การสังเคราะห์ตัวเร่งปฏิกิริยาซีโอไลต์บีตาที่เสถียรต่ออุณหภูมิสูงสำหรับการเปลี่ยนกลีเซอรอลเป็นโซลคีทาลอย่างเลือกจำเพาะ

นางสาวศิริลักษณ์ เทศนา

วิทยานิพนธ์นี้เป็นส่วนหนึ่งของการศึกษาตามหลักสูตรปริญญาวิทยาศาสตรมหาบัณฑิต
สาขาวิชาเคมี ภาควิชาเคมี
คณะวิทยาศาสตร์ จุฬาลงกรณ์มหาวิทยาลัย
ปีการศึกษา 2557

SYNTHESIS OF HIGHLY THERMAL STABLE ZEOLITE BETA CATALYST FOR SELECTIVE CONVERSION OF GLYCEROL TO SOLKETAL

Miss Siriluck Tesana

A Thesis Submitted in Partial Fulfillment of the Requirements
for the Degree of Master of Science Program in Chemistry
Department of Chemistry
Faculty of Science
Chulalongkorn University
Academic Year 2014

Thesis Title	SYNTHESIS OF HIGHLY THERMAL STABLE ZEOLITE BETA CATALYST FOR SELECTIVE CONVERSION OF GLYCEROL TO SOLKETAL
By	Miss Siriluck Tesana
Field of Study	Chemistry
Thesis Advisor	Aticha Chaisuwan, Ph.D.

Accepted by the Faculty of Science, Chulalongkorn University in Partial Fulfillment of the Requirements for the Master's Degree

.....Dean of the Faculty of Science
(Professor Supot Hannongbua, Dr.rer.nat.)

THESIS COMMITTEE

.....Chairman
(Associate Professor Vudhichai Parasuk, Ph.D.)

.....Thesis Advisor
(Aticha Chaisuwan, Ph.D.)

.....Examiner
(Duangamol Tungasmita, Ph.D.)

.....Examiner
(Numpon Insin, Ph.D.)

.....External Examiner
(Associate Professor Kulaya Otaka, Ph.D.)

ศิริลักษณ์ เทศนา : การสังเคราะห์ตัวเร่งปฏิกิริยาซีโอไลต์บีตาที่เสถียรต่ออุณหภูมิสูงสำหรับการเปลี่ยนกลีเซอรอลเป็นโซลคีทาลอย่างเลือกจำเพาะ (SYNTHESIS OF HIGHLY THERMAL STABLE ZEOLITE BETA CATALYST FOR SELECTIVE CONVERSION OF GLYCEROL TO SOLKETAL) อ.ที่ปรึกษาวิทยานิพนธ์หลัก: อ. ดร.อธิชา ฉายสุวรรณ, 113 หน้า.

ได้สังเคราะห์ซีโอไลต์บีตาสำเร็จจากซิลิกาฟูมซึ่งผสมกับโซเดียมอะลูมิเนตและโซเดียมไฮดรอกไซด์โดยใช้สีดนาโนซึ่งมีสภาพเป็นผลึกแทนสารต้นแบบอินทรีย์เพื่อเร่งการเกิดผลึกซีโอไลต์บีตา ได้นำเจลตั้งต้นที่มีอัตราส่วนของซิลิกาต่ออะลูมินาต่อโซเดียมออกไซด์ต่อน้ำเป็น 1:0.027:0.36:35 ไปตกผลึกในออโตเคลฟแบบไฮโดรเทอมัลภายใต้ความดันที่เกิดขึ้นเอง ได้ศึกษาผลของอุณหภูมิที่ใช้ในการตกผลึก เวลาของการตกผลึก และปริมาณสีดนาโนที่นำไปเผาแล้วต่อสมบัติของผลิตภัณฑ์ซีโอไลต์บีตา ได้ตรวจสอบลักษณะเฉพาะของซีโอไลต์บีตาด้วยเทคนิคเอกซ์อาร์ดี เอฟอีเอสอีเอ็ม การดูดซับไนโตรเจน อะลูมิเนียม 27-เอ็มเอเอส-เอ็นเอ็มอาร์ และไอซีพี-เอ็มเอส การเพิ่มอุณหภูมิและเวลาที่ใช้ในการตกผลึกนำไปสู่การเกิดซีโอไลต์โซเดียม-พีหนึ่งและมอร์ดีไนต์เป็นสารเจือปน การเพิ่มปริมาณสีดจากร้อยละ 0.17 เป็น 0.83 โดยน้ำหนักต่อเจลตั้งต้นมีผลให้ซีโอไลต์บีตาที่มีสภาพผลึกสูงมีขนาดอนุภาคเล็กลงจาก 620 นาโนเมตร x 840 นาโนเมตร เป็น 140 นาโนเมตร x 150 นาโนเมตรและลดเวลาที่ใช้ในการตกผลึกจาก 5 วัน เป็น 2 วัน ตามลำดับ พื้นที่ผิวจำเพาะชนิดบีอีทีของซีโอไลต์บีตาที่สังเคราะห์ได้มีค่าประมาณ 600 ตารางเมตรต่อกรัม ซีโอไลต์บีตาที่สังเคราะห์ได้มีความสูงของพีกหลักในเอ็กซ์อาร์ดีลดลงเพียงเล็กน้อยจากการเผาที่อุณหภูมิสูง 550 องศาเซลเซียส ซึ่งบ่งชี้ให้เห็นถึงความเสถียรสูงของซีโอไลต์บีตาที่สังเคราะห์ด้วยวิธีการใช้สีดนาโนเป็นตัวช่วย การไม่มีพีกของอะลูมิเนียมชนิดนอน-เฟรมเวิร์กในสเปกตรัมอะลูมิเนียม 27-เอ็มเอเอส-เอ็นเอ็มอาร์บ่งชี้ว่าไม่มีอะลูมิเนียมหลุดออกจากโครงสร้างหลังจากการนำไปเผา ตัวเร่งปฏิกิริยาซีโอไลต์มีค่าอัตราส่วนของซิลิกาต่ออะลูมินาในช่วง 8.8 ถึง 10.0 ได้สำรวจฤทธิ์ของสารตัวอย่างซีโอไลต์บีตาในการเร่งปฏิกิริยาอะซีทาลไลเซชันของกลีเซอรอลด้วยแอซีโตนโดยใช้ไดเมทิลฟอร์มาไมด์เป็นตัวทำละลาย ค่าการเปลี่ยนกลีเซอรอลและปริมาณของผลิตภัณฑ์โซลคีทาลไม่ได้รับผลกระทบจากปริมาณสีดนาโนที่ใช้ในการสังเคราะห์ตัวเร่งปฏิกิริยาเพราะได้คัดเลือกตัวเร่งปฏิกิริยาที่นำมาทดสอบจากการสังเคราะห์ในภาวะที่เหมาะสมจึงมีสมบัติใกล้เคียงกัน จากการเปลี่ยนค่าตัวแปรหลายชนิดพบว่าได้ค่าการเปลี่ยนกลีเซอรอลสูงสุดร้อยละ 35 และความเลือกจำเพาะต่อโซลคีทาลร้อยละ 93 หลังทำปฏิกิริยา 150 นาที ตัวเร่งปฏิกิริยาที่ผ่านการใช้งานแล้วสามารถทำให้กลับคืนสภาพเดิมได้โดยการเผาที่อุณหภูมิสูง และมีประสิทธิภาพในการเร่งปฏิกิริยาใกล้เคียงของเดิม

ภาควิชา เคมี ลายมือชื่อนิสิต .....

สาขาวิชา เคมี ลายมือชื่อ อ.ที่ปรึกษาหลัก .....

ปีการศึกษา 2557

5672106723 : MAJOR CHEMISTRY
KEYWORDS: ACETALIZATION / ACETONE / BEA / CATALYST / GLYCEROL / NANOSEED / SOLKETAL / SYNTHESIS / ZEOLITE BETA

SIRILUCK TESANA: SYNTHESIS OF HIGHLY THERMAL STABLE ZEOLITE BETA CATALYST FOR SELECTIVE CONVERSION OF GLYCEROL TO SOLKETAL. ADVISOR: ATICHA CHAISUWAN, Ph.D., 113 pp.

Highly thermal stable zeolite beta was successfully synthesized from fumed silica mixed with sodium aluminate and sodium hydroxide using crystalline nanoseeds instead of the organic template to encourage formation of the zeolite beta crystals. The starting gel with a composition of SiO_2:0.027Al_2O_3:0.36Na_2O:35H_2O was hydrothermal crystallized in an autoclave under autogenous pressure. The effects of crystallization temperature, crystallization time, and calcined nanoseed amounts on the properties of zeolite beta products were studied. The zeolite beta products were characterized by XRD, FESEM, nitrogen adsorption, ^{27}Al-MAS-NMR and ICP-MS techniques. The increase in temperatures and crystallization time leads to formation of zeolites Na-P1 and mordenite as impurities. The increase in seed amounts from 0.17 to 0.83 wt% to the starting gel resulted in high crystallinity zeolite beta with smaller average particle sizes from 620 nm x 840 nm to 140 nm x 150 nm, and shorter optimal crystallization time from 5 to 2 days, respectively. Their BET surface areas were approximately 600 m^2/g. The intensities of the XRD parent peak of zeolite beta products were slightly decreased upon calcination at 550 °C indicating the high stability of the samples prepared by the nanoseed-assisted method. The absence of the non-framework peak in ^{27}Al-MAS-NMR spectra indicated no dealumination after calcination. The zeolite catalysts contained SiO_2/Al_2O_3 ratios in a range of 8.8-10.0. The catalytic activities of zeolite beta samples were investigated for acetalization of glycerol with acetone using dimethylformamide as solvent. The glycerol conversions and solketal yields were not influenced by nanoseed amounts used in the catalyst synthesis because all tested catalysts were selected from the optimal conditions of synthesis resulting in similar properties. Upon varying several parameters, the highest glycerol conversion of 35% with 93% selectivity to solketal were achieved after 150 minutes. The used catalyst was regenerated by calcinations and maintained similar activity.

Department: Chemistry Student's Signature .....
Field of Study: Chemistry Advisor's Signature .....
Academic Year: 2014

ACKNOWLEDGEMENTS

The author would like to deeply thank Dr. Aticha Chaisuwan, her thesis advisor for valuable advice and guidance in this research as well as the extraordinary experiences throughout the work.

She would like to give her gratitude to Associate Professor Dr. Vudhichai Parasuk, the chairman, Dr. Duangamol Tungasmita, Dr. Numpon Insin and Associate Professor Dr. Kulaya Otaka, the members of the thesis committee, for all of their kindness and useful advice in the research.

She appreciates Department of Chemistry, Faculty of Science, Chulalongkorn University for the valuable instruments and laboratories. Furthermore, she would like to thank the Office of The High Education Commission for a Science Achievement Scholarship for financial support. In addition, she appreciates Thailand Japan Technology Transfer Project, a loan supported by Japan Banks for International Cooperation (TJTTP-JBIC) for instrument support.

Many thanks are given in particular to the members of Materials Chemistry and Catalysis Research Unit for their help and encouragement throughout the course of her research. Finally, she would like to greatly thank her family, all of her chemistry professors and friends for their assistance and encouragement during her graduate study.

CONTENTS

Page

Page

Page

Page

LIST OF TABLES

LIST OF FIGURES

LIST OF SCHEMES

LIST OF ABBREVIATIONS

AIP	aluminium isopropoxide
MAS-NMR	magic-angle-spinning-nuclear magnetic resonance
BEA	zeolite beta
BET	Brunauer-Emmett-Teller
BJH	Barret, Joyner and, Halenda
°C	degree Celsius
cps	counts per second
FESEM	field emission scanning electron microscopy
FID	flame ionization detector
GC	gas chromatograph or gas chromatography
h	hour (s)
ICP-MS	inductively coupled plasma-mass spectroscopy
M	molar
XRD	X-ray diffraction
g	gram (s)
min	minute (s)
ppb	part per billion or µg/L
SBA-15	Santa Barbara Amorphous-15
TEOS	tetraethyl orthosilicate
TEAOH	tetraethylammonium hydroxide
%	percent

CHAPTER I

INTRODUCTION

1.1 Background

Zeolites are considered as efficient catalysts for a number of acid-catalyzed reactions due to their high crystallinity, large specific surface area, unique shape and size selectivity and controllable acidity. Among all zeolites, zeolite beta is one of the most attractive large pore zeolites. Zeolite beta has an open-framework structure of three dimensional channels with 12 membered-ring pore openings. The pore sizes of zeolite beta are 0.66 nm x 0.67 nm along the straight channels and 0.56 nm x 0.56 nm along the zigzag channels [1]. Zeolite beta is formed by the intergrowth of two polymorphs A and B which have tetragonal and monoclinic symmetries, respectively [2]. Similar to other zeolites, zeolite beta can adsorb or exclude molecules depending on their shapes and sizes [3]. Due to its appropriate pore size and structure, zeolite beta appears to be a potential candidate as a solid acid catalyst in a broad range of catalytic reactions such as alkylation [4, 5], isomerization [6-8], catalytic cracking [9-11], esterification [12, 13] and acetalization [14-16].

Zeolite beta was first synthesized at Mobile Research and Development Laboratories by Wadlinger and coworkers in 1967 [17]. Zeolite beta is typically synthesized by a hydrothermal method using tetraethylammonium hydroxide (TEAOH) as pore directing agent to shorten crystallization time and to obtain nanocrystal zeolites [18]. In the presence of an organic template, a high silica zeolite beta with the Si/Al mole ratio of 11 to higher was obtained [19]. Unfortunately, combustion of the organic template during thermal activation of zeolite beta at an elevated temperature may cause the partial degradation of zeolite structure resulting in aluminum migration and loss of its acidity during catalyst activation [20, 21]. To avoid degradation of zeolite beta structure during calcination, the TEAOH amount used in the starting mixture must be controlled as low as possible.

The aluminum-rich zeolite beta (Si/Al ratios in a range of 3.9-6.2) was synthesized by adding template-containing zeolite beta as seeds [22]. Among various inorganic cations in gel, only sodium ions provided the structure of zeolite beta with the crystal size around 400 nm. Zeolite beta with highest crystallinity was obtained after crystallization at 125 °C for 6 days in the presence of 2.5 wt% seeds.

In 2008, the synthesis of zeolite beta with the low Si/Al mole ratio of 4.5 was achieved without using any organic template but the addition of calcined zeolite beta as seeds was attempted. High crystallinity of zeolite beta with the particle sizes ranging from 100 to 160 nm was found. The purpose of addition of inorganics seeds was not only to induce formation of zeolite beta structure but also to reduce the crystallization time of zeolite beta. It was reported that zeolite beta could not be obtained in the absence of seeds [23].

The template-free zeolite beta was used as seeds in the synthesis of zeolite beta and highly crystalline zeolite beta with Si/Al mole ratios in the range of 5.2-6.8 was obtained [24, 25]. The influences of gel compositions as well as amounts and Si/Al ratios of seeds on properties of zeolite beta were revealed. An increment of seed Si/Al ratios led to a decrease of crystallization time for zeolite beta formation. In the presence of sodium in the starting gel, mordenite was thermodynamically more stable than zeolite beta but in the presence of seeds, zeolite beta phase was kinetically favored. To obtain pure zeolite beta, seeds were needed to initiate crystal growth of zeolite beta phase prior to nucleation of mordenite phase. Crystallization rate and crystal sizes of zeolite beta products were affected by seed amounts. In the presence of seeds in a small amount, rate of crystallization was slower resulting in larger crystal sizes.

The core-shell crystallization mechanism of the seed-directed synthesis was proposed as shown in Scheme 1.1 supported by SEM, TEM and EDX results [26]. At the early stage, the crystal seeds were dispersed in the starting gel prior to form condensed amorphous aluminosilicates. During hydrothermal treatment the crystal seeds were partially dissolved and gradually grew in the amorphous aluminosilicates. Finally, the pure phase of zeolite beta was obtained. Thus, achieved product

comprised of the core of non-dissolved seeds and shell growing from the transformation of the amorphous aluminosilicates.

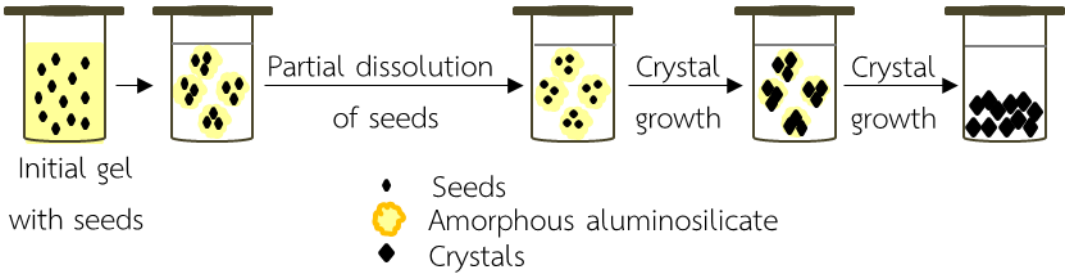

Scheme 1.1 Crystallization mechanism in the organic template-free synthetic route [25]

Large quantity of seeds and high crystallization temperature resulted in fast crystallization rate, but more defects could be found for a synthesis of zeolite beta [21]. The synthesis of zeolite beta at two different temperatures of 120 °C and 140 °C was investigated. Zeolite beta with better properties including higher thermal stability, larger specific surface area and micropore volume and less defects was obtained at 120 °C. The other factor affecting crystallinity of zeolite products is the type of seeds.

Recently, the influence of nature of zeolite beta seeds on properties of achieved zeolite beta product synthesized by organic template-free route was reported [27]. Various types of seeds were added into the initial mixture. At the induction period, the partially dissolution of seeds took place. Crystal sizes of seeds considerably influenced the induction process. Smaller crystals dissolved faster than larger ones, thus shorter induction period was consumed for the nuclei formation. During the crystal growth period, growth rate of zeolite beta was affected by both crystal size and Si/Al mole ratio of seeds. The higher Si/Al mole ratio of seed, the faster induction and crystal growth rate were observed. However, rate of crystal growth significantly decreased according to an increment of seed crystal size resulting in reduction of nuclei number generated by seeds. They also concluded that seeds

with high Si/Al ratios gave zeolite beta product with high crystallinity, whereas high crystal size of seed was favorable for the synthesis of zeolite beta product with large crystal size. To obtain a pure zeolite beta product with small crystal size and high crystallinity, the small zeolite beta seeds with suitable high Si/Al mole ratio could be applied as structure directing agent. Moreover, the quality of zeolite was also significantly influenced by crystallization conditions.

Nowadays, petroleum and natural gas are still the most powerful energy source for modern society. There is an increasing trend of fuel consumption due to global economic growth. Rising oil prices as well as more concern about greenhouse gas concentrations have motivated many researchers to seek new alternative energy sources. Biodiesel has received a great interest as alternative fuel with low greenhouse gases emission. Biodiesel is produced by base-catalyzed transesterification of triglyceride with methanol (Scheme 1.2). From the biodiesel manufacturing process, glycerol is obtained as by product approximately 10 wt%. An increment of biodiesel production has led to a massive oversupply of low cost crude glycerol [28-30].

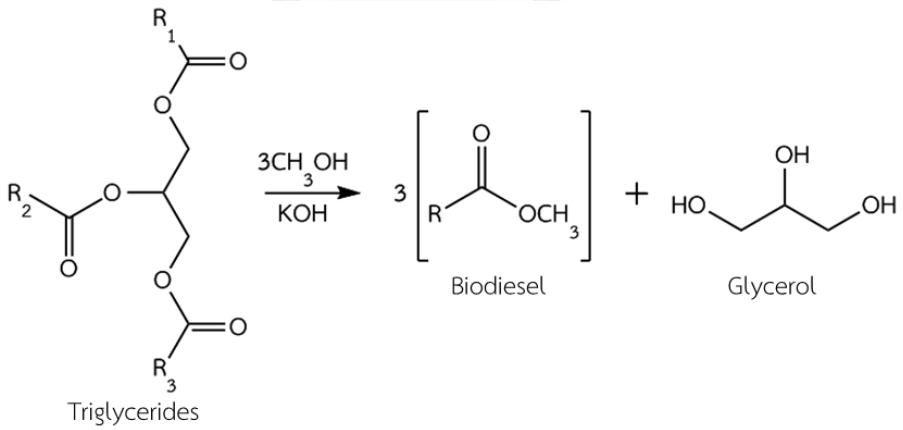

Scheme 1.2 Biodiesel production via transesterification of triglycerides

Glycerol is commonly used in food, cosmetic, soap and pharmaceutical industries but a surplus of crude glycerol still piles up. New applications for glycerol have been investigated. A great number of reactions could be applied to glycerol, thus providing lots of value-added products such as acrolein [31], acetol [32], propanediols [33], acrylic acid [34] and acetal [35]. Those glycerol derivatives can be used in fuels, chemicals, pharmaceutical, and plastic industries. One of the most attractive chemical routes of glycerol conversion is acid-catalyzed acetalization of glycerol to solketal (Scheme 1.3).

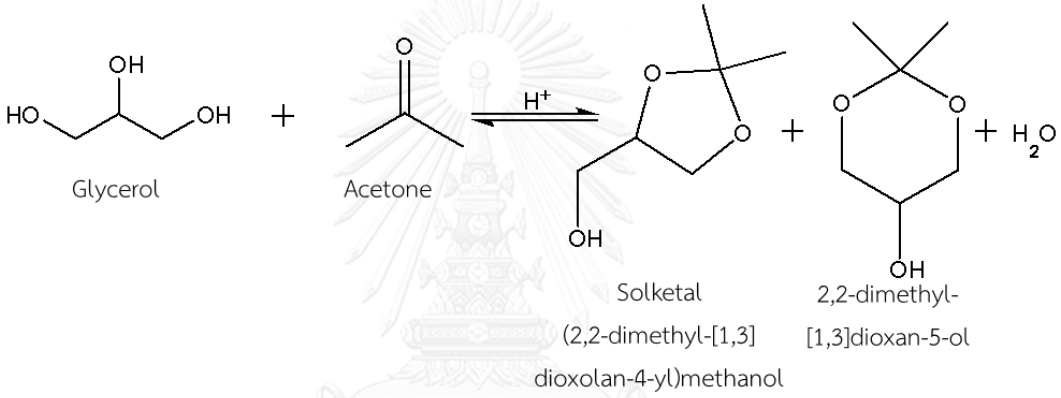

Scheme 1.3 Acid-catalyzed acetalization of glycerol to solketal

Solketal or (2,2-dimethyl-[1,3] dioxolan-4-yl)methanol, is a useful fuel additive for gasoline, diesel and biodiesel. This compound can improve cold flow properties and flash point in addition to reducing fuel viscosity. Recent studies indicate that solketal is a high potential oxygenated fuel which can significantly increase the octane number of gasoline. In addition, it is also used as solvent, plasticizer and suspension agent in pharmaceutical industry [36, 37].

Traditionally, acetalization of glycerol with acetone was carried out in a batch reactor using homogeneous acid catalysts for example sulfuric acid [38], *p*-toluene sulfonic acid [39] and tin(II) chloride solution [40]. Solketal production from glycerol using a flow continuous process was developed in 2011 by Monbaliu and coworkers [38]. A 69% conversion of glycerol was observed using 10 mol% of sulfuric

acid with 4 equivalents of acetone. But the higher acid concentration, the lower glycerol conversion was found due to degradation reaction of glycerol. Since sulfuric acid has been known as a highly corrosive mineral acid, the reaction is required to perform in a glass reactor. The synthesis of solketal using p-toluenesulfonic acid as catalyst was reported [39]. The reaction was carried out in a batch reactor under reflux. After 12 hours of reaction with a large excess amount of acetone, a high glycerol conversion up to 80% was observed. It could not reach a 100% conversion due to the effect of water, a by-product which drove solketal back to glycerol. Recently, $SnCl_2$ was claimed to be an efficient catalyst for solketal formation due to its solubility in the reaction medium and high water resistance. The maximum glycerol conversion was 81% with high selectivity to solketal [40]. However, it was reported that $SnCl_2$ could induce DNA damage and hazard to embryo. Thus, in order to obtain high solketal yield, long reaction time and large excess amount of acetone as well as water-resistance of catalyst are required.

Even though the homogeneous acid catalysts showed good catalytic activities, they still had several drawbacks such as reactor corrosion, complicated separation process and catalysts toxicity. Most of these problems could be overcome by using heterogeneous catalysts like amberlyst [14], heteropolyacids [41], sulfonated-mesoporous silica [42], zeolites and others [15]. The effects of impurities on catalytic performance of Amberlyst-15 and zeolite beta toward acetalization of glycerol with acetone were reported [14]. Three main impurities which were water, methanol and sodium chloride were added at various amounts in the reaction medium. All impurities, especially water and sodium chloride caused glycerol conversion decreased. Amberlyst-15 was affected by impurities more than zeolite beta due to poor water tolerant properties of the former. Acetalization of glycerol over heteropolyacids immobilized in silica was reported [41]. The stronger acid catalysts, the better catalytic activity and the higher selectivity to solketal were achieved. However, all of immobilized catalysts showed a lower conversion after the fourth run due to catalysts degradation. Other catalysts, *i.e.* Amberlyst and heteropolyacids showed poor thermal stability, low surface area and difficulty in

catalyst regeneration [43]. Carbon-mesoporous silica composite was synthesized using glucose as both carbon source and structure directing agent in 2013 [42]. This material was functionalized with sulfonic acid to form an acid catalyst which exhibited a high glycerol conversion and also remained an efficient catalyst after the fourth use. However, the disadvantage is that several synthesis steps were needed to obtain these composite materials.

The conversion of glycerol to solketal using nanoparticles of zeolite beta as catalyst showed high selectivity toward solketal [44]. However, formation of by-product especially water can drive the solketal back to glycerol [45]. To make the reaction forward a large excess of acetone will be required. Moreover, molecular sizes of reagents become the importance factor for this catalytic reaction because most of reactions took place at the acid sites inside zeolite pore. From Chemdraw 3D Ultra, the kinetic diameter of glycerol is 0.63 nm x 0.27 nm while the average pore size of zeolite beta is about 0.67 nm [3]. Thus large pore zeolite beta allows glycerol to diffuse into zeolite structure. However the kinetic pore size of zeolite beta can change a little depending on temperature [46].

A mechanism was proposed for acetalization of glycerol with acetone over zeolite beta to form the synthesis of solketal as shown in Scheme 1.4 [15, 47, 48]. The mechanism involves four importance steps. First, the oxygen atom of excess acetone attaches proton at the acid site of zeolite. Secondary, the hydroxyl oxygen atom of glycerol attack at the C of carbonyl group, the hemiacetal intermediate is created. Finally, the dissociation of water molecule occurs, followed by self-condensation to form solketal.

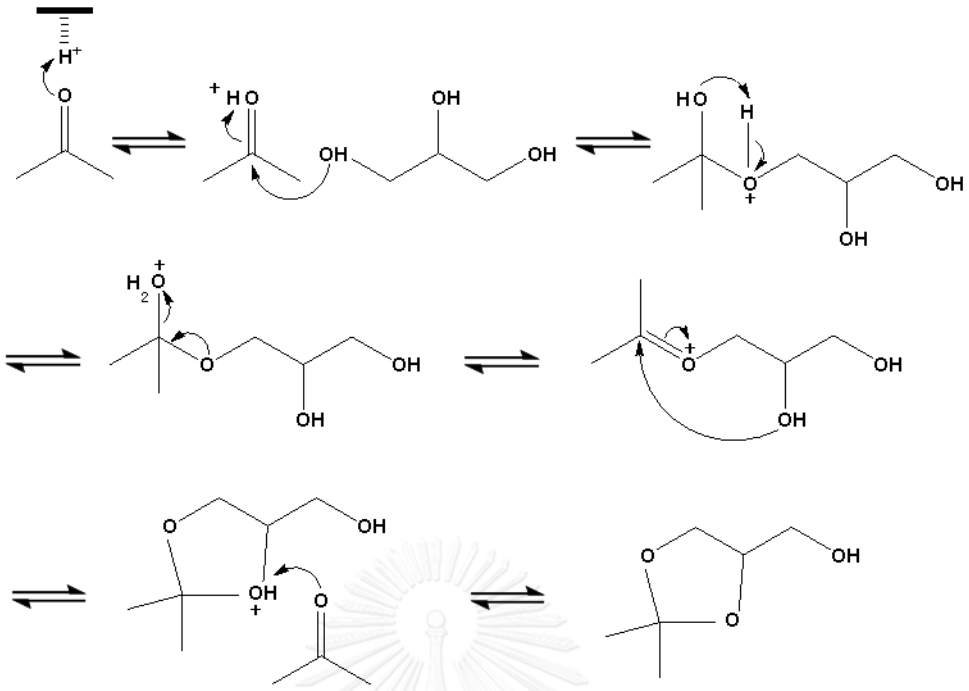

Scheme 1.4 Mechanism for acid-catalyzed acetalization reaction of glycerol with acetone

Zeolites beta tended to be an appropriate acid catalyst for glycerol conversion to solketal due to its appropriate pore size and structure [14-16]. Nevertheless, the structure of zeolite beta always partially collapses at elevated activation temperature of at least 500 °C, resulting in aluminum leaching from the zeolite framework to its surface [20, 21]. This project aims to develop the synthesis of zeolite beta with stable structure upon thermal activation using the organic template-free route. Instead, crystalline nanoseeds will be replaced for the organic template to encourage formation of the zeolite crystals upon hydrothermal treatment. To obtain the appropriate condition of synthesis, some parameters such as effects of crystallization temperature, crystallization periods and amounts of crystalline nanoseeds were studied. The catalysts obtained were characterized for their structures, crystallinities, crystal sizes, pore sizes and specific surface areas. The thermal stability and structure collapse were investigated by XRD and ^{27}Al-MAS-NMR techniques. The zeolite products were also tested for their catalyst activities in acetalization of glycerol to solketal. Reaction parameters in view of reaction periods,

amounts of catalysts, mole ratios of glycerol to acetone and Si/Al ratios in the starting gel were also reported.

1.2 Objectives

To synthesize highly thermal stable zeolite beta catalyst for conversion of glycerol to solketal

1.3 Scope of Work

1. To prepare SBA-15 from tetraethylorthosilicate using Pluronic® P123 as structure-directing agent.
2. To prepare crystalline nanoseeds from on-site-prepared SBA-15 silica in the presence of aluminium isopropoxide and tetraethylammonium hydroxide.
3. To synthesize zeolite beta catalyst from fumed silica with addition of crystalline nanoseeds under various conditions.
4. To study the effects of crystallization periods, crystallization temperature and crystalline nanoseed amounts on the formation of zeolite beta products.
5. To apply selected zeolite products to acetalization of glycerol to solketal by investigating the effects of reaction time and mole ratios of glycerol to acetone with different amounts of crystalline nanoseeds in gel.
6. To study activity of the regenerated catalyst.

CHAPTER II

THEORY

2.1 Zeolites

Zeolites are a crystalline microporous aluminosilicates of, typically, alkali and alkaline earth metal ions. The zeolite structure consisting of oxides of Si and Al in tetrahedral coordination connected in three dimensions by the sharing oxygen atoms as shown in Figure 2.1 [49] resulting in a negative charge delocalizing around each AlO_2 unit. Metal ions are needed to balance the framework charges.

Figure 2.1 The general framework structure of zeolites

According to the incorporation of aluminium into the silica framework, the negative charges of tetrahedral $[AlO_2]^-$ units make the overall framework negatively charged which must be balanced by the extra framework cations. A general unit cell formula of a zeolite is:

$$M_{x/n}\,[\,(AlO_2)_x(SiO_2)_y\,]\cdot zH_2O$$

where M atoms are extra framework cations with the valence of n, generally group I or II ions, but it can be other metals, nonmetals or even organic cations. Total number of alumina and silica per unit cell are represented by x and y, respectively. Thus, summation of x and y is the total amount of tetrahedral units in the unit cell. The portion [ ] is the framework composition and z is the number of water molecule located in the channels and cavities inside the zeolite structure.

2.1.1 Zeolite structures

There are more than 200 types of zeolites discovered in nature and synthesized in laboratories. Types of zeolites are classified by structures. A general zeolite structure is three-dimensional framework of tetrahedral primary building units (TO_4). Each of primary building unit (PBU) consists of the tetrahedral atoms (T) which are silicon or aluminum tetrahedrally coordinated to four atoms of oxygen as shown in Figure 2.2. The angle of T-O-T linkage is flexible in the range of 120°-180° [49].

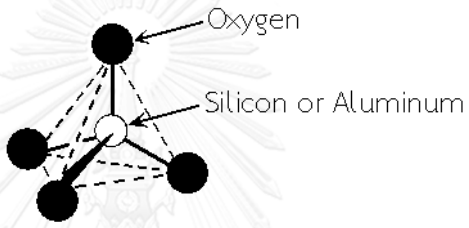

Figure 2.2 A primary building unit (PBU) of a zeolite

The PBUs are arranged into larger structures by sharing four oxygen atoms with another tetrahedral unit by corner sharing, so called secondary building units (SBUs). These SBUs units are the true criteria used in classifying groups of all zeolite structures. The SBUs are usually shown by connected dots which is corners of polyhedral referred to the tetrahedral (Al, Si) atoms. The connecting lines represent the distance between the centers of neighboring tetrahedral units while oxygen atoms are omitted. Some SBUs are shown in Figure 2.3. The simplest SBUs are single polygons or rings for example 4, 5, 6 and 8-membered rings. The extensive SBUs are the double rings such as 4-4, 5-5, 6-6 and 8-8 membered double rings and 4-1, 5-1, 6-2 and 4-1=1 branched rings or two rings with unequal members.

The different framework structures of zeolites can be built from different SBUs. The SBUs units are interconnected to create a broad range of tertiary building units or polyhedrons which are arranged in a three-dimensional

structure forming the characteristic framework of each zeolite crystal structure. For instance, zeolite A framework (LTA) can be generated from either the 4-member single ring or the 6-member single ring. Some of them are shown in Figure 2.4.

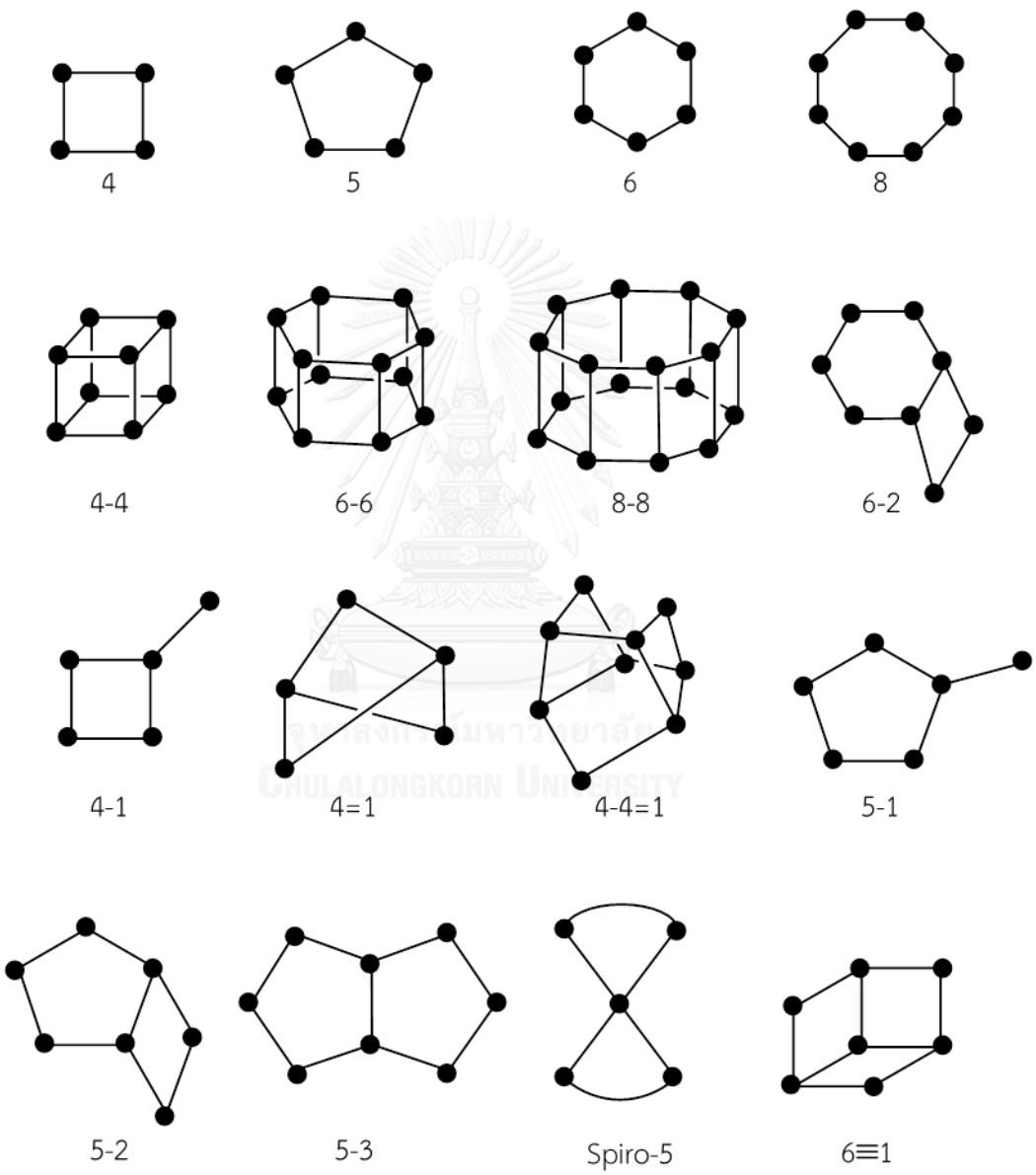

Figure 2.3 Secondary building units (SBUs) in zeolite framework [50]

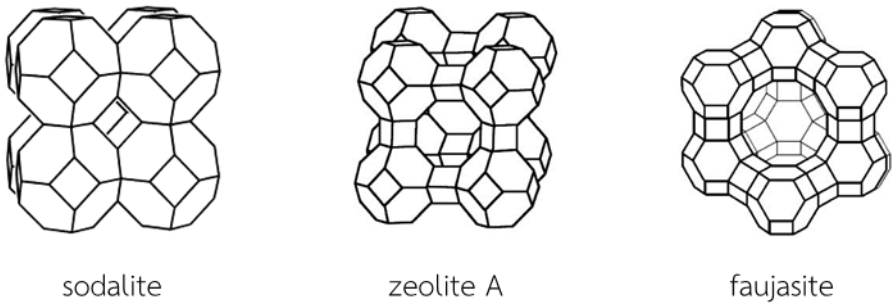

Figure 2.4 The structures of some zeolites: sodalite, zeolite A, and faujasite [51]

The pore openings or pore sizes are usually mentioned as the number of oxygen atoms which are equal to the number of tetrahedral atoms. According to the different pore sizes, zeolites can be classified into three groups as shown in Figure 2.5. The small pore means the 8-membered oxygen ring opening ranging from 0.30-0.45 nm, zeolite A, erionite and chabazite, for instance. The medium pore means the 10-membered oxygen ring opening ranging from 0.45-0.60 nm such as ZSM-11, ZSM-5 and TS-1. The large pore means 12-membered oxygen ring opening bigger than 0.60 nm such as zeolite rho, mordenite, faujasite and zeolite beta [52].

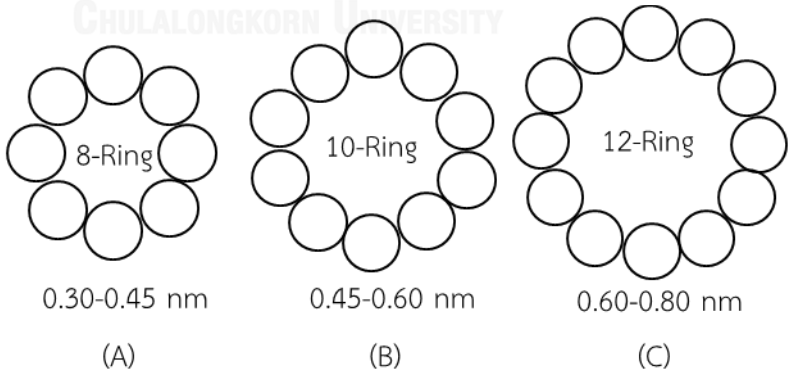

Figure 2.5 Examples of the three types of pore openings in the zeolite framework (A) small pore, (B) medium pore and (C) large pore

2.1.2 Acid Sites of Zeolites

Acidity is one of the most important properties of zeolite catalysts since the activity in an acid-catalyzed reaction is related to the type and the amount of active sites inside the zeolite structure. A well understanding of nature of zeolite acidity is necessary for developing a catalyst for chemical reactions. Acidity of zeolites is mainly based on the alumina content which is related to the Si/Al mole ratio. As previously described, the alumina units in the structure of zeolite have the negative charges which need to be balanced by the extra framework cations. When the cations are proton (H^+), the zeolite becomes acidic and can be used as acid catalyst. Normally, zeolites are synthesized in the presence of sodium ions, thus Na^+ ions become extra-framework cations balancing the framework charges. The acid form of zeolite is obtained when Na^+ is replaced by H^+. However, the direct proton exchange cannot be performed according to the instability of zeolite structure in a strong mineral acid solution.

Commonly, the preparation of the acid zeolite was done via indirect exchange with an ammonium salt solution followed by calcination above 375 °C in order to decompose NH_4^+ ions into H^+ and NH_3. After the elimination of ammonia molecules, protons are bonded with surface oxygen giving the bridging form –SiO(H)Al- of the Brønsted acid sites. At high temperature, the bridging OH is in equilibrium with the terminal OH, so called a silanol group adjacent to tricoordinated aluminium ion which has a property of electron-pair acceptor which is known as Lewis acid [53-55]. The formation of these acids sites is shown in Figure 2.6.

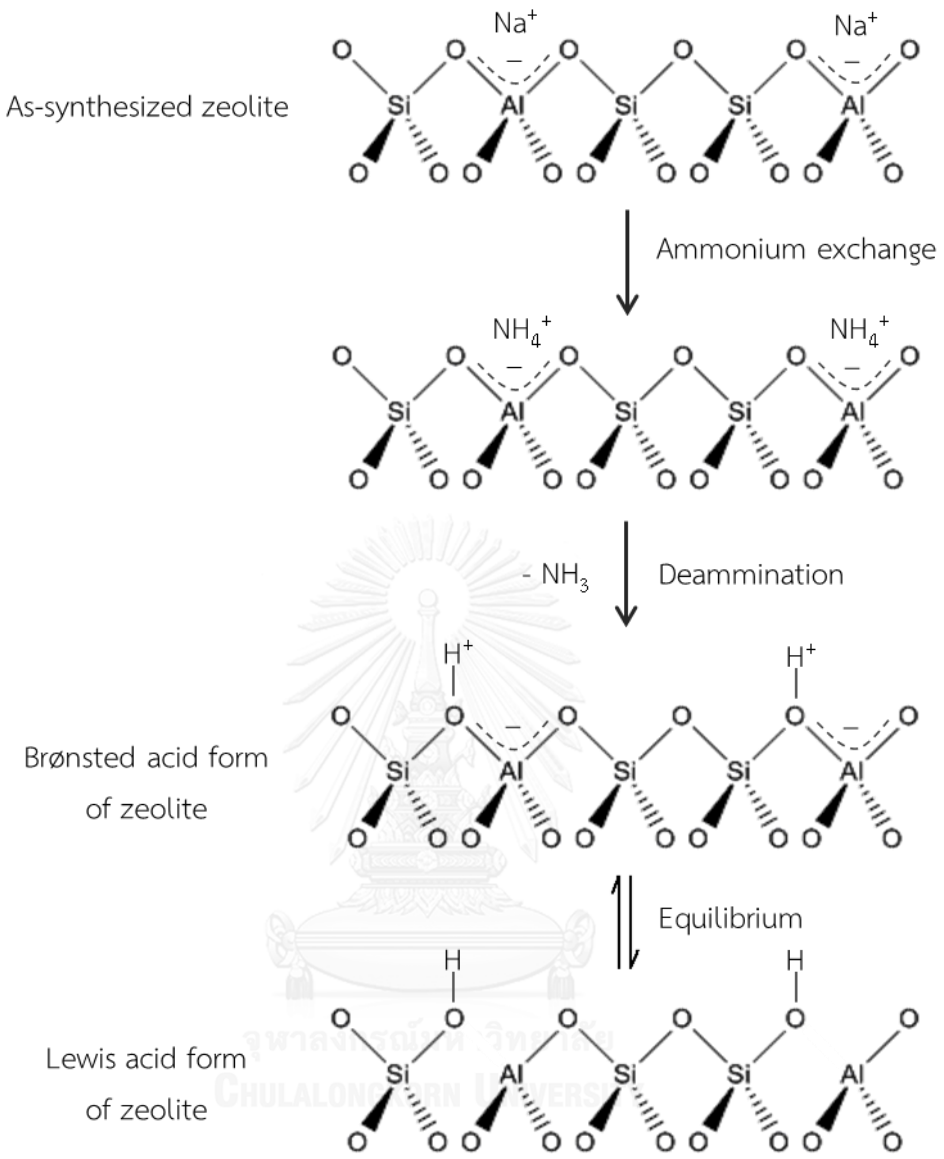

Figure 2.6 The generation of Brønsted and Lewis acid sites in zeolite

2.1.3 Shape and Size Selectivity

The high crystallinity and rigid channel structures of zeolites lead to shape and size selective properties of zeolites. This unique property plays an important role in catalytic reaction making zeolites as potential catalysts better than other materials. Shape selectivity of zeolites can be classified into 3 types: reactant selectivity, transition state selectivity and product selectivity as shown in Figure 2.7. Due to the rigid pores of any zeolite, only appropriate shapes and sizes of reactants can effectively enter and diffuse inside the zeolite channel. Thus, the reactant molecules with larger size than the pore size of zeolite cannot reach the acid sites, so the reaction cannot take place. Considering the transition state selectivity, the local environment around the acid site affects the rate constant of certain reaction mechanism. If the transition state is too bulky, reaction rate is retarded and those transition states are easily decomposed. When products of the reaction are obtained inside the zeolite pores, the product will be also selected by size and shape. Some product molecules cannot escape from the zeolite structure. However, the zeolite framework can exhibit some flexibility in kinetic pore diameter with changes in temperature [55, 56].

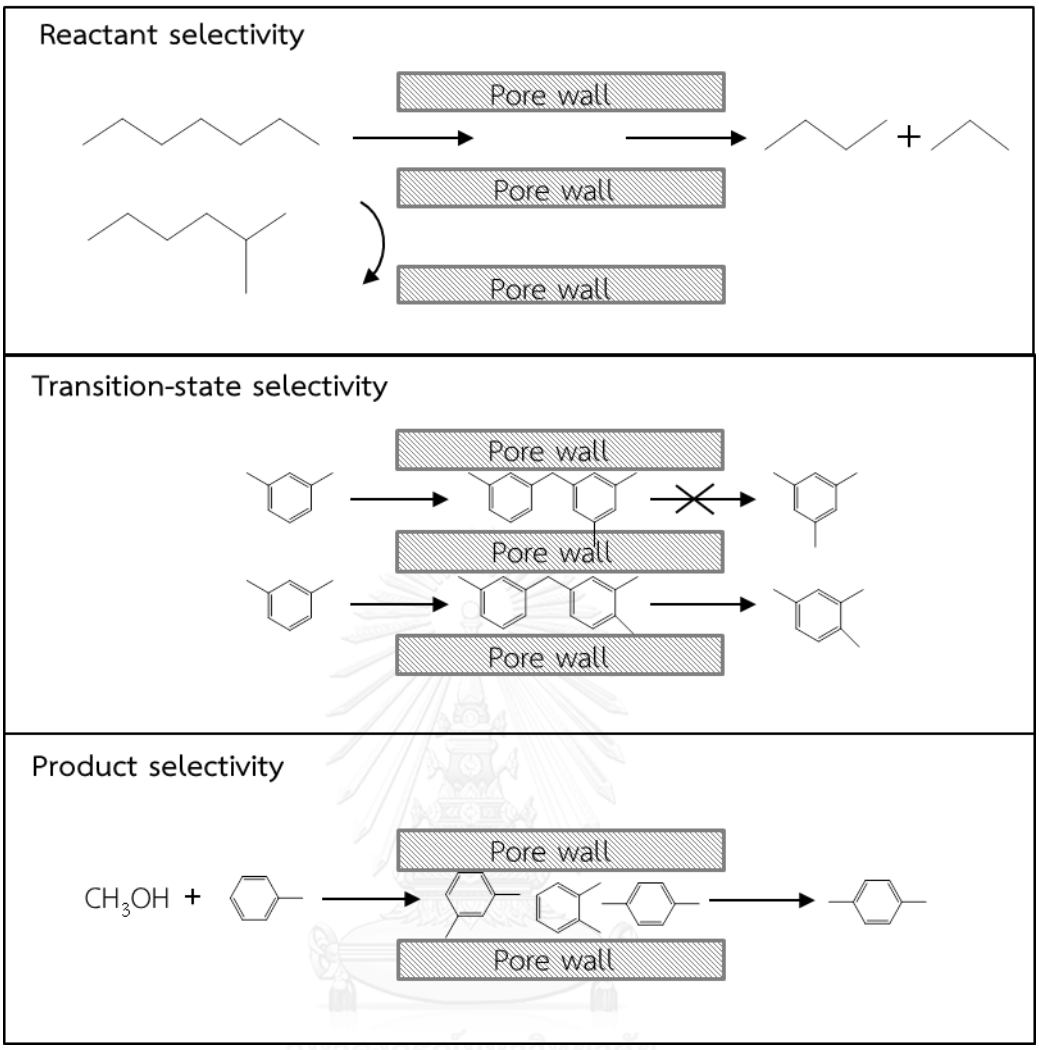

Figure 2.7 Three types of selectivity in zeolites: reactant, transition-state and product shape and size selectivity

2.2 Zeolite Synthesis

Zeolites are conventionally synthesized at various temperatures by a hydrothermal method in a closed cylindrical vessel, so called an autoclave. The starting mixture used in the zeolite synthesis is composed of mixed sources of silicon, aluminium and inorganic base, usually NaOH, in water resulting in the four-component system Na_2O-Al_2O_3-SiO_2-H_2O. The common silica sources are silica gel, water glass, colloidal silica, sodium silicate and tetraethylorthosilicate (TEOS) while sodium aluminate, aluminium isopropoxide (AIP) and aluminium hydroxide are used as alumina sources in the zeolite synthesis. The copolymerization of silicate and aluminate species takes place according to the condensation mechanism. The resulted amorphous aluminosilicates gel is heated in an autogenic pressure autoclave at the appropriate temperature and time to form zeolite crystals. The autogenous pressure is approximately equivalent to the saturated vapor pressure of water at crystallization temperature. The crystallization time varies from a few hours to several days depending on type of zeolites and reactant composition. The zeolite crystals are separated from the reaction media by filtration, washing and drying [57].

$$M^+OH^- + Al_2O_3 + SiO_2 + H_2O\ (aq)$$
$$\downarrow$$
$$[\ M_a(AlO_2)_b(SiO_2)_c\ NaOH\ H_2O\ ]\ (gel)$$
$$\downarrow$$
$$[\ M_x(AlO_2)_x(SiO_2)_y\ zH_2O\ ] + solution$$
(zeolite crystals)

For the zeolite with high silica content, an excess amount of OH^- is required to dissolve the high concentration of silica, but a very high pH solution also encourages the formation of quartz instead of zeolite. Template theory was then developed for the synthesis of the high silica zeolite in order to avoid quartz formation. By adding an organic template as the structure directing agent, the zeolite containing the encapsulated organic cations inside the zeolite pores are easily

formed [57]. After calcination at evaluated temperature, the organic template decomposes and leaves H^+ as the balancing cation. The organic template is usually a quaternary ammonium ion which has halides or hydroxide as a counter ion. Several types of organic templates are regularly used in zeolite synthesis, for example, tetraethylammonium hydroxide, tetrapropylammonium hydroxide and tretapropyl ammonium bromide. One type of template can be used for several types of zeolites, while the same type of zeolites can be synthesized by using different organic templates.

2.3 Zeolite Beta

Zeolite beta was discovered a long time ago but it received more interest since it became important for some dewaxing operation. Due to the complication of zeolite beta structure, it was recently investigated for structure identification. In 1967, zeolite beta with high silica was first synthesized by Wadlinger and coworkers using tetraethylammonium hydroxide as organic template [17]. The unit cell composition of zeolite beta is:

$$Na_n [(AlO_2)_n (SiO_2)_{64-n}] \cdot zH_2O$$

2.3.1 Structure of Zeolite Beta

In 1988, Newsam and Higgins reported the determination of the framework structure [2, 58]. Zeolite beta contains a large pore system of 12-membered rings. Zeolite beta structure consists of small building units of double 6-rings connected by two of single 4-rings and four of single 5-rings. There building units connected together to form the chains along the (001) direction. The framework of zeolite beta is disordered along this direction [59]. The structure of zeolite beta consists of three polymorphs illustrated as projection sheets as shown in Figure 2.8 [1, 60]. Polymorphs A and B have closely related structures of tetragonal and monoclinic symmetries, respectively. Each system

consists of 12-membered rings connected together to form two types of channels which are straight channels along (100) plane and sinusoidal channels along (001) plane. The straight channels have an elliptical opening, while the sinusoidal channels have a circular opening of 0.56 nm. Polymorph A has the tetragonal crystal system with two different pore openings of 0.60 nm x 0.56 nm and 0.60 nm x 0.73 nm. Polymorph B has the monoclinic crystal system with two different pore openings of 0.68 nm x 0.55 nm and 0.68 nm x 0.73 nm. While a hypothetical monoclinic polymorph C was first described by Newsam and coworkers [2] in 1988 and in 2001 pure polymorph C of a type of germanosilicates analogous to zeolite beta was first synthesized by Corma and coworkers [61]. Normally, zeolite beta consists of an intergrowth hybrid of two polymorphs A and B.

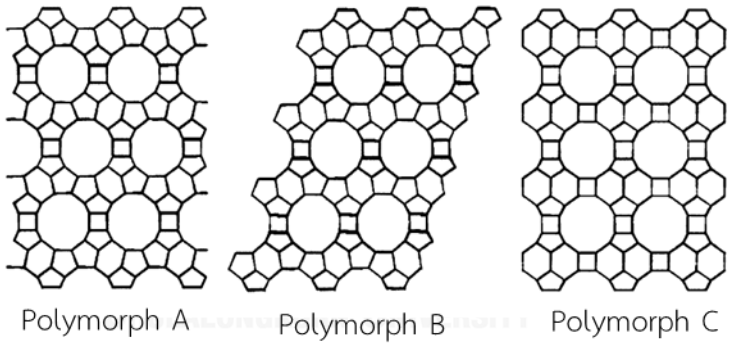

Figure 2.8 Illustration of three polymorphs of zeolite beta

2.3.2 Characterization of Zeolite Beta

2.3.2.1 X-ray Powder Diffraction (XRD)

X-ray powder diffraction is a non-destructive analytical technique used for structural identification of a crystalline material, including unit cell parameters and an interplanar spacing between lattice planes. Moreover, XRD can provide the degree of crystallinity of sample relative to a reference compound.

The X-ray region falls in the range of the electromagnetic spectrum between ultraviolet and gamma-rays. The x-ray wavelength about 0.1 nm is approximately similar to the distance between the atomic structures of interest making it suitable for structural investigation in a wide range of materials. X-rays are produced when high speed electrons collide with a metal target which is usually copper (Cu). When a high accelerating voltage is applied between tungsten filament as the cathode and Cu target as the anode, the high speed electrons are produced and then collide with the target. As a high speed electron strikes on one core electron of the target atom, the energy is transferred to the core electron and the core electron with excess energy is ejected from the atom forming a hole instead. An electron from an outer, higher-energy shell then fills the hole and reduces it extra energy by emitting X-ray with a characteristic wavelength. The energy (E) and wavelength (λ) of X-ray photon are related by the equation of $E = hc/\lambda$, where h is Planck's constant and c is the light speed.

As shown in Figure 2.9 [62], a monochromatic incident beam of X-ray on the surface of crystal at an angle θ, the scattered beam intensity can be measured as a function of diffraction angle 2θ. The peaks in XRD pattern directly depend on the interplanar d spacing of the samples. The size of unit cell of sample can be determined easily by using Braggs' law:

$$n\lambda = 2d\sin\theta$$

Where the integer n is the order of diffracted beam, λ is the X-ray wavelength, d is the interplanar spacing and 2θ is the angle between the detector position and the extrapolation of the incident beam, in other word, θ is the angle between the incident beam and the lattice plane.

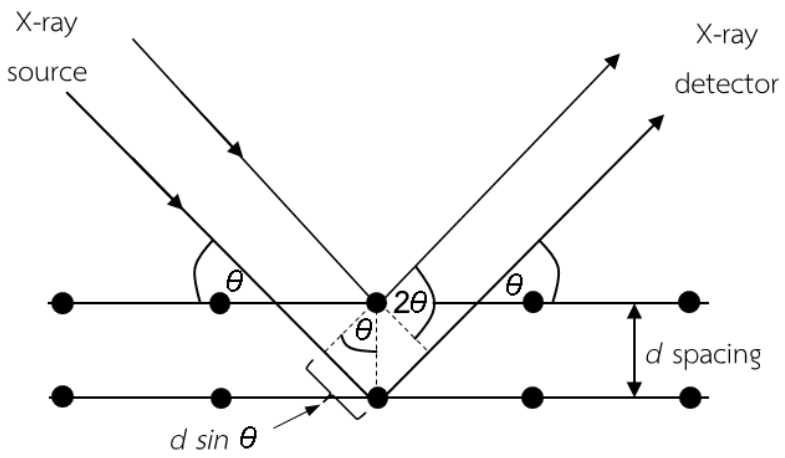

Figure 2.9 Bragg reflection from a set of crystal planes with a *d* spacing

An incident wave is directed into a material and a detector is typically moved about to record the directions and intensities of the outgoing diffracted waves. The relationship plotted between peak intensities and direction of waves or detector positions in angles of 2θ is so called an X-ray diffraction pattern or an X-ray diffractogram. The diffracted waves from different atoms of different types and positions can interfere constructively and destructively with each other resulting in different peak intensities. Therefore, the diffraction pattern obtained can reveal the distribution of atoms in the lattice planes in the material.

The X-ray powder diffraction technique is widely used for structural characterization of various crystalline materials including zeolites. The XRD data are useful for identification of framework type of zeolite base on the reference XRD database. The XRD peak intensities refer to the relative crystallinities of zeolite samples. The zeolite with higher degree of crystallinity exhibits more the XRD pattern with higher intensities than the one with lower degree of crystallinity. As other materials, the peak position can indicate the size of unit cell and the peak width can inform the crystal size. [63]. In addition, XRD pattern can be used to study the chemical formula of zeolites since it varies by the Si to Al ratios as well as ratio of

difference polymorphs. Figure 2.10 [64] presents the simulated XRD patterns of zeolite beta. As shown, the intensities of XRD peak are varied by the ratios of two polymorphs of zeolite beta.

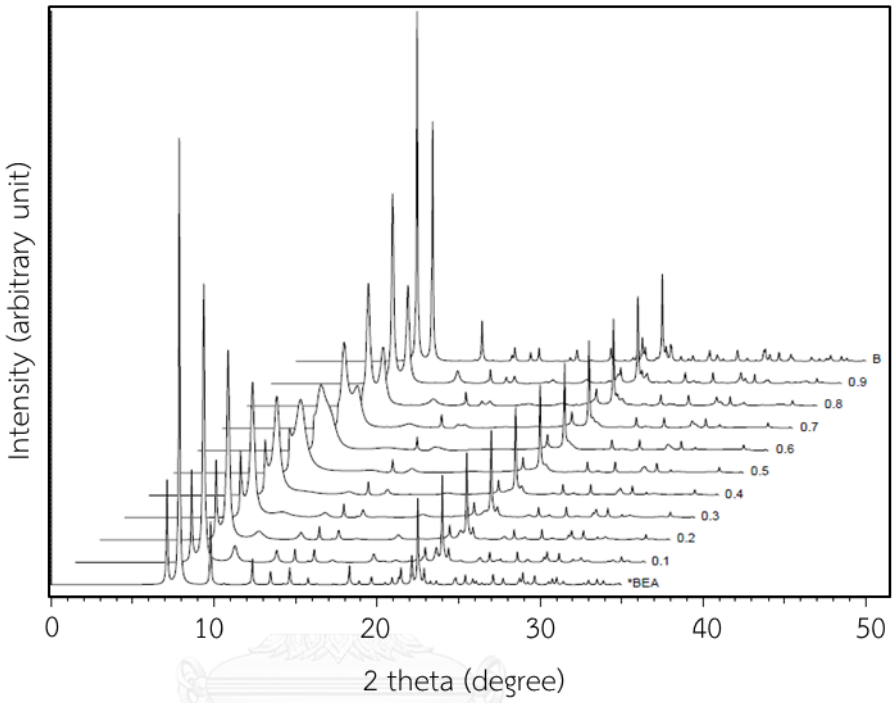

Figure 2.10 Simulated XRD patterns of zeolite beta with different ratios of two polymorphs (A and B)

2.3.2.2 Field Emission Scanning Electron Microscopy (FESEM)

High resolution field emission scanning electron microscopy (FESEM) is achieved when a field emission electron gun is used instead of the conventional thermal electron gun. When an intense electric field is applied to a needle-shaped tip of tungsten single crystal in the field emission gun, an electron beam with an extremely high current density is generated. The ultra-high vacuum (10^{-10} Torr) is required for this field emission gun. Due to the extremely small emission source of electrons and the greater number of electrons emitted per unit area as well as the

much narrower range of emitted electron energies than those obtained from the thermal emission guns, higher resolution at high magnification power can be achieved [65]. Similar to the conventional scanning electron microscope, an electron beam is used for producing a variety of signals at the surface of solid specimens from interactions between electrons and sample atoms. The final image is built up from the number of electrons emitted from each spot on the sample. The FESEM image shows very detailed three-dimensional black and white images revealed valuable information about textural morphology, crystal size, purity, homogeneity as well as orientation of materials.

For characterization of zeolites and non-conductive samples, a conductive coating on the sample specimen with a very thin layer of gold by a sputter coater is required [66]. Not only crystal shape and size, an amorphous phase which cannot be detected by XRD, can also be easily distinguished by using FESEM. Figure 2.11 presents the FESEM images of SBA-15 [67] and zeolite beta [24].

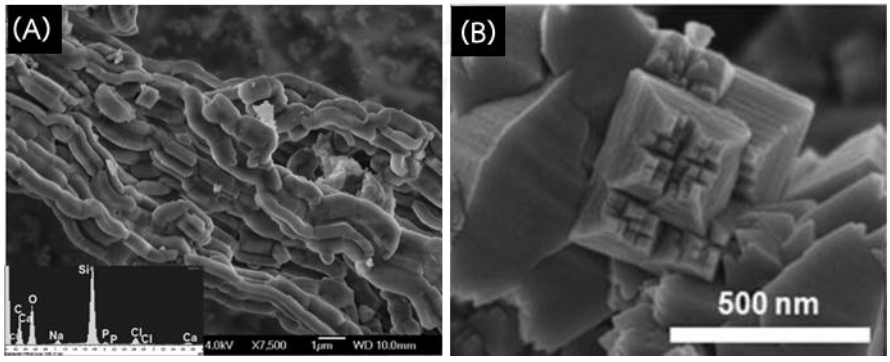

Figure 2.11 Field emission scanning electron micrographs of (A) SBA-15 and (B) zeolite beta

2.3.2.3 Nitrogen Adsorption-Desorption Technique

According to International Union of Pure and Applied Chemistry (IUPAC) definition of pore sizes, porous solid materials are classified into 3 types as shown in Table 2.1. In the adsorption process, a so-called adsorbent is the solid of which the surface is to adsorb a so-called adsorbate which is the gas adsorbed on the surface. The nitrogen adsorption is classified as the physical adsorption or physisorption because the attraction force between the nitrogen molecules and the surface of solid material is van der Waals force. The force of attraction in physisorption is very weak; therefore, molecules adsorbed by this type of adsorption can be easily desorbed by heating or decreasing the pressure.

Table 2.1 IUPAC classification of pores according to the pore width

Type	Pore width
Micrpores	< 2 nm
Mesopores	2-50 nm
Macropores	> 50 nm

The nitrogen adsorption-desorption technique can be used for determination of the adsorption-desorption behavior of microporous and mesoporous materials. Adsorption behaviors of materials are described by an adsorption isotherm, a plot between the amounts of adsorbed gas on the surface of adsorbent as a function of relative pressure at a constant temperature and so does a desorption isotherm. Many different types of adsorption isotherms have been observed depending on the type of adsorbate, the type of adsorbents and intermolecular interaction between the gas and the surface. The adsorption isotherms has been classified by IUPAC into the into six types as illustrated in Figure 2.12 [68]. The isotherm

of Type I is typical behavior of microporous materials (pore sizes <2 nm) such as zeolites. The micropore filling takes place only at very low relative pressure with reaching the saturation very fast. The isotherm of Type II where adsorption occurs at the region of very high relative pressure is assigned to porous materials with high external surface area. The isotherm of type III is observed for the macroporous (pore sizes >50 nm) or non-porous materials, only a small adsorption capacity can be observed. Type IV and V isotherms are typical for mesoporous materials (pore sizes = 2-50 nm). Type IV is the adsorption behavior of a mesoporous system containing micropores while Type V does not present any micropores. The reverse plots of the adsorption isotherms represent desorption isotherms backward to low relative pressure. The hysteresis loop usually observed in mesopores is due to the bottle neck effect referring to much different sizes of pores. However, some reports showed the observation of the hysteresis loop in the micropore materials. Type VI shows multilayer adsorption [69].

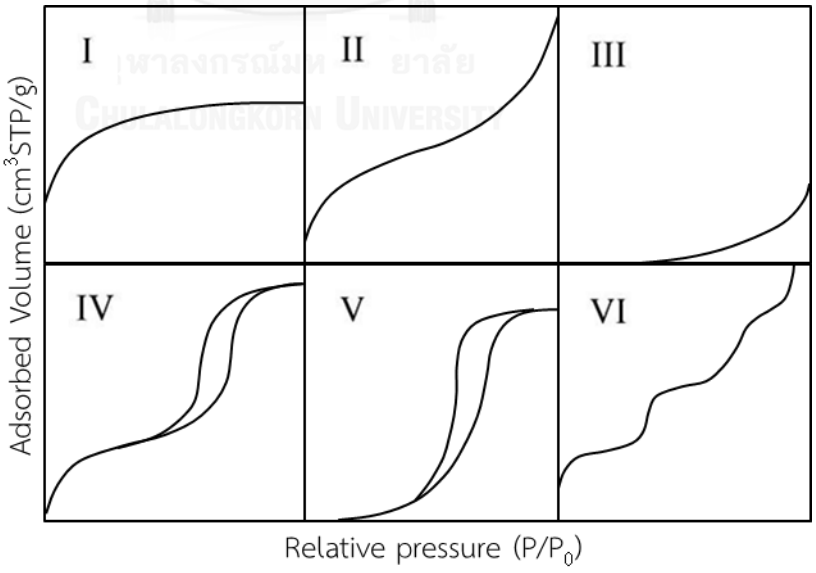

Figure 2.12 The IUPAC classification of six types of adsorption isotherms

A lot of theoretical models are applied to the data obtained from nitrogen adsorption isotherms allowing the study of textural properties of materials including microporous materials like zeolites. One of the most useful models is the BET model proposed by Brunauer, Emmett and Teller, and very useful for the measurement of the specific surface area of all types of porous materials [70]. The BET model was assumed on multilayer adsorption which is different from Langmuir monolayer adsorption. The BET specific surface area can be obtained from the measurement of adsorption isotherm which is carried out at the temperature of liquid nitrogen, -196 °C or 77 K. The data of adsorption isotherms are then treated by the BET equation:

$$\frac{P}{V(P_o - P)} = \frac{1}{V_m C} + \frac{C-1}{V_m C}\left(\frac{P}{P_0}\right)$$

where P and P_0 are the equilibrium and atmospheric pressure of adsorbed gas at the adsorption temperature, V is the volume of adsorbed gas, V_m is the volume of monolayer adsorbed gas, and C is the BET constant. A plot of $P/V(P_0-P)$ versus P/P_0 gives a straight or nearly straight line with the slope $(C-1)/V_mC$ and the intercept $(1/V_mC)$. If the monolayer adsorbed gas volume (V_m) is known, the surface area can be calculated using the equation below, where S_{total} is total surface area, N is Avogadro's number and σ is the gas cross section which is 0.162 nm^2 for the molecule of nitrogen gas.

$$S_{total} = \frac{V_m N \sigma}{M}$$

Pore size distribution can be measured by using various methods. The Barrett, Joyner and Halenda-plot, BJH-plot, is employed to determine pore size distributions from experimental isotherm which is modified from the BET plot. It can be applied only to mesopores such as SBA-15, MCM-41, silica gel, etc. HJ plot or t plot is a procedure for calculating the external surface area and the micropore volume of microporous materials. This method is accurate for pore sizes in the range of 0.7 to 1.2 nm. MP plot is a modified t-plot method. It is used for determination of pore size distribution of both mesoporous and microporous materials.

2.3.2.4 ^{27}Al-MAS-NMR Spectroscopy

The ^{27}Al-MAS-NMR technique is used for characterization of the coordination site of aluminium atoms which is tetrahedral for framework sites and octahedral for non-framework sites of zeolites. By applying the magic angle spinning technique, the higher magnetic fields of superconducting magnets is obtained resulting in the high-resolution spectra. The presence of aluminium in the zeolite framework generates a negative charge which can be balanced by protons producing bridging ≡Si-OH-Al≡ hydroxyl groups, which are Brønsted acid sites. Therefore, the structural investigation of aluminium sites of zeolite implies the acid property of zeolite which is really important for industrial catalytic applications. Two types of aluminium atoms in zeolite framework can be distinguished by the chemical shift in ^{27}Al-MAS-NMR spectra. A peak at the chemical shift approximately 50 ppm corresponds to tetrahedrally coordinated aluminium or aluminium in the framework site while the octahedrally coordinated aluminium in zeolite framework presents the NMR peak at or near 0 ppm. However, the ^{27}Al-MAS-NMR is reliable only for the qualitative analysis. The other technique, ICP-MS is required to find out the total number of aluminium atoms in zeolite framework.

2.3.2.5 Inductively Coupled Plasma-Mass Spectroscopy

Inductively coupled plasma-mass spectroscopy (ICP-MS) is multi-elemental analytical technique with very low detection limits in the range of part per billion to part per trillion levels. ICP-MS combines a high-temperature ICP source with a mass spectrometer. Figure 2.13 demonstrates an ICP source in ICP-MS. Inside the concentric channels of the ICP torch, argon gas is flowed. When the spark is applied to the argon flowing through the ICP torch, electrons are stripped off from the argon atom, producing argon ions. These ions are caught in the oscillating fields and collide with other atoms, generating plasma [71].

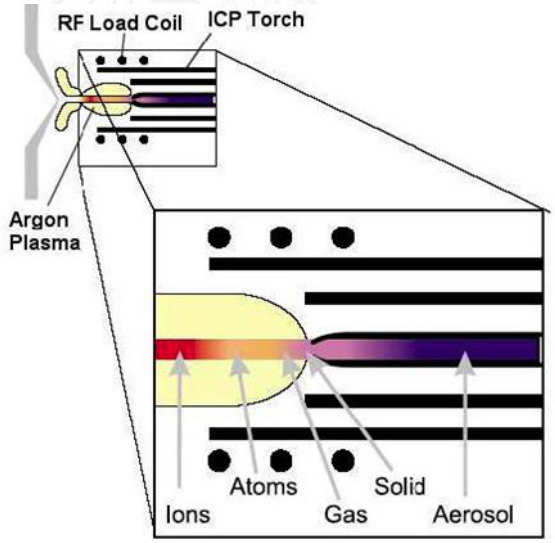

Figure 2.13 The ICP Torch showing the states of the sample [71]

The sample to be analyzed is introduced via a nebulizer into the ICP plasma as aerosol. After the aerosol sample enters the center of ICP torch, it evaporates and the elements in the aerosol are broken down into gaseous atoms prior to ionization towards the end of the plasma. The singly-charged ions from the plasma are extracted through a series of cones into a quadrupole mass spectrometer. These ions are separated by its mass-to-charge ratio using quadrupole mass filter which only allows ions of a single mass-to-charge ratio pass the rods to the detector at a given time. The main processes of ICP-MS are shown in Figure 2.14.

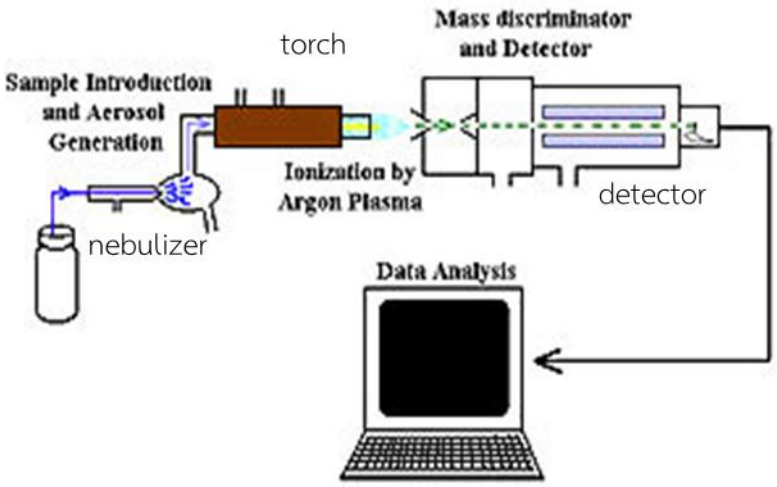

Figure 2.14 The main processes of ICP-MS [71]

2.4 Acetalization of Alcohols to Form Acetals

Acetalization is the chemical reaction for the synthesis of acetal, which is an organic compound having two separate oxygen atoms singly bonded to the same carbon atom. Acetal has the chemical structure of $R^1R^2C(OR^3)_2$, where both R^1 group is either alkyl or aryl or hydrogen, R^2 and R^3 groups are either alkyl or aryl groups. Ketal is a subclass of acetal compounds derived from the addition of alcohol to ketone where neither R group is a hydrogen atom. Acetal is usually prepared by an acid-catalyzed dehydration reaction of ketone or aldehyde with alcohol as shown in Scheme 2.1. The organic carbonyl compound and hemiacetal are in equilibrium. The further reaction between alcohol and hemiacetal takes place to form acetal which is stable at room temperature. Formation of acetal occurs after heating with acid and an excess amount of alcohol. The hydroxyl group of hemiacetal is protonated and then dehydration takes place to form the carbocation. Alcohol rapidly attacks the carbocation leading to the deprotonation giving the acetal [72].

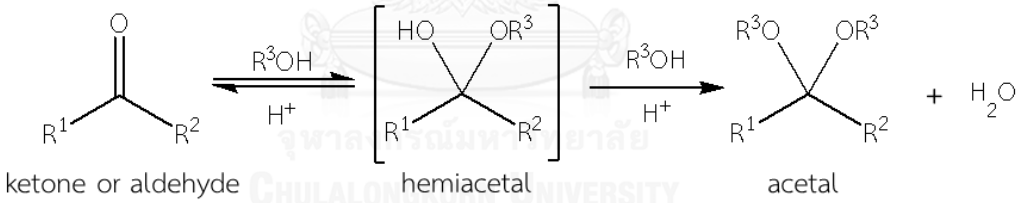

Scheme 2.1 Typical acetalization of alcohol with ketone or aldehyde

Two pathways were proposed for the formation of hemiacetal, one is the neutral pathway and the other is the acid-catalyzed pathway [73]. The neutral pathway requires only two steps as shown in Scheme 2.2 (A). First, a [1,2]-addition of alcohol to aldehyde or ketone takes place. Secondly, the proton transfer produced a tetrahedral compound. Similar to all types of [1,2]-additions to carbonyls with neutral or weak nucleophiles, the presence of an acid lead to the faster rate of reaction. Scheme 2.2 (B) presents the acid-catalyzed pathway to form the hemiacetal.

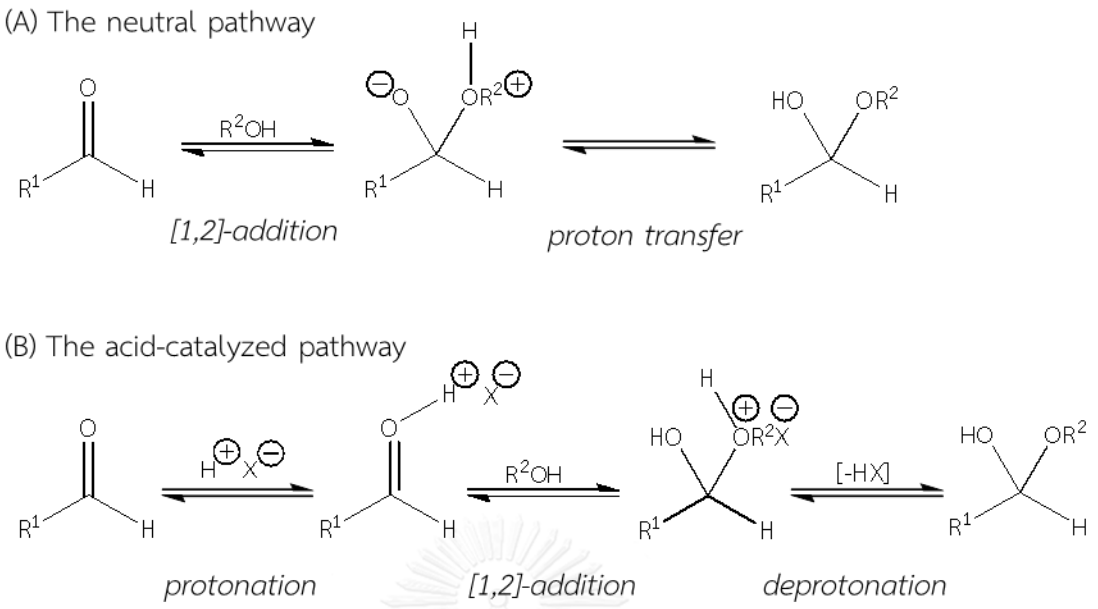

Scheme 2.2 Two pathways of hemiacetal formation [73]

In order to achieve the full acetal, acid treatment is required to forward the further reaction. Scheme 2.3 demonstrates six steps of acetal formation. Similar to the formation of hemiacetal, protonation of carbonyl group takes place followed by [1,2]-addition to obtain hemiacetal. The hydroxyl group as a poor leaving group of hemiacetal is protonated and transformed into water which is an excellent leaving group. Due to the high magnitude of increase in leaving group ability, oxygen lone pair is allowed to expel water from carbonyl carbon via [1,2]-elimination reaction. The oxonium ion which is really active is formed. The oxygen of oxonium has positive charge indicating that C=O bond is weaker than those in neutral form. The highly electrophilic carbon rapidly combines with alcohol, even a weaker nucleophile, resulting in [1,2]-addition. The final step is deprotonation to form neutral acetal. All steps are reversible. Thus, to drive the reaction forward, the reaction has to be carried out using acid catalyst [73].

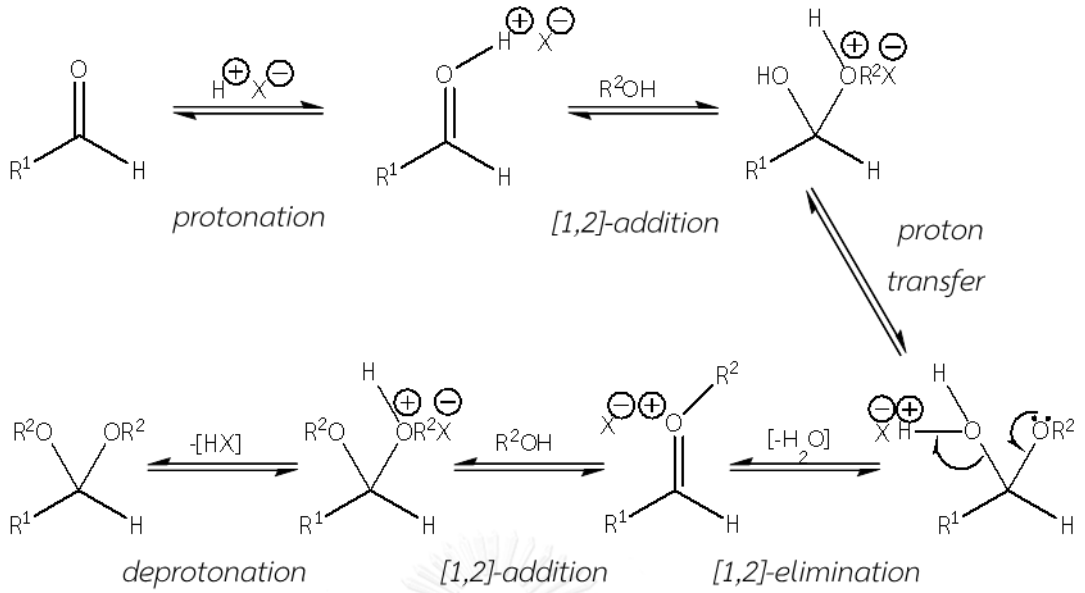

Scheme 2.3 Pathway of acetal formation [73]

The reaction pathways shown above can be applied to the acetalization of glycerol to solketal. The mechanism shown in Scheme 2.4 was proposed for the acid-catalyzed acetalization of glycerol with acetone. In the first step, the carbonyl group of acetone is protonated by an acid. In the second step, hydroxyl group of glycerol attacks the activated carbonyl group of acetone, followed by proton transfer to form hemiacetal intermediate. This intermediate undergoes cyclization via the following steps. The forth step is water elimination. Nucleophilic attack of terminal hydroxyl group on the tertiary carbon atom takes place followed by deprotonation by acetone to form either solketal (five-membered ring acetal) or six-membered ring acetal [72, 73].

1. Protonation of the carbonyl

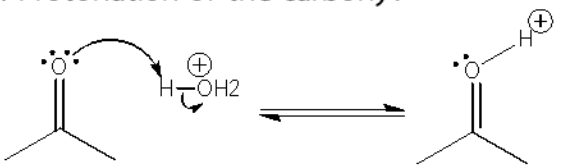

2. Nucleophilic attack by the hydroxyl group of glycerol

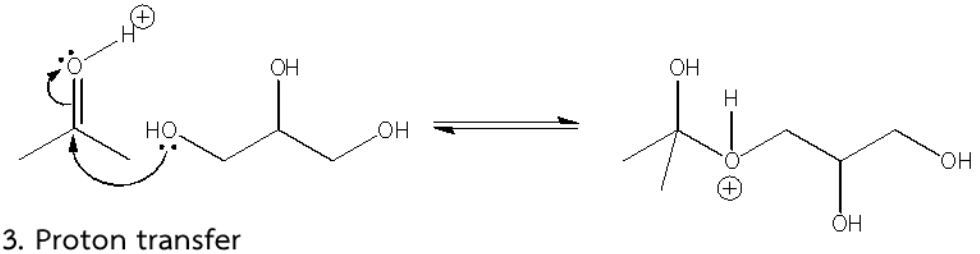

3. Proton transfer

4. Water elimination

5. Nucleophilic attack by glycerol and deprotonation

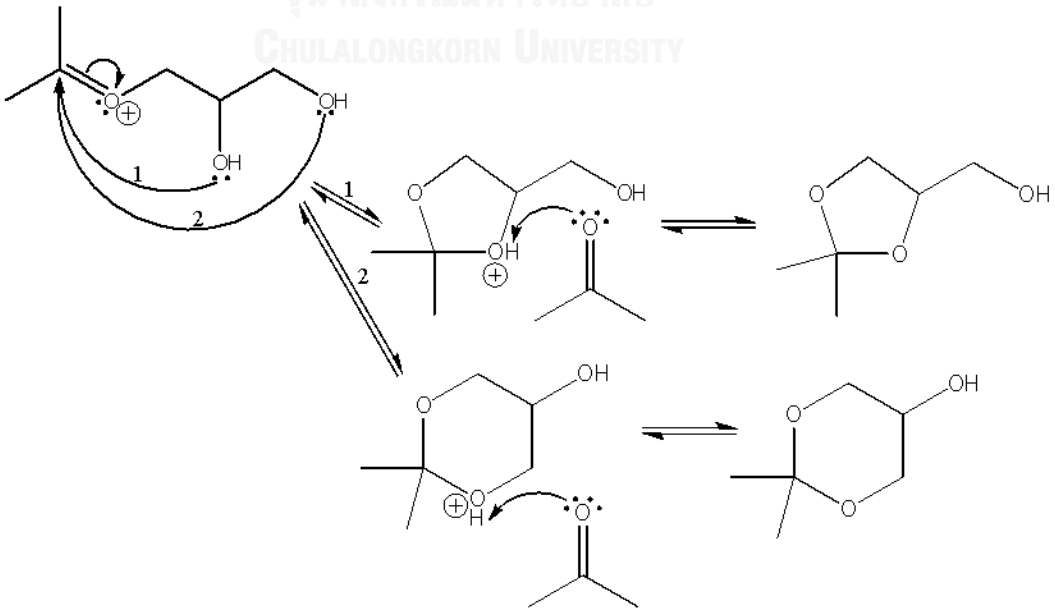

Scheme 2.4 Acid-catalyzed acetalization of glycerol with acetone [72, 73]

CHAPTER III

EXPERIMENTS

3.1 Instruments and Apparatus

Ultrasonicator

To make uniform gel, the ultrasonic probe of a ultrasonicator (SONICS, VC 505) was equipped with a power supply (net power output: 500 Watts, frequency 20 kHz), sealed converter (piezoelectric lead zirconate titanate crystals) and a titanium alloy probe (13-mm-diameter tip). The starting mixture was subjected to ultrasound irradiation with the amplitude of 40%

Ovens and Furnaces

The crystallization of SBA-15 and zeolite samples was carried out in a Memmert UM-500 oven at a required temperature. The calcination of solid samples was achieved in a Lenton AWF furnace with programmable heating rate of 1 °C/min.

X-ray Powder Diffractrometer (XRD)

All XRD patterns were collected for phase and structural analysis using a Rigaku, Dmax 2200/utima+ X-ray powder diffractrometer with a monochromater and Cu K_{α} radiation (40 kV 30 mA). For the analysis of SBA-15 phase, 2-theta was ranged from 0.7 to 5.0 degrees with a scan speed of 2 degrees/min and a scan step of 0.02 degree. The scattering, the divergent and the receiving slits were fixed at 0.05 degree, 0.5 degree and 0.15 mm, respectively, for SBA-15. For the investigation of zeolite beta samples and crystalline nanoseeds 2-theta was in the range of 5.0 to 40.0 degrees with scan speed of 5 degrees/min and a scan step of 0.02 degree. The scattering, the divergent and the receiving slits were fixed at 0.5 degree, 0.5 degree and 0.3 mm for crystalline nanoseeds and zeolite beta catalysts. The measured diffractograms were analyzed by Jade 6.0 software purchased from material database Incorporation (MDI).

Scanning Electron Microscope (SEM) and Field Emission Scanning Electron Microscope (FESEM)

JEOL, JSM-5410LV and JSM-7610F FESEM were used for investigation of morphology and particle size of SBA-15, crystalline nanoseeds and zeolite beta catalysts. The samples were sprinkled over double sided carbon sticky tape mounted on sample holders before coated with sputtering gold under vacuum prior to the FESEM measurements.

^{27}Al-MAS-NMR Spectrometer

Solid state ^{27}Al-MAS-NMR spectra were obtained using a Bruker Advance, DPX 300 MHz NMR spectrometer at 20 ℃. All of spectra were recorded at a frequency of 78 MHz. The spectral parameters were set as follows: scan number of 800, relaxation delay of 4 seconds, spin rate of 5 kHz and spectral size 4 K with 2 K time domain size.

ICP-MS Spectrometer

A Thermo Scientific, iCAP Qc inductively coupled plasma equipped with a mass spectrometer was used for analyzing aluminium content in the zeolite samples.

Nitrogen Adsorptometer

The porosity of samples in term of nitrogen adsorption-desorption isotherms were performed in a BELSORP, mini-II nitrogen adsorptometer. The samples were pretreated at 400 ℃ for 3 hours just prior to analysis. Specific surface areas were calculated by BET equation. The t-plot method was used to analyze micropore volume and external surface area. The micropore size distribution was figured out by MP-plot method while the mesopore size distribution was obtained by the BJH-plot method.

Gas Chromatograph

A Varian CP-3800 gas chromatograph equipped with a flame ionization detector (FID) and a 30 m length x 0.32 mm CP-WAX-52CB capillary column was used to analyze liquid samples. The heating program used for 0.2 µL liquid sample analysis is shown in Scheme 3.1.

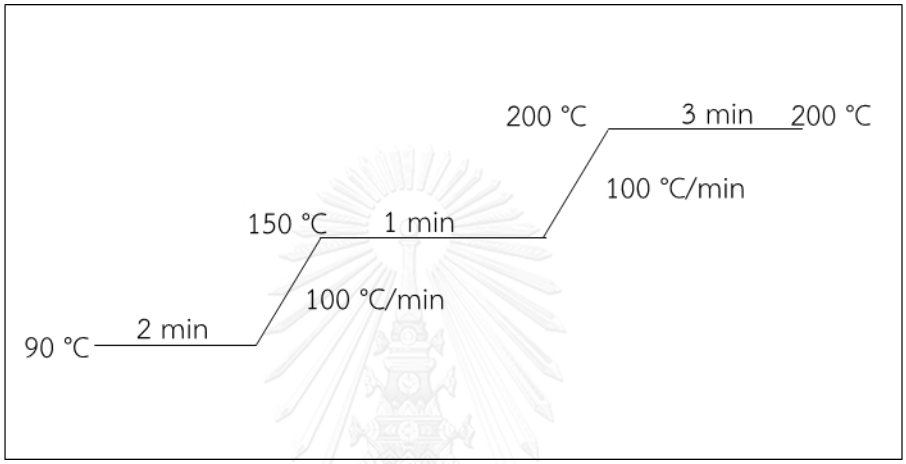

Scheme 3.1 The GC heating program for analysis of products from acetalization of glycerol with acetone

3.2 Chemicals and Gases

1. Pluronic® P123, PEO_{20}-PPO_{70}-PEO_{20}, average molecular weight = 5800 (Aldrich)
2. Hydrochloric acid, HCl (Merck, 37 wt%)
3. Tetraethylorthosilicate, TEOS (Fluka, 98 wt%)
4. Tetraethylammonium hydroxide, TEAOH (Fluka, 40 wt%)
5. Aluminium isopropoxide, AIP (Merck, 98 wt%)
6. Sodium aluminate, $NaAlO_2$ (Riedel-deHaën, 46 wt% of Al_2O_3)
7. Sodium hydroxide, NaOH (Merck, 99 wt%)

8. Fumed silica, SiO_2, powder, 0.007 μm (Aldrich)
9. Ammonium nitrate, NH_4NO_3 (Fluka, 99 wt%)
10. Anhydrous glycerol, $C_3H_8O_3$ (Fisher, 99.95 wt%)
11. Acetone, C_3H_6O (Merck, highly pure grade)
12. Dimethylformamide, DMF (ACI Labscan, 99.8 wt%)
13. Solketal, $C_6H_{12}O_3$ (Aldrich, 98 wt%)
14. Toluene, C_7H_8 (Carlo erba, 99.5 wt%)
15. Hydrofluoric acid, HF (Merck, 48 wt%)
16. Nitric acid, HNO_3 (Merck, 65 wt%)
17. Aluminium standard solution, Al (Fluka, 1000 mg/L))
18. Liquid nitrogen, N_2 (Linde, highly pure grade)
19. Nitrogen gas, N_2 (Thai Industrial Gases, TIG, highly pure grade)

3.3 Preparation of SBA-15

SBA-15, a silica source in the synthesis of crystalline nanoseeds was prepared according to the method reported by Zhao and coworkers [74]. A starting solution was prepared in acid media using triblock copolymer Pluronic® P123 as a structure directing agent. First, Pluronic® P123 template was dissolved in the presence of deionized water and 2M HCl. TEOS was added under nitrogen atmosphere. The mixture was stirred at room temperature for an hour and then aged at 40 ℃ for 48 hours. The resulting gel was transferred into a Teflon-lined autoclave, tightly capped and crystallized at 100 ℃ for 48 hours. After crystallization, the capped Teflon-lined autoclave was quenched with running tap water to room temperature. The product was separated by filtration, washed several times with deionized water and dried overnight at 100 ℃. The resulted as-synthesized SBA-15 was calcined at 550 ℃ for 5 hours to remove the structure directing agent from pores. The white powder of calcined SBA-15 was characterized for its structure and pore properties by using XRD, SEM, and nitrogen adsorption techniques. The

schematic diagram of the preparation procedure for SBA-15 is shown in Scheme 3.2. The heating program for template removal from SBA-15 is shown in Scheme 3.3. The calcined product was kept in desiccator prior to use.

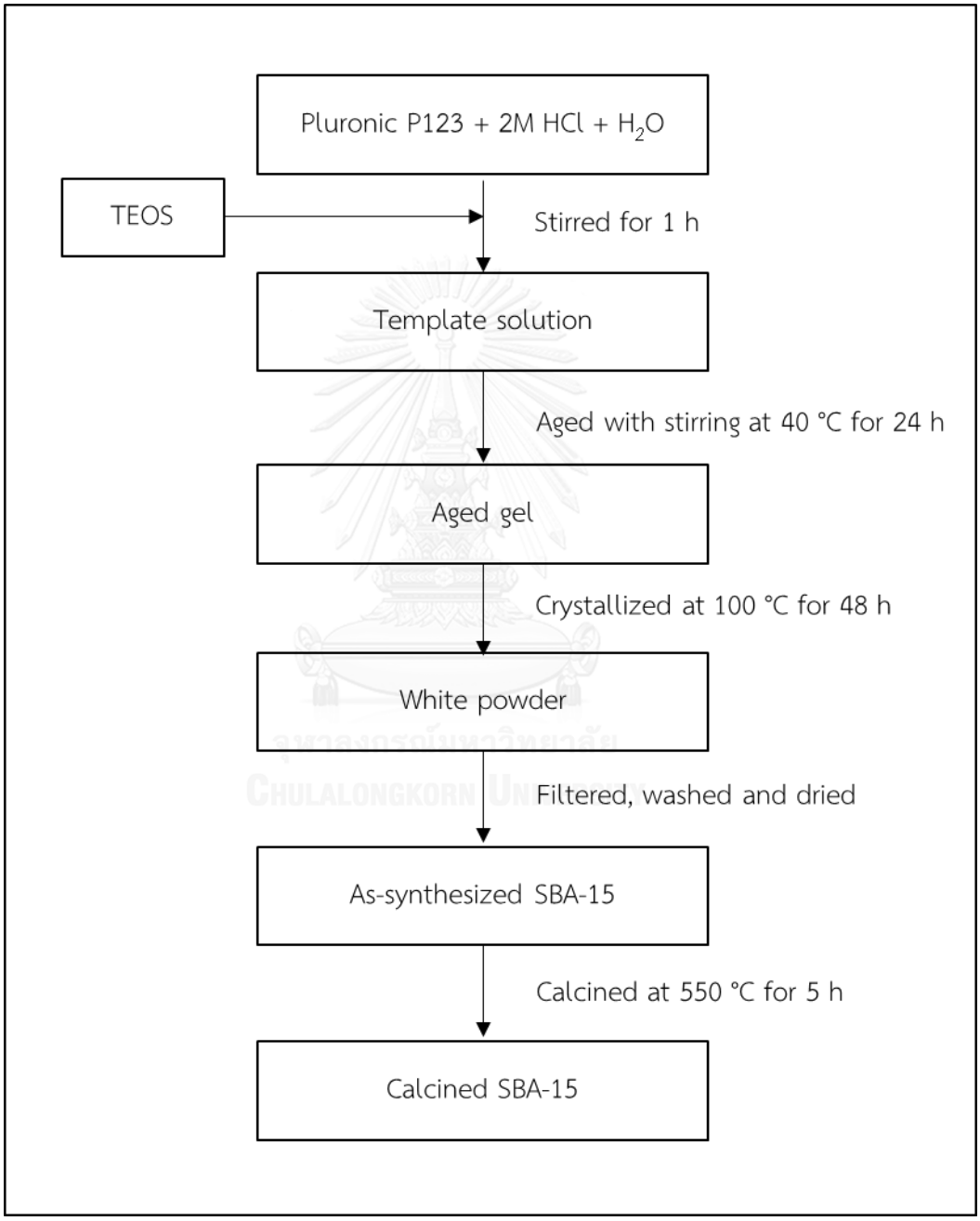

Scheme 3.2 The preparation of SBA-15 procedure

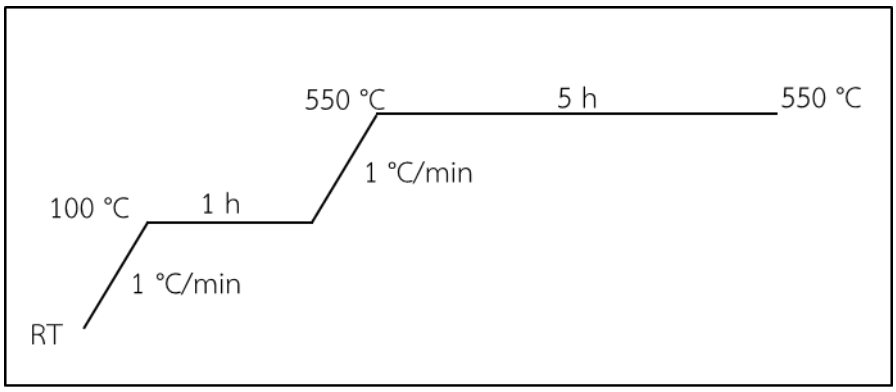

Scheme 3.3 A heating program for removal of organic template from SBA-15 and crystalline nanoseed pores

3.4 Preparation of Crystalline Nanoseeds

Crystalline nanoseeds were prepared from calcined SBA-15 by wetness impregnation with an organic template solution of TEAOH [75]. First, an amount of 63.8 g of 40 wt% TEAOH solution was mixed with a 1.4751 g of AIP and added dropwise into 26.00 g of calcined SBA-15 which was placed in a 4-necked round bottom flask and agitated with a propeller stirrer during mixing. The mixture of reactant sources with the mole ratio of SiO_2:0.008Al_2O_3:0.4TEAOH:7.5H_2O was aged at room temperature for 12 hours, and then transferred into a stainless-steel autoclave containing a Teflon cup. The gel mixture of crystalline nanoseeds was subjected to ultrasound irradiation with 40% amplitude for 10 minutes in order to mix thoroughly. The autoclave was capped tightly and place in an oven at 135 °C. After crystallization for 48 hours, the capped autoclave was quenched with running water to stop the crystallization. A white solid sample was separated by centrifugation, washed with deionized water for several times and dried in an oven at 110 °C. Crystalline nanoseeds obtained were calcined at 550 °C for 5 hours to remove organic template from pores. The as-synthesized and calcined crystalline nanoseeds were characterized for its structure and properties by using XRD, SEM, and nitrogen adsorption instruments. The schematic diagram of this preparation procedure is

shown in Scheme 3.4. The heating program in Scheme 3.3 was also used for template removal from crystalline nanoseeds. The calcined crystalline nanoseeds achieved were used as structure directing agent for the synthesis of zeolite beta catalyst, prior to use sample was kept in desiccator.

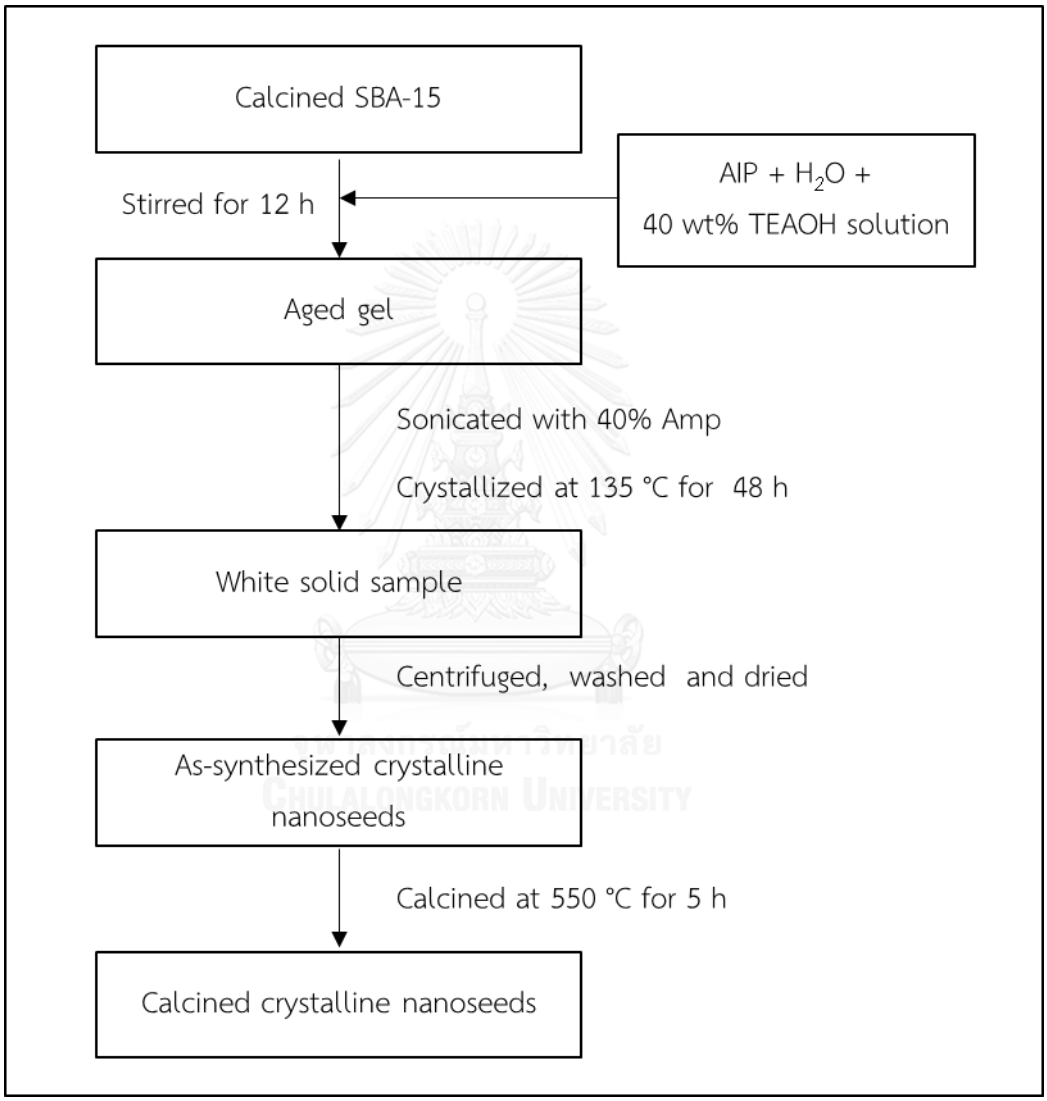

Scheme 3.4 The synthesis of crystalline nanoseeds

3.5 Synthesis of Zeolite Beta Catalyst

3.5.1 Effect of Crystallization Temperature

A catalyst was synthesized hydrothermally via the seed-assisted method [21]. An amount of 0.84 g of sodium aluminate was dissolved in a small amount of deionized water and then mixed with a solution of 10 wt% sodium hydroxide. The clear solution was added dropwise on 8.31 g of fumed silica which was previously dried overnight at 200 °C. Then the mixture was stirred thoroughly to form uniform gel with mole composition of SiO_2:0.027Al_2O_3:0.36Na_2O:35.09H_2O. An amount of calcined crystalline nanoseeds was mixed well with the gel at the weight ratio of 0.17:100. The resulted mixture was transferred into an autoclave which was capped tightly and then placed in and oven at a required temperature in the range of 120-150 °C for 5 days. The capped autoclave was quenched by running tap water. Then the white solid sample was separated by filtration, washed several times with deionized water and dried in an oven at 100 °C overnight. The products were kept in a desiccator prior to use. The schematic diagram of zeolite beta synthesis at various temperatures is presented in Scheme 3.5. The code of each sample was used as assigned in Table 3.1. The samples were characterized for structure and morphology by using XRD, FESEM, nitrogen adsorption-desorption and ^{27}Al-MAS-NMR instruments.

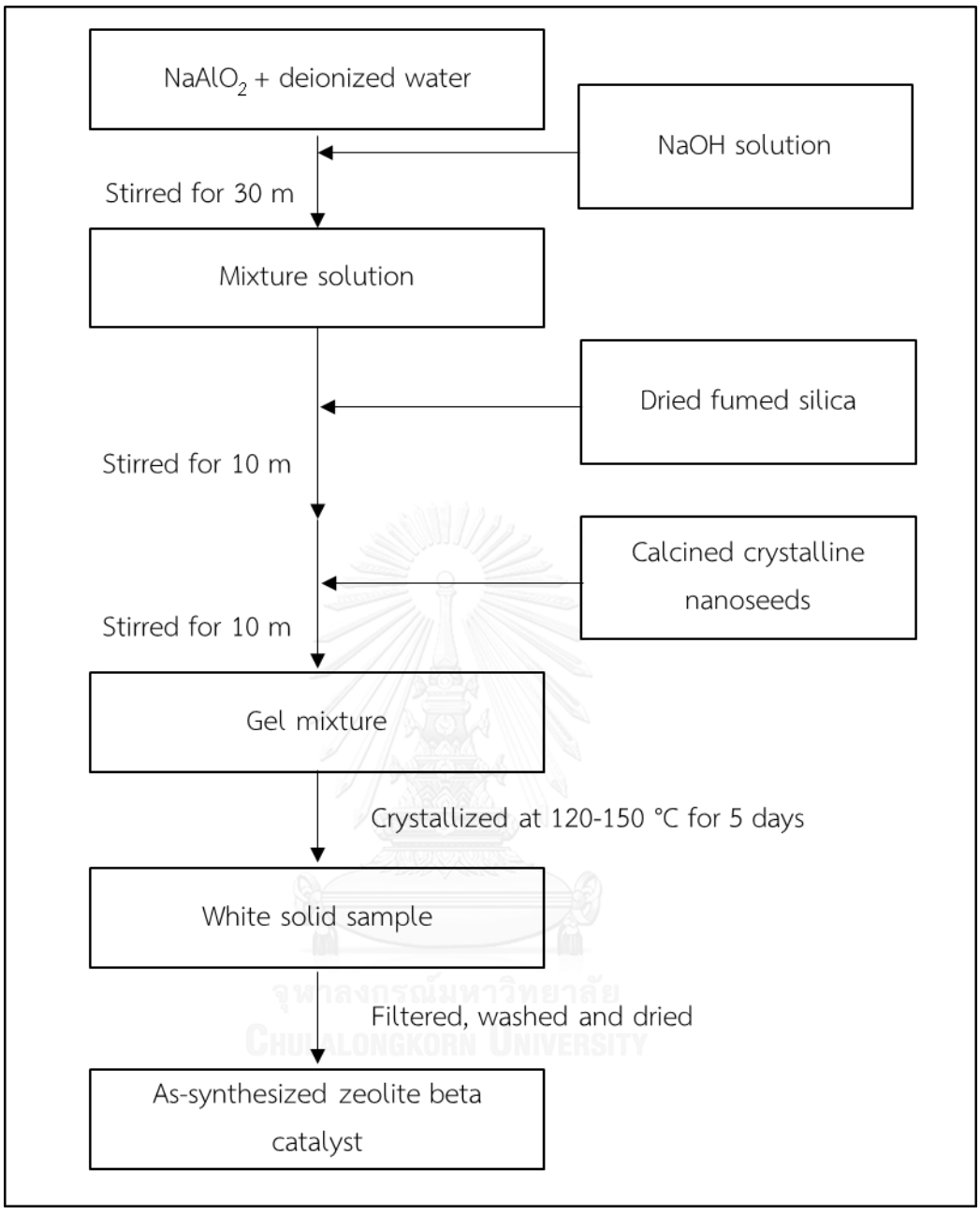

Scheme 3.5 The synthesis of zeolite beta via the seed-assisted method by varying temperatures

Table 3.1 The conditions for zeolite beta crystallized for various crystallization temperatures

Sample code	Seed amounts (wt% to the starting gel)	Crystallization temperature (°C)	Crystallization period (day)
BEA-0.17%s-120℃-5d	0.17 wt%	120 ℃	5
BEA-0.17%s-130℃-5d	0.17 wt%	130 ℃	5
BEA-0.17%s-135℃-5d	0.17 wt%	135 ℃	5
BEA-0.17%s-140℃-5d	0.17 wt%	140 ℃	5
BEA-0.17%s-150℃-5d	0.17 wt%	150 ℃	5

3.5.2 Effect of Crystallization Time

Zeolite beta samples were prepared using a series of starting gel with the same composition and similar procedure as reported in Section 3.5.1 but the crystallized temperature was fixed at 130 ℃ and the crystallization periods were varied from 1-6 days. The sample codes are explained in Table 3.2. The products were characterized by using XRD, FESEM and nitrogen adsorption-desorption instruments.

Table 3.2 The conditions for zeolite beta crystallized for various crystallization periods

Sample code	Seed amounts (wt% to the starting gel)	Crystallization temperature (°C)	Crystallization period (day)
BEA-0.17%s-130℃-1d	0.17 wt%	130 ℃	1
BEA-0.17%s-130℃-2d	0.17 wt%	130 ℃	2
BEA-0.17%s-130℃-3d	0.17 wt%	130 ℃	3
BEA-0.17%s-130℃-4d	0.17 wt%	130 ℃	4
BEA-0.17%s-130℃-5d	0.17 wt%	130 ℃	5
BEA-0.17%s-130℃-6d	0.17 wt%	130 ℃	6

3.5.3 Effect of Crystalline Nanoseed Amounts

In order to study the effect of crystalline nanoseed amounts on the formation of zeolite beta, a series of starting gel with the same composition as described in Section 3.5.1 were crystallized at 130 °C in the presence of crystalline nanoseed amounts varied from 0.17-1.00 wt%. The sample codes are demonstrated in Table 3.3. The products were characterized by using XRD, FESEM, nitrogen adsorption-desorption, ^{27}Al-MAS-NMR and ICP-MS techniques.

Table 3.3 The conditions for zeolite beta synthesis in the presence of various crystalline nanoseed amounts

Sample code	Seed amounts (wt% to the starting gel)	Crystallization temperature (°C)	Crystallization period, X (day)
BEA-0.17%s-130℃-Xd	0.17 wt%	130 ℃	1 to 5
BEA-0.33%s-130℃-Xd	0.33 wt%	130 ℃	1 to 5
BEA-0.50%s-130℃-Xd	0.50 wt%	130 ℃	1 to 5
BEA-0.66%s-130℃-Xd	0.66 wt%	130 ℃	1 to 5
BEA-0.83%s-130℃-Xd	0.83 wt%	130 ℃	1 to 5
BEA-1.00%s-130℃-Xd	1.00 wt%	130 ℃	1 to 5

3.6 Activation of Zeolite Beta Catalyst

To make zeolite beta active as acid catalyst, sodium ions of the zeolite prepared by crystalline nanoseed-assisted method must be exchanged by ammonium ions and subsequently converted to proton (H^+) by calcination at elevated temperature [76]. An amount of 2.0 g amount of as-synthesized sample of zeolite beta catalyst was mixed with 40 mL of 0.5M ammonium nitrate solution under reflux at boiling temperature overnight. The ammonium ion exchanged zeolite was separated by filtration and washed with deionized water until no nitrate ions detected in the filtrate. If nitrate ions still remained, a brown ring at the liquid

interface must be found according to brown ring test. The ammonium ion exchange was repeated twice more in order to reach the highest degree of exchange. The sample was air dried for 6 hours, dried in an oven at 100 ℃ overnight and subsequently calcined in a muffle furnace at 500 ℃ for 5 hours to obtain zeolite beta in H^+ form (H^+-BEA). The activation process for zeolite beta samples is shown in Scheme 3.6.

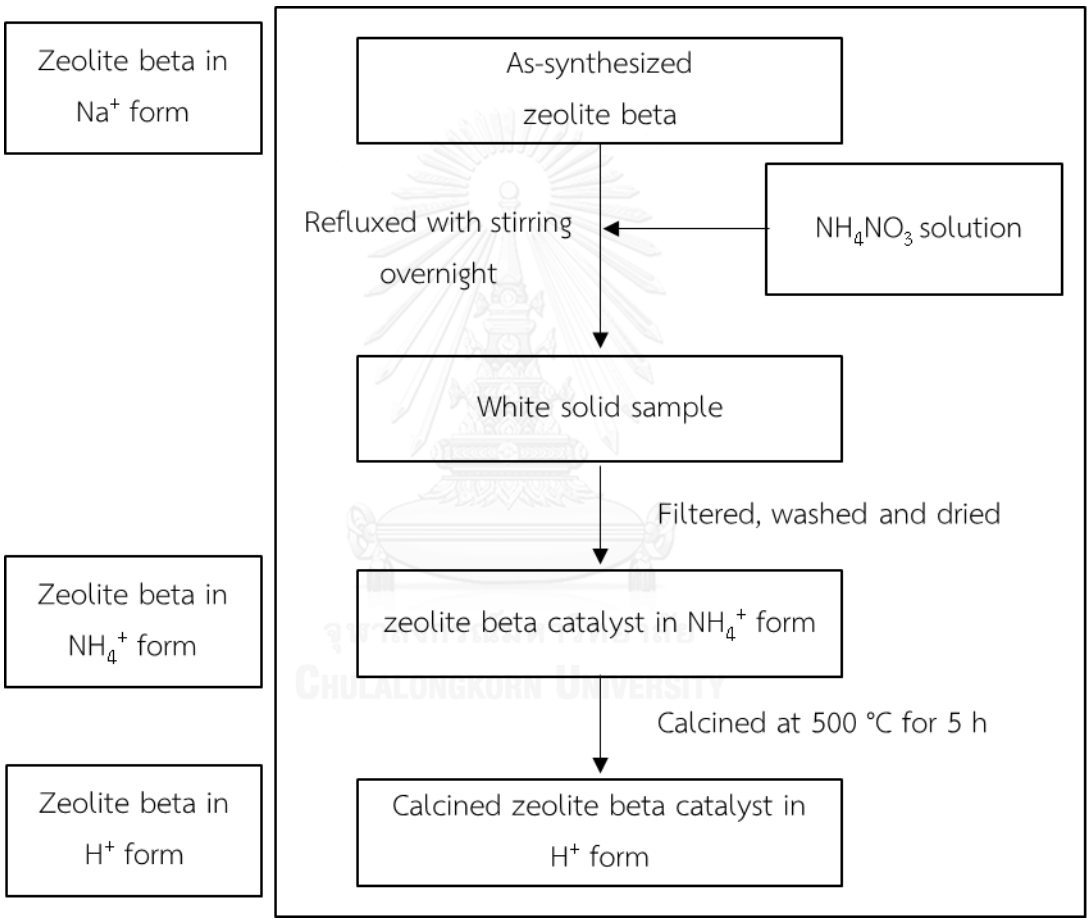

Scheme 3.6 Procedure for activation of zeolite beta via ammonium ion exchange

3.7 Elemental Analysis

The determination of Si to Al mole ratio was performed using ICP-MS. The fluoride treatment was needed to get rid of silica from the zeolite sample. A 0.0500 g of zeolite beta sample was soaked with 10 mL of 6M HCl in a TEFLON beaker. An amount of 10 mL 48% hydrofluoric acid was added dropwise to the mixture. The sample was heated but not boiled until the solution was dried on a hot plate. The fluoride treatment was repeated twice more in order to make sure that all of silica atoms were removed as volatile SiF_4 species. To digest the remained sample, an amount of 10 mL of aqua regia, 6M HCl: 6M HNO_3 at a ratio of 1:3 v/v was added into the Teflon beaker and heated to dryness again. Subsequently, an amount of 25 mL of 6M HNO_3 was poured slowly on a trace amount of the dried sample in the Teflon beaker and warmed for 5 minutes to dissolve the sample. The sample solution with all rinsing water was transferred into a 250-mL volumetric flask, brought to the mark with deionized water, and mixed well. The sample solution was analyzed for total aluminium content by ICP-MS. The standard solutions of aluminium were prepared in HNO_3 in the range of 10, 20, 40, 60 and 100 ppb to achieve calibration curve. The silica content was analyzed by calculated from the unit cell formula of zeolite beta and the aluminum content from ICP-MS measurement.

3.8 Activity Test of Zeolite Beta Catalysts in Acetalization of Glycerol to Solketal

3.8.1 Effect of Catalyst Amounts

The catalytic reaction between glycerol and acetone were carried out at boiling temperature under reflux for 150 minutes using H^+-BEA-0.17%s-130°C-5d catalyst. The reactions were carried out in a 50-mL 3-necked round bottom flask using under reflux at the boiling temperature under reflux and atmospheric pressure. The mixture of 2.50 g glycerol and 4.00 mL acetone (mole ratio of 1:2) was used as reactants and 20.00 mL DMF as a solvent. The catalyst amount was

varied in a range of 1, 5, 10 and 20 wt% with respect to glycerol. A small portion of the liquid mixture was taken from the reaction media through a microfilter at 30-minute intervals until the end of 150 minutes. A volume of 0.2 mL of sampling liquid was mixed with 10 µL toluene as internal standard for analysis by GC. The values of %conversion, %selectivity to solketal and %yield were calculated based on the following equations:

$$\%\text{conversion} = \frac{\text{Reacted mole of glycerol}}{\text{Initial mole of glycerol}} \times 100$$

$$= \frac{\text{mole}_{\text{all products}}}{\text{mole}_{\text{all products}} + \text{mole}_{\text{remained glycerol}}} \times 100$$

$$\%\text{selectivity} = \frac{\text{mole of solketal}}{\text{Total mole of all products}} \times 100$$

$$\%\text{yield} = \frac{\text{Actual mole of solketal}}{\text{Theoritical mole of solketal}} \times 100$$

$$= \frac{\%\text{conversion} \times \%\text{selectivity}}{100}$$

3.8.2 Effect of Glycerol to Acetone Mole Ratio

The experiments were set up similar to Section 3.8.1 but the catalyst amount was fixed as of 20 wt% of H^+-BEA-0.17%s-130°C-5d while the glycerol to acetone mole ratio was varied in a range of 1:2, 1:4, 1:6 and 1:10. The total

volume of reaction mixture was fixed by adjusting the volume of acetone and DMF. After the reaction was performed for 150 minutes, a 0.2-mL portion of the liquid mixture was taken from the reaction media through a microfilter and internal standard to Section 3.8.1 for the analysis by GC.

3.8.3 Effect of Crystalline Nanoseed Amounts in Catalyst

The acetalization reaction was performed using zeolite beta catalysts with various crystalline nanoseed amounts of 0.17, 0.33 and 0.83 wt% in the preparation of zeolite catalysts (denoted as H^+-BEA-0.17%s-130℃-5d,H^+-BEA-0.33%s-130℃-3d and H^+-BEA-0.83%s-130℃-2d, respectively). A 20 wt% of each zeolite beta catalyst was subjected to the reaction flask containing glycerol and acetone with the mole ratio of 1:10. After 150 minutes of reaction, a 0.2-mL portion of the liquid mixture was taken from the reaction media through a microfilter and treated similarly to Section 3.8.1 for the analysis by GC. The used H^+-BEA-0.83%s-130℃-2d catalyst from the first run was separated from the reaction media and kept for further study.

3.8.4 Catalyst Reuse

The used H^+-BEA-0.83%s-130℃-2d catalyst from the first run of acetalization reaction in Section 3.8.3 was collected by filtration, washed with DMF and then acetone. The washed catalyst was air dried for 30 minutes, placed in an oven at 100 ℃ for 2 hours and calcined in air at 500 ℃ for 5 hours. The resulted zeolite was denoted as the 1^{st} regenerated catalyst which was characterized by XRD and FESEM prior to the test for its catalytic activity. The acetalization reaction was carried out in the same way as the first run reported in Section 3.8.3. The spent H^+-BEA-0.83%s-130℃-2d catalyst from the second run was regenerated in the same way, resulted in the 2^{nd} regenerated catalyst.

CHAPTER IV

RESULTS AND DISSCUSSIONS

4.1 Physical Properties of SBA-15

SBA-15 was prepared in order to be used as an active silica source for the synthesis of zeolite beta catalyst. The gel containing a liquid silica source and Pluronic® P123 as a structure directing agent was crystallized at 100 °C for 2 days and the organic substance was removed by calcination in air at 550 °C for 5 hours. The as-prepared sample of SBA-15 exhibited an XRD pattern as shown in Figure 4.1 (A) similar to that of hexagonal structure SBA-15 [74]. The X-ray diffractogram consists of three peaks correspondent to (100), (110) and (200) lattice planes which are located at 2θ of 0.86°, 1.46° and 1.68°, respectively. These XRD peaks are located at rather low Bragg angles indicating long interplanar d-spacing values in the structure lacking of short range order. No indication of other crystalline phases was found.

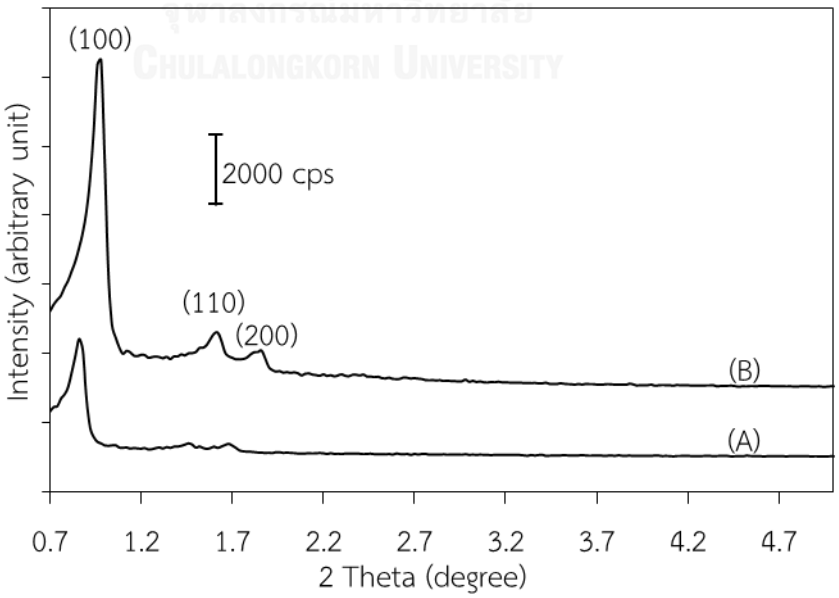

Figure 4.15 XRD pattern of (A) as-prepared and (B) calcined SBA-15

The XRD peak intensities of calcined sample in Figure 4.1(B) are more remarkably higher than those of the as-synthesized sample. This phenomenon was normally observed in porous materials after the removal of the structure directing agent from its pores. All peaks shifted to larger Bragg angles, 2θ due to the smaller d-spacing values. The contraction of unit cell contributed to a decrease of d-spacing values which is inversely proportional to θ values according to Bragg theory, $n\lambda = 2d \sin\theta$.

Scanning electron microscopy (SEM) images in Figure 4.4 reveals similar morphologies for both as-synthesized and calcined SBA-15, *i.e.* rod-like particles at 1000X magnification and aggregates of worm-like morphology at 5000X magnification. After calcination, the thickness of SBA-15 rods shrinks from 5.5 μm to 3.4 μm is the evidence for the structure shrinkage confirming the XRD results. The twisted worm-like morphology indicates the lack of short range order of the SBA-15 structure resulting in the XRD peaks observed at an unusal range of very small Bragg angles.

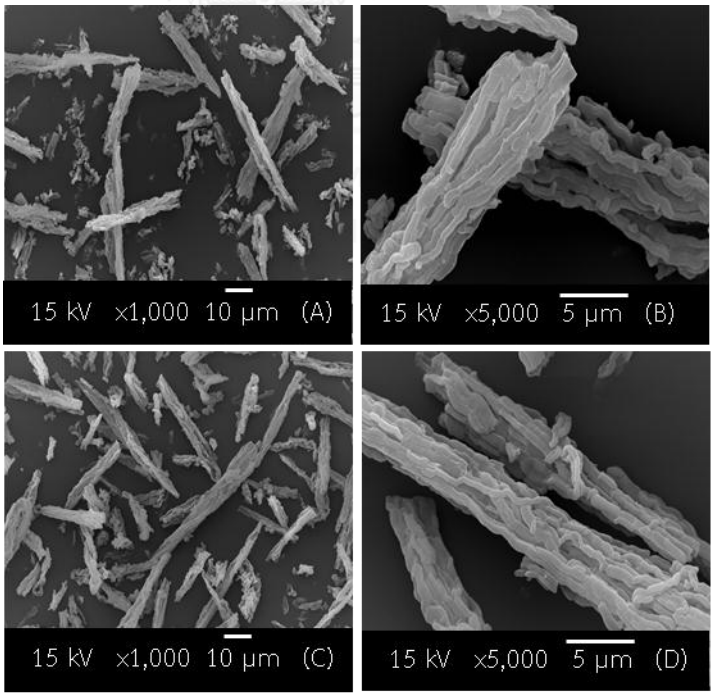

Figure 4.16 SEM images of (A and B) as-prepared SBA-15 and (C and D) calcined SBA-15

The SBA-15 sample was also characterized for it pore properties. The nitrogen adsorption-desorption isotherm of calcined SBA-15 is illustrated in Figure 4.3. Calcined SBA-15 exhibits a type IV adsorption isotherm which is a characteristic pattern of a majority of mesopores with some micropores. At very low relative pressure below $P/P_0<0.2$, a steep increase in the adsorbed volume was observed. At the intermediate pressure region (P/P_0 = 0.2-0.9), the adsorption-desorption isotherms exhibit a hysteresis loop corresponding to capillary condensation due to the well-known bottleneck effect which is caused by the significant difference in diameters of pore cavity and pore window causing difficult evacuation of gas molecules during desorption process at high relative pressure range of 0.6-0.8.

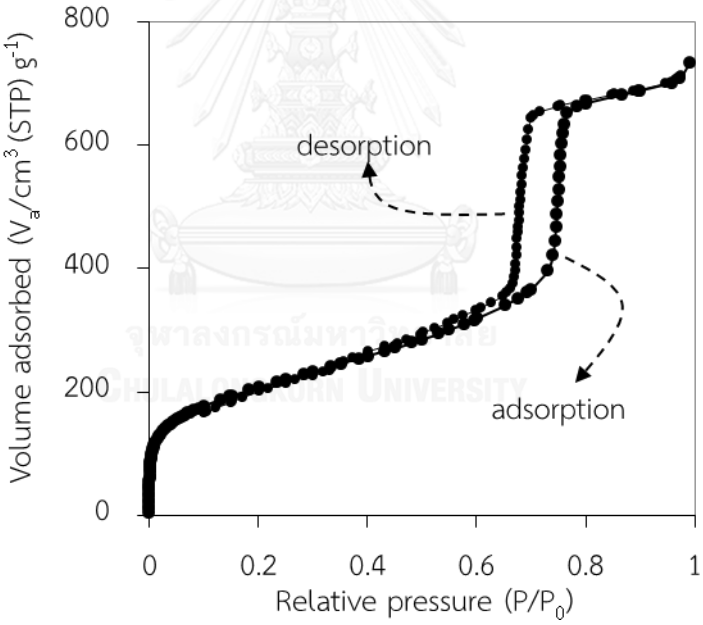

Figure 4.17 Nitrogen adsorption-desorption isotherm of calcined SBA-15

The calcined SBA-15 sample has a BET Brunauer-Emmett-Teller (BET) specific surface area of 740 m^2/g and pore volume of 1.13 cm^3/g. The Barrett-Joyner-Halenda (BJH) analysis was used for measuring pore size distribution. As shown in Figure 4.4, a single narrow peak was found indicating the uniform pore

size distribution with the average pore diameter of 8.1 nm lying in a mesopore range.

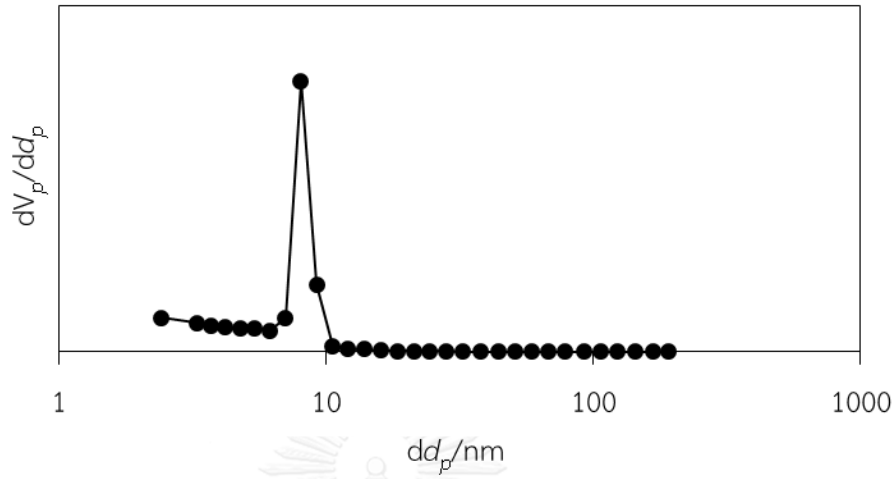

Figure 4.18 BJH pore size distribution of calcined SBA-15

4.2 Physicochemical Properties of Crystalline Nanoseeds

4.2.1 XRD Patterns of Crystalline Nanoseeds

The XRD patterns of the as-synthesized and calcined crystalline nanoseeds are illustrated in Figure 4.5. They are similar to the typical pattern of zeolite beta [77]. The as-synthesized nanoseeds pattern presents the highest peak located at 2θ of 22.56° and other peaks at 2θ of 7.78°, 21.56°, 25.44°, 26.96° and 29.62°. The broad peak at 2θ of 7.78° is resulted from the convolution of four peaks due to the cocurrence of zeolite beta polymorph A (2θ of 6.98° and 7.74°) and polymorph B (2θ of 7.34° and 8.31°) [77]. After the removal of organic template at 550 °C for 5 hours, the intensity of the parent peak at 2θ of 22.56° decreases to about one half of that belonging to the as-synthesized sample. This circumstance is resulted from the partial decomposition of zeolite structure due to high temperature of calcination process which is in agreement with the previous reports [20, 21]. There is no peak of SBA-15 at 2θ below 5° indicating the complete phase transformation from SBA-15 to the crystalline nanoseeds having BEA structure.

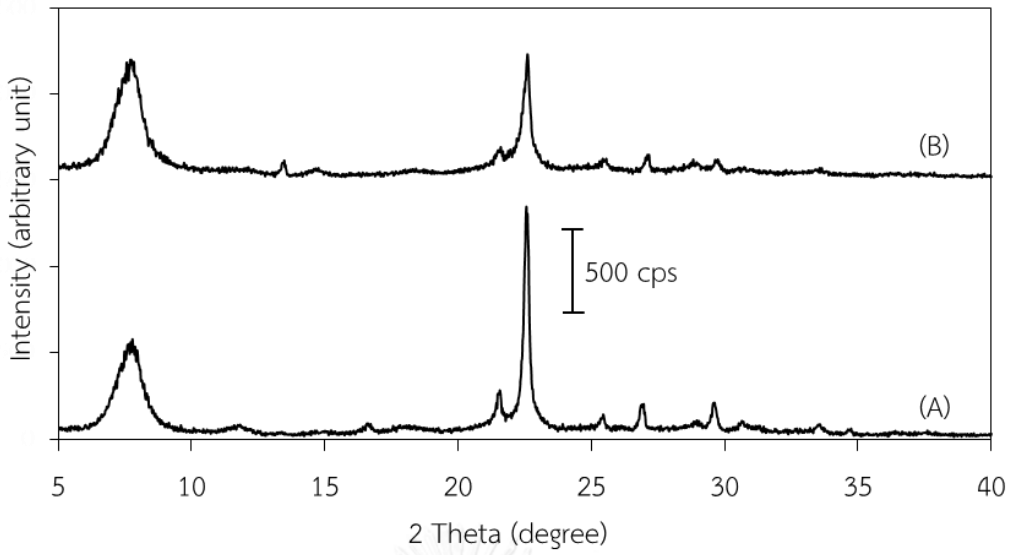

Figure 4.19 XRD patterns of (A) the as-synthesized and (B) the calcined crystalline nanoseeds

4.2.2 SEM Images of Crystalline Nanoseeds

The SEM image of crystalline nanoseeds in Figure 4.8 illustrates the fairly spherical shaped of nano-sized particles. The nanoparticles have rough surface resulting in a high external surface area which corresponds to an unusual tail of nitrogen adsorption isotherm as reported previously. The size of particles is in the range of 116-147 nm. No amorphous phase was found indicating the complete phase transformation of SBA-15 into crystalline nanoseeds with BEA structure.

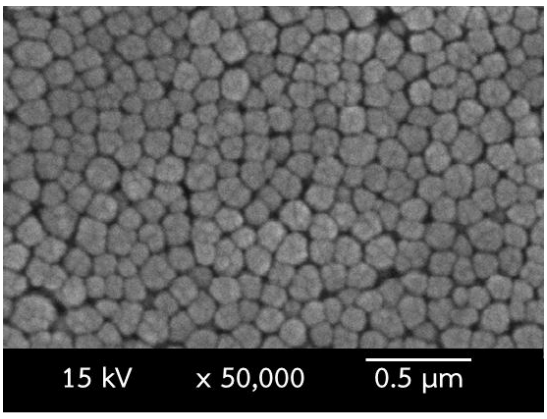

Figure 4.20 SEM image of calcined crystalline nanoseeds at 50,000 magnifications

4.2.3 Nitrogen Adsorption-Desorption of Crystalline Nanoseeds

The nitrogen adsorption-desorption isotherms of calcined crystalline nanoseeds as shown in Figure 4.6 can be assigned to the Type I which is typical for the behaviour of microporous material. An increase of the nitrogen adsorbed volume was observed at two regions. The gas adsorption at very low relative pressure indicates the microporous behavior. There is another adsorption tail at the relative pressure around 0.9-1 due to the unusual adsorption on the external surface area. No adsorption behavior of mesopores at the relative pressure between 0.2-0.8 indicating the complete reaction of SBA-15. In conclusion SBA-15 was transformed completely to microporous material i.e. the crystalline BEA nanoseeds identified by the XRD technique. The specific surface area of crystalline nanoseeds sample evaluated by BET theory, was about 730 m^2/g. The external surface area of sample is 72 m^2/g calculated by t-plot analysis. The distribution data of pore sizes determined by MP-plot in Figure 4.7 shows the average pore size of 0.7 nm which is in agreement with the pore size of meterials having the BEA struture. From t-plot calculation, crystalline naoseeds show a large micropore volume of 0.27 cm^3/g comparable to other reports [24, 25].

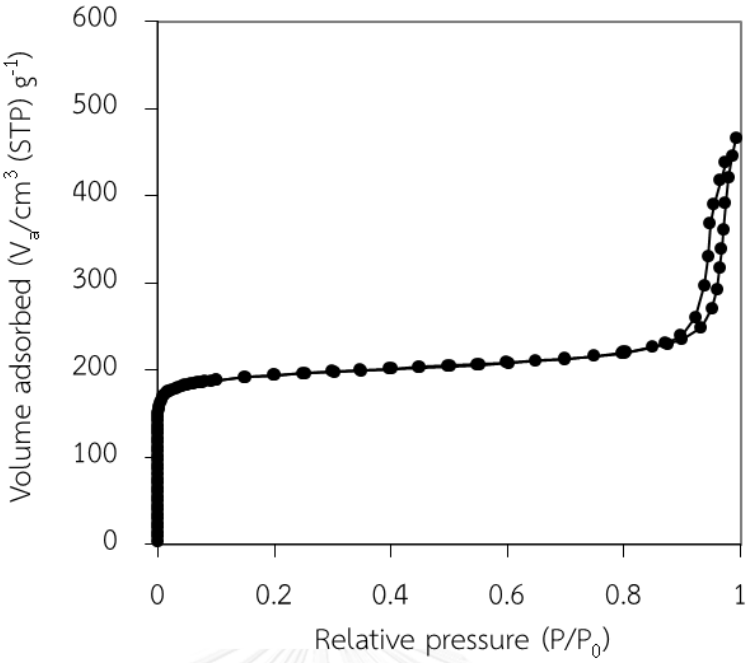

Figure 4.21 Nitrogen adsorption-desorption isotherm of the calcined crystalline nanoseeds

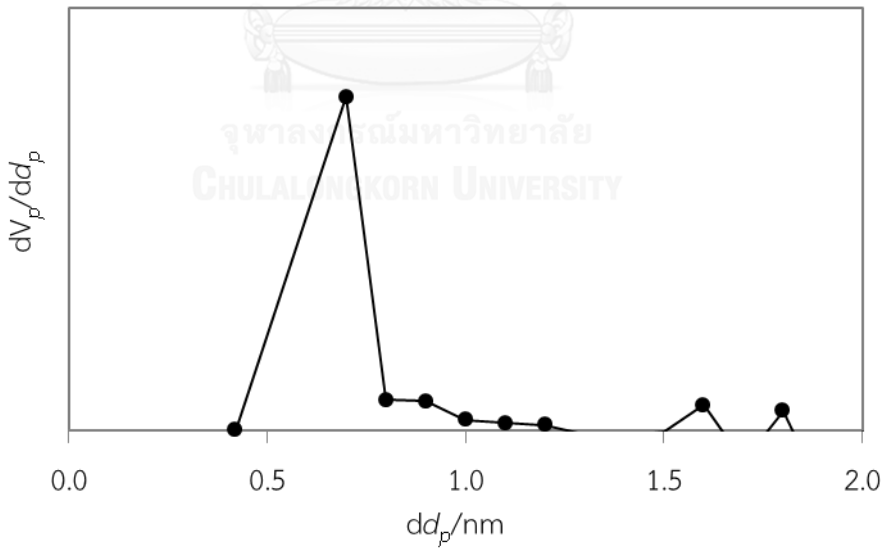

Figure 4.22 Pore size distribution of crystalline nanoseeds calculated by the MP-plot analysis

4.2.4 ^{27}Al-MAS-NMR Spectra of Crystalline Nanoseeds

The ^{27}Al-MAS-NMR spectrum of calcined crystalline nanoseeds is shown in Figure 4.9. The strong signal at a chemical shift of 54.9 ppm belongs to the tetrahedral aluminium atoms in zeolite framework. The weak signal was observed at the chemical shift nearly 0 ppm which can be assigned to the octahedral coordination aluminium atoms. The octahedrally coordinated aluminium atoms are located on the non-framework position according to template removal at high temperature which is believed to cause dealumination from framework site to extra-framework site. The framework Al to non-framework Al peak integral of 26.3:1 indicates that around 4% of total aluminium atoms are at the extra framework site.

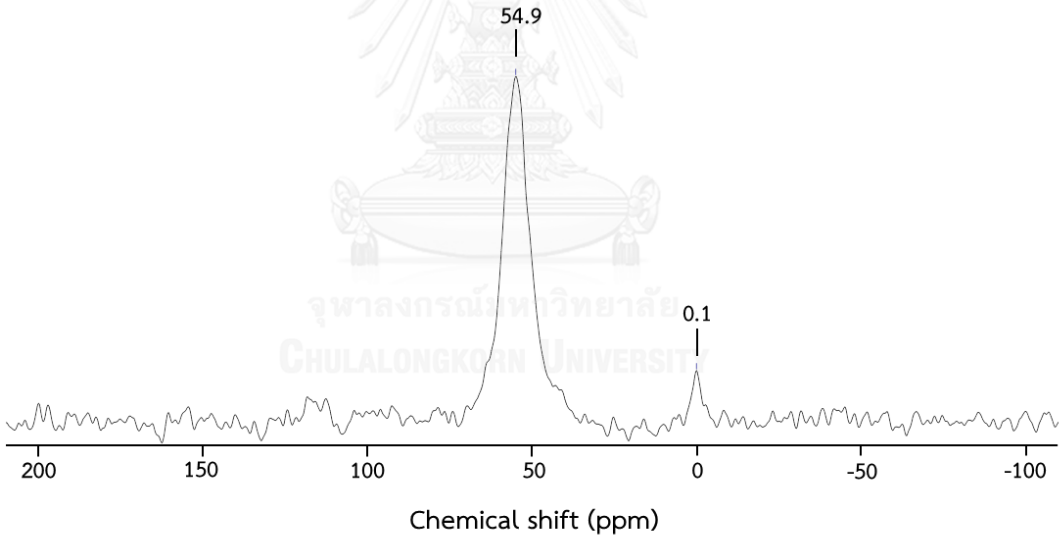

Figure 4.23 ^{27}Al-MAS-NMR spectra of calcined crystalline nanoseeds with BEA structure

4.3 Physicochemical Properties of Zeolite Beta

4.3.1 Effect of Crystallization Temperature on Formation of Zeolite Beta

4.3.1.1 X-ray Powder Diffraction Patterns

An amount of 0.17% by weight of calcined crystalline nanoseeds to the starting gel was used as structure directing agent for the study on effect of crystallization temperature on formation of zeolite beta. A range of crystallization temperature from 120 ℃ to 150 ℃ was studied. Figure 4.10 shows XRD patterns of as-synthesized products at various crystallization temperatures for 5 days. It is obvious that temperature is a factor playing a key role in the type and crystallinity of products. By comparing the sample XRD patterns to the typical ones of zeolites in literature and the intensities of its parent peak of each zeolite structure, it was found that the products of zeolite beta were achieved only at the crystallization temperatures of 120 ℃ and 130 ℃. The XRD peak at 2θ of 22.2° of the sample crystallized at 120 ℃ has lower intensities than that at 130 ℃ and the result implied the existence of other phase which may be an amorphous phase, which cannot be detected at all by XRD. The concurrence of other zeolites Na-P1 and mordenite was found as minor phases in the samples crystallized at 135 ℃ and 140 ℃. Zeolites Na-P1 and mordenite became more preferable than zeolite beta at 150 ℃. Temperatures play an important role in zeolite structure and crystallinity. Pure zeolite beta with high crystallinity can be prepared at 130 ℃. Thus, crystallization temperature of 130 ℃ providing a pure phase of zeolite beta with the highest crystallinity is selected as the optimal temperature for studies on other parameters.

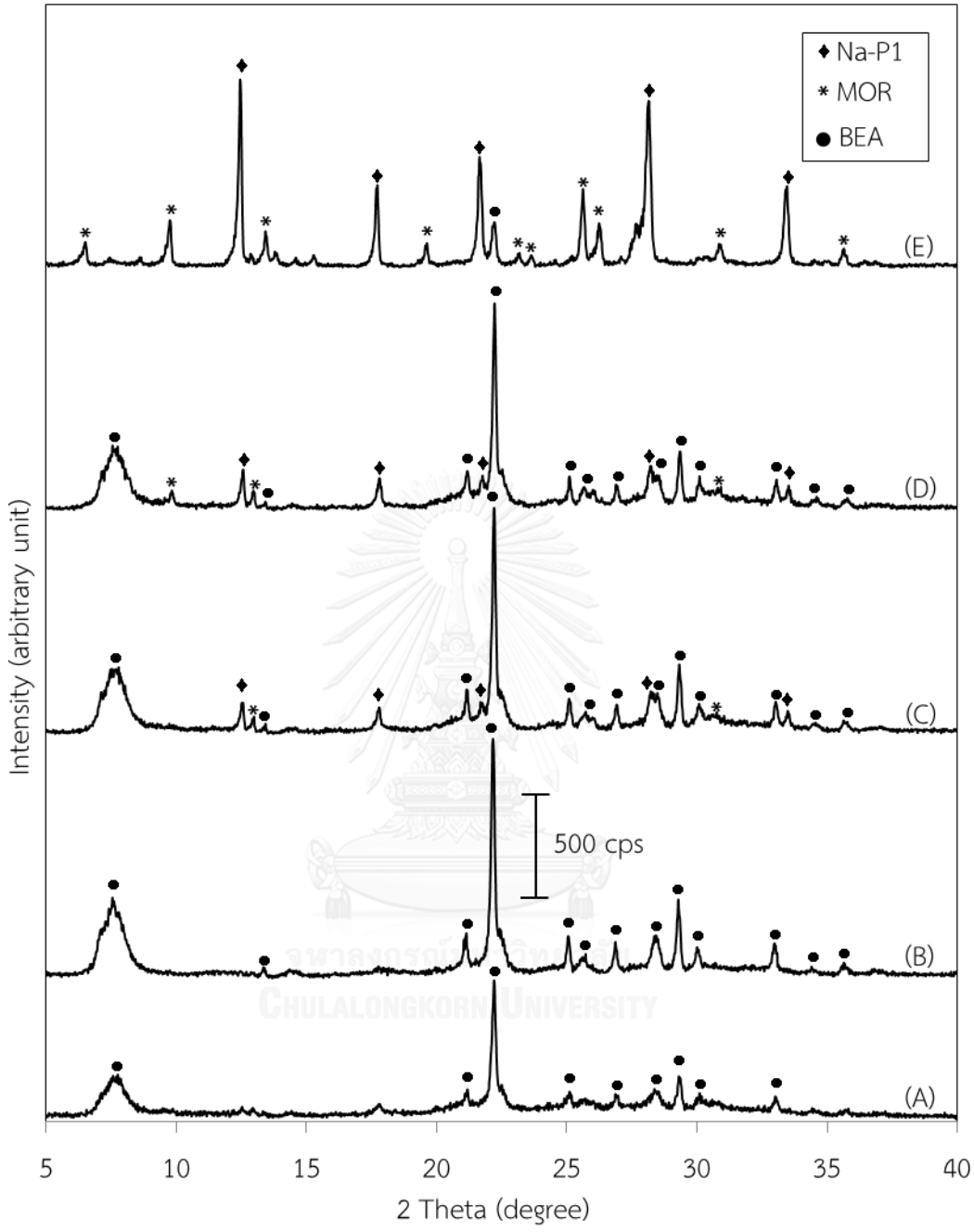

Figure 4.24 XRD patterns of as-synthesized zeolite beta products crystallized at various temperatures: (A) 120 °C; (B) 130 °C; (C) 135 °C; (D) 140 °C and (E) 150 °C

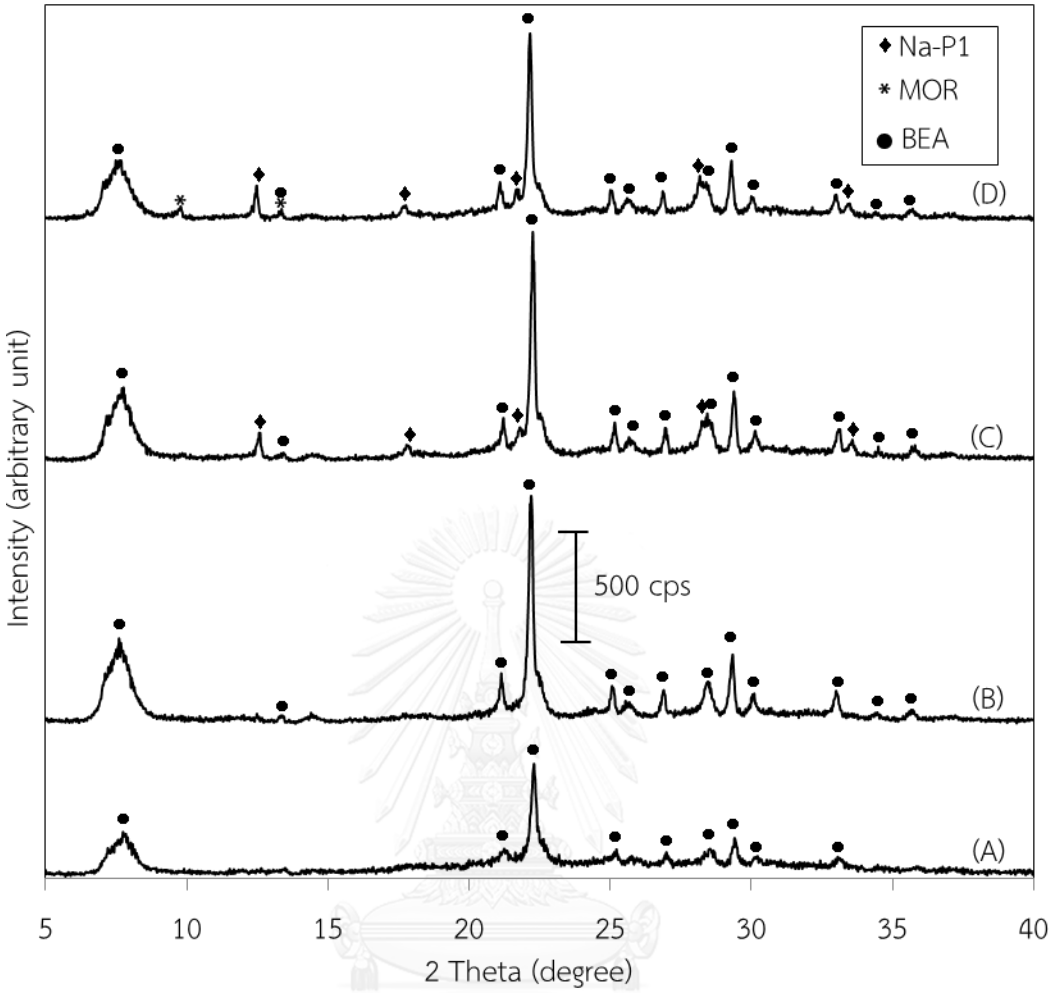

Figure 4.25 XRD patterns of calcined zeolite beta products crystallized at various temperatures: (A) 120 °C; (B) 130 °C; (C) 135 °C and (D) 140 °C

In general for zeolite beta, the significant decrease in intensity of the parent peak at 2θ of 22.2° is always found after calcination. But, zeolite beta products prepared by addition of crystalline nanoseeds show a small decrease of intensity comparing to those prepared by conventional method using an organic template. The samples prepared in this work having zeolite beta as major phase were tested for their thermal stability by calcination at 550 ℃ for 5 hours. As shown in Figure 4.11, all of XRD peak positions were still not shifted and no new peak was found. The decrease of intensities (peak area) of the parent peak by about 10, 5, 2, and 5% for the calcined samples crystallized at 120, 130, 135, and 140 ℃, respectively. Although the sample crystallized at 135 ℃ is the most thermal stable, it is not a pure beta phase. The pure zeolite beta obtained from the crystallization at 130 ℃ is the most thermally stable. This is a good sign indicating the high thermal stability of zeolite beta product upon calcination. This is also evidenced by the absence of a peak at non-framework aluminium position in ^{27}Al-MAS-NMR spectra of the calcined zeolite beta products to be discussed.

4.3.1.2 ^{27}Al-MAS-NMR Spectra

^{27}Al-MAS-NMR spectra of calcined zeolite beta samples crystallized at 120 ℃ and 130 ℃ are presented in Figure 4.12. The spectra of both calcined zeolite beta products present only one intense signal at around 56.2 ppm which is assigned to the tetrahedral aluminium atoms located in zeolite framework. The signal at 0 ppm was not found, indicating the absence of octrahedral non-framework aluminium species, in other words, all aluminium atoms incorporated into the tetrahedral framework site. These results confirmed that there were no aluminium migration from the tetrahedral site to the octahedral site during the calcination process at the elevated temperatrure. This is a good sign indicating the high thermal stability of seed-assisted zeolite beta products which is consistent with the XRD results.

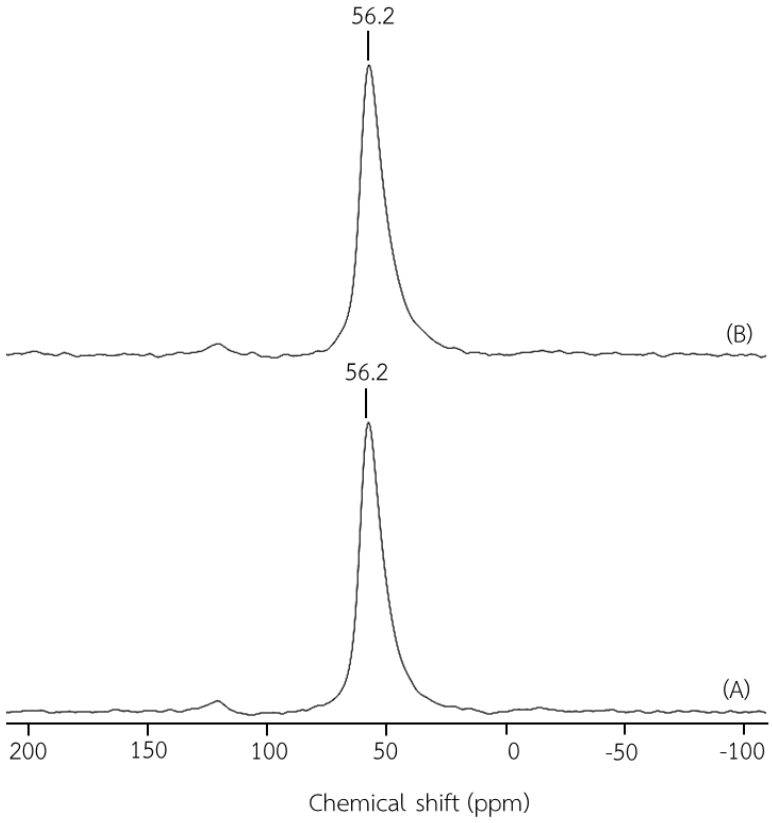

Figure 4.26 ^{27}Al-MAS-NMR spectra of calcined zeolite beta products crystallized at (A) 120 ℃ and (B) 130 ℃ for 5 days

4.3.1.3 Field Emission Scanning Electron Microscopy Images

The morphology of zeolite beta samples synthesized at 120 ℃ and 130 ℃ were investigated using field emission scanning electron microscope. FESEM images in Figure 4.12 (A and B) reveal the truncated square bipyramidal crystals of zeolite beta obtained after crystallization at 120 ℃ for 5 days. The average size of the zeolite crystals is about 440 nm x 640 nm. These results are in agreement with a previous report [22]. A few large spherical particles as shown in Figure 4.13 (B) were identified as sodalite in comparison with that reported by Xing-dong, L. and Novembre, D. [78, 79]. However, no characteristic peaks of sodalite were observed in the X-ray diffractogram of the sample indicating that only a trace amount of the sodalite phase was formed. The higher crystallization temperature, the larger crystal sizes of zeolite beta are. Figure 4.13 (C and D) shows the products crystallized at 130 ℃. The larger average particle size of 620 nm x 840 nm was obtained within the same crystallization period of 5 days. The aggregation of small particles can be noticed on crystal surface in Figure 4.13 (D).

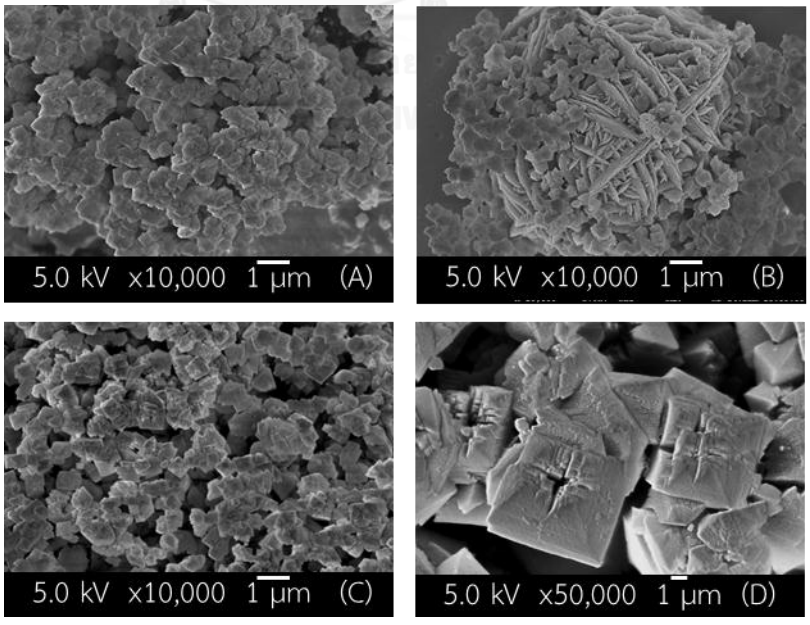

Figure 4.27 FESEM images of zeolite beta samples synthesized at (A and B) 120 ℃ and (C and D) 130 ℃ using the same crystallization time of 5 days

4.3.1.4 Nitrogen Adsosorption-Desorption Isotherms

Figure 4.14 shows the adsorption-desorption isotherms of all zeolite beta samples crystallized at different temperatures. All of them exhibit the steep adsorption curve at very low pressure which can be assigned to Type I adsorption-desorption isotherm, indicating a typical behaviour of microporous materials. The sample synthesized at 130 ℃ shows the highest volume of adsorbed nitrogen followed by those samples synthesized at 135 ℃, 140 ℃ and 120 ℃, respectively. Considering at high relative pressure around 0.9-1.0, only the sample crystallized at 130 ℃ showed a small adsorption tail according to the existence of the external surface area which in agreement with the FESEM images as discussed before.

The textural properties of zeolite beta sample crystallized at various temperatures are compiled in Table 4.1. The specific surface areas of all samples were calculated by BET calculation. The external surface area and micropore volumes were determined by the t-plot method. The sample synthesized at 130 ℃ has the largest specific surface area of 595 m^2/g whereas other samples have particularly lower BET specific surface areas according to the presence of other crystalline and/or amorphous phases. Zeolite beta sample synthesized at 130 ℃ shows the greatest external surface area of 22.5 m^2/g as well as the highest micropore volume of 0.23 cm^3/g. The distribution data of pore sizes were determined by the MP-plot method as shown in Figure 4.15. The pore size distribution peaks of all samples are centered at 0.7 nm which is the typical average value for zeolite beta [3, 80, 81].

From the above results, crystallization temperature of 130 ℃ is the appropriate temperature for the synthesis of seed-assisted zeolite beta, since it is the lowest temperature to provide pure zeolite beta with high crystallinity, greatest surface area and largest micropore volume which are important properties required for a good catalyst.

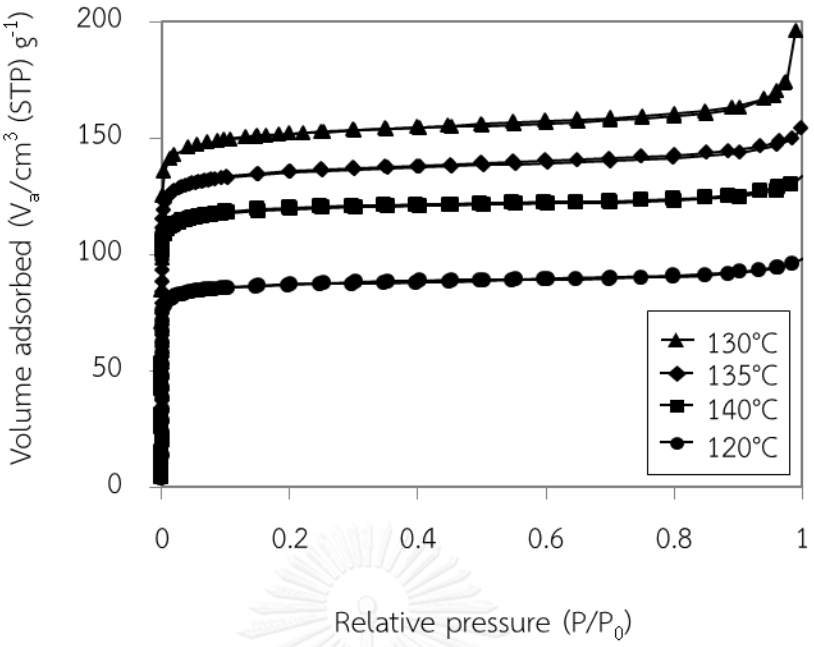

Figure 4.28 Nitrogen adsorption-desorption isotherms of calcined zeolite beta products crystallized at various temperatures

Table 4.1 Textural properties of calcined zeolite beta products prepared by adding 0.17 wt% nanoseeds and crystallized at various temperatures

Sample code	BET plot	t-plot		MP-plot
	specific surface area (m^2/g)	external surface area (m^2/g)	micropore volume (cm^3/g)	micropore size distribution (nm)
BEA-0.17%s-120℃-5d	344	9.9	0.13	0.7
BEA-0.17%s-130℃-5d	595	22.5	0.23	0.7
BEA-0.17%s-135℃-5d	534	18.0	0.20	0.7
BEA-0.17%s-140℃-5d	473	10.4	0.18	0.7

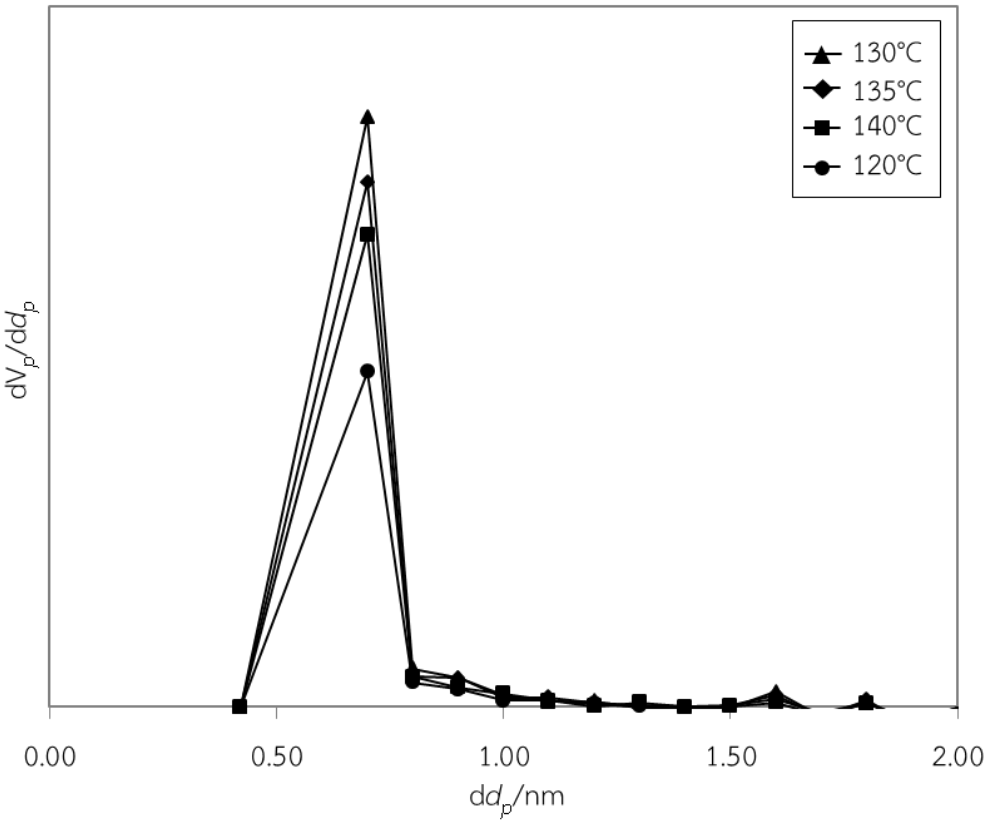

Figure 4.29 MP plots for pore size distributions of calcined zeolite beta products prepared by adding 0.17 wt% nanoseeds and crystallized at various temperatures

4.3.2 Effect of Crystallization Time on Formation of Zeolite Beta

4.3.2.1 X-ray Powder Diffraction Patterns

The effect of crystallization time from 1 day to 6 days on formation of zeolite beta structure was investigated. Figure 4.16 shows XRD patterns of as-synthesized zeolite beta synthesized at 130 ℃ for various crystallization periods. For the first 3 days of crystallization, no reflection peaks can be observed indicating that only an amorphous phase was obtained in those three samples. Thus, 3 days of crystallization is not enough for formation of the BEA structure. By prolongation of crystallization time, the characteristic peaks of zeolite beta are found at 2θ of 7.6° and 22.2° after crystallization for 4 days. The longer crystallization period, the higher crystallinity of zeolite beta phase can be obtained. The characteristic peak of zeolite beta exhibits the maximum intensity after 5 days of crystallization and remained the same until 6 days. Nevertheless, when the crystallization time reaches 6 days, the impurity of zeolite Na-P1 appears. Thus, the duration of 5 days is the most appropriate for the crystallization of zeolite beta at 130 ℃.

When the as-synthesized zeolite samples crystallized for 4-6 days were calcined at 550 ℃ for 5 hours, all of XRD peaks positions still the same as shown in Figure 4.17. Only 10%, or less, decrease of intensities of the peak at 2θ of 22.2° was observed after calcination. This result suggests that zeolite beta synthesized by addition of crystalline nanoseeds have high thermal stability of structure upon calcination. Thus, to obtain high crystallinity of zeolite beta and avoid formation of Na-P1 zeolite as impurity, the crystallization condition of zeolite beta catalyst must be controlled at 130 ℃ for 5 days.

Figure 4.30 XRD patterns of as-synthesized zeolite beta products crystallized at 130 °C with various periods of crystallization: (A) 1 day; (B) 2 days; (C) 3 days; (D) 4 days; (E) 5 days and (F) 6 days

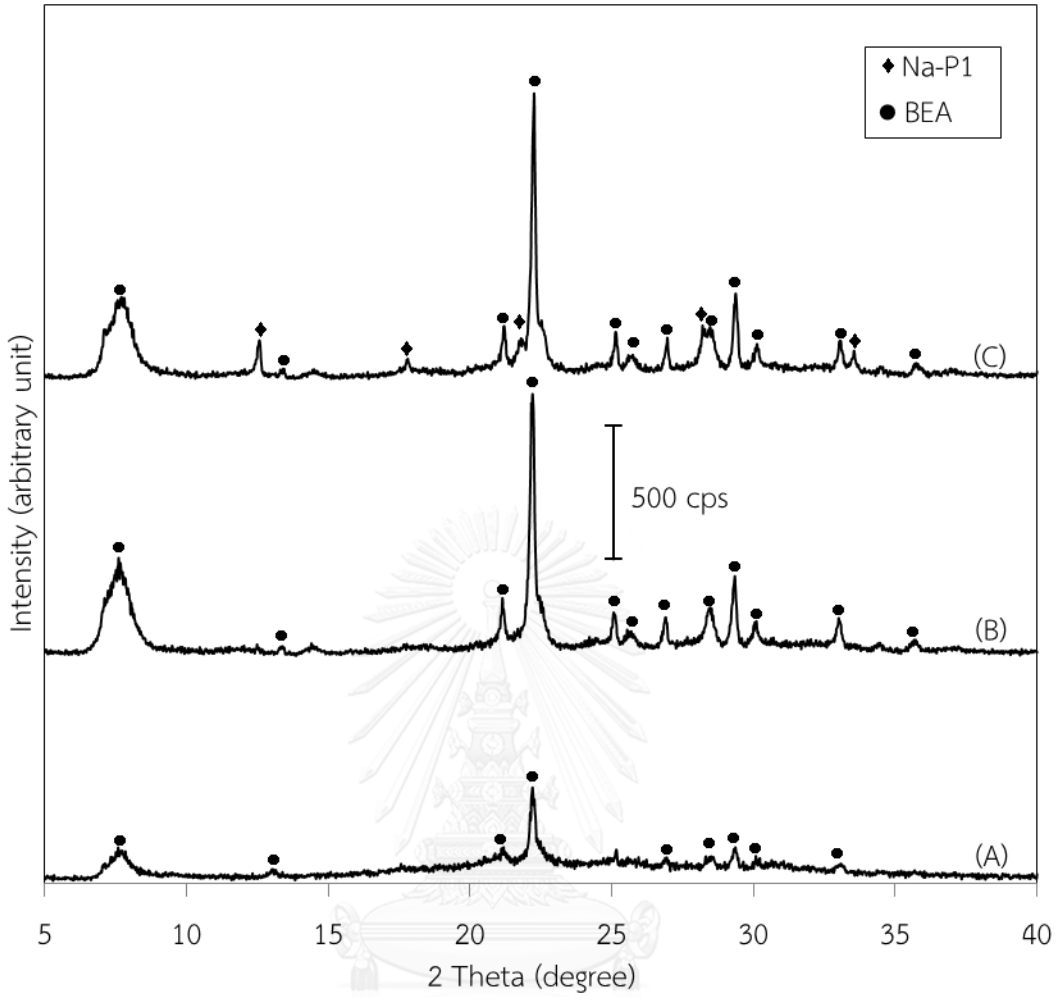

Figure 4.31 XRD patterns of calcined zeolite beta products crystallized at 130 °C with various periods of crystallization: (A) 4 days; (B) 5 days and (C) 6 days

4.3.2.2 Field Emission Scanning Electron Microscopy Images

The morphology of the calcined zeolite beta products synthesized at 130 ℃ for 4 days and 5 days were investigated using field emission scanning electron microscope as shown in Figure 4.18. FESEM image in Figure 4.18 (A) obviously reveals the incomplete phase transformation of the amorphous gel into crystals after 4 days of crystallization, only a trace amount of small complete crystal was observed. When the product was crystallized for 5 days, the highly crystalline, truncated square bipyramidal crystals of zeolite beta were obtained as shown in Figures 4.18 (B). No amorphous phase was found indicating the complete transformation from amorphous gel into zeolite beta phase which is in agreement with the higher intensity of the XRD parent peak as discussed above. The average size of crystals is about 620 nm x 840 nm.

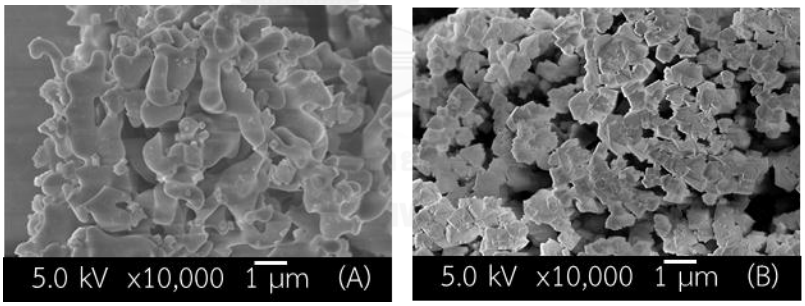

Figure 4.32 FESEM images of zeolite beta samples synthesized at 130 ℃ for (A) 4 days and (B) 5 days

4.3.2.3 Nitrogen Adsosorption-Desorption Isotherms

The calcined zeolite beta products crystallized for 4-6 days were characterized for its textual properties using the nitrogen adsorption-desorption technique. After the gel mixture was crystallized for 4 days, a significant increase of volume of adsorbed gas was observed at very low relative pressure, giving a so-call type I isotherm which is typical for micropores. The zeolite beta products synthesized at the longer period of crystallization depict the same type of isotherm as shown in Figure 4.19. The longer period of crystallization, the higher volume of adsorbed gas was found according to complete formation of the zeolite beta structure. Considering at very high relative pressure, only sample crystallized for 5 days presents the small tail according to the external surface of sample.

The textural properties of the samples crystallized for various periods are compiled in Table 4.2. The specific surface area of products was calculated by the BET method. The product crystallized for 4 days exhibits BET area of 255 m^2/g which is remarkably lower than those crystallized for 5 days due to the incomplete phase transformation of amorphous gel into crystal phase. Prolongation of crystallization period from 5 days to 6 days did not significantly affect the BET surface area. The sample crystallized for 6 days presents slightly lower surface area than the sample crystallized for 5 days according to the coexistence of impurity phase, zeolite Na-P1, as reported by XRD data. The external surface area and micropore volume of those samples were analyzed by the t-plot. The Zeolite beta products synthesized for 5 and 6 days show the large micropore volume of 0.2 cm^3/g, whereas the sample crystallized for 4 days exhibits only 0.1 cm^3/g of micropore volume which is rather too small for its application and it implies the incomplete transformation of the amorphous gel to the microporous crystals. The pore size distribution, determined by MP-plot method was found in a micropore range with an average pore size of 0.7 nm.

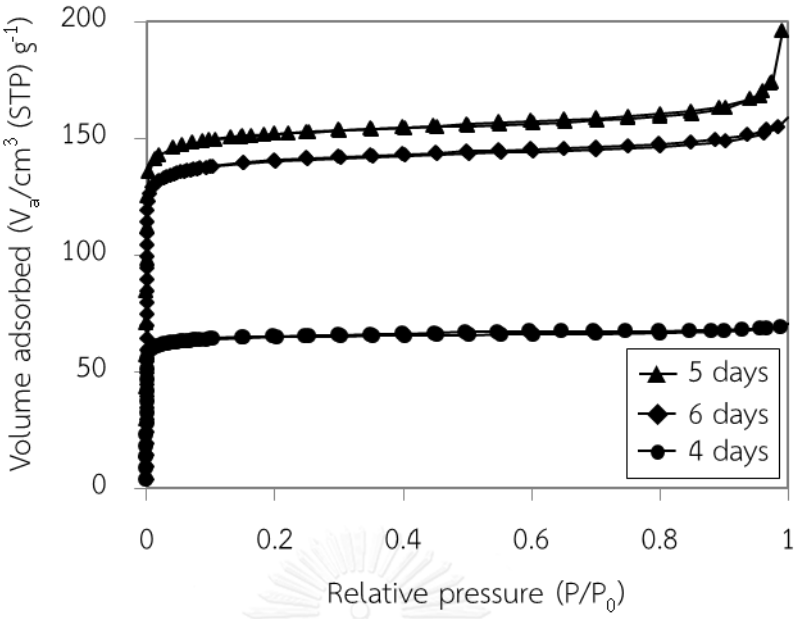

Figure 4.33 Nitrogen adsorption-desorption isotherm of calcined zeolite beta products synthesized at 130 °C with various periods of crystallization

Table 4.2 Textural properties of calcined zeolite beta products synthesized at 130 °C with various periods of crystallization

Sample code	BET plot	t-plot		MP-plot
	specific surface area (m^2/g)	external surface area (m^2/g)	micropore volume (cm^3/g)	micropore size distribution (nm)
BEA-0.17%s-130℃-4d	255	5.2	0.10	0.7
BEA-0.17%s-130℃-5d	595	22.5	0.23	0.7
BEA-0.17%s-130℃-6d	552	15.6	0.21	0.7

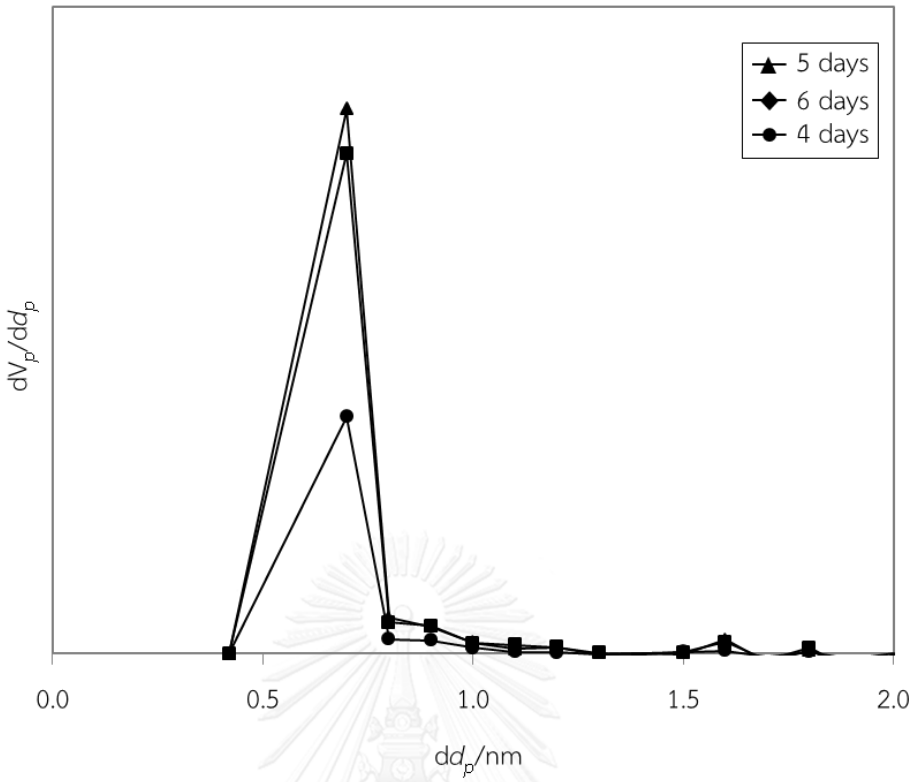

Figure 4.34 MP plots for pore size distribution of calcined zeolite beta products synthesized at 130 °C with various periods of crystallization

4.3.3 Effect of Crystalline Nanoseed Amounts on Formation of Zeolite Beta

4.3.3.1 X-ray Powder Diffraction Patterns

All results in the previous sections were the study of other parameters but the seed amount was kept at 0.17 wt% constantly. In this section various amounts of seeds will be studied for their effect on formation of zeolite beta. Figure 4.21 shows XRD patterns of as-synthesized zeolite beta prepared in the presence of 0.33 wt% crystalline nanoseeds at different periods of crystallization from 1 day to 5 days. The sample crystallized for 1 day presents no reflection peaks indicating that only the amorphous phase was found. Upon prolongation of crystallization time, characteristic peaks of zeolite beta with low intensities were observed after 2 days. The parent peak at 2θ of 22.2° reaches the maximum intensity after 4 days and remained constant during crystallization for longer than 4 days. However, the phase of MOR zeolite was revealed in the samples crystallized at 4 days. When the crystallization time was extended to 5 days, the co-existence of zeolites Na-P1 and MOR was found as impurities in the zeolite beta sample. The crystallization at 130 °C for 3 days which provided the pure phase of zeolite beta with high crystallinity is the optimal condition for the synthesis of zeolite beta in the presence of 0.33% crystalline nanoseeds. The zeolite products synthesized by adding of 0.50 and 0.66 wt% crystalline nanoseeds showed similar tendency of XRD results after crystallization for various periods from 1 day to 5 days as shown in Figure 4.22 and 4.23. The BEA phase with low crystallinities was found since 2 days in the presence of 0.33, 0.50 and 0.66 wt% of crystalline nanoseeds. Comparing the crystallization for 2 days, when the larger amounts of seeds were added, the higher the peak intensities of zeolite beta were observed. Prolongation of crystallization period to 3 days, all of samples exhibited the maximum crystallinity of zeolite beta phase with no impurity. Thus, 3 days is suitable for the synthesis of zeolite

beta at 130 ℃ when 0.33, 0.50 and 0.66 wt% of seed amounts were added.

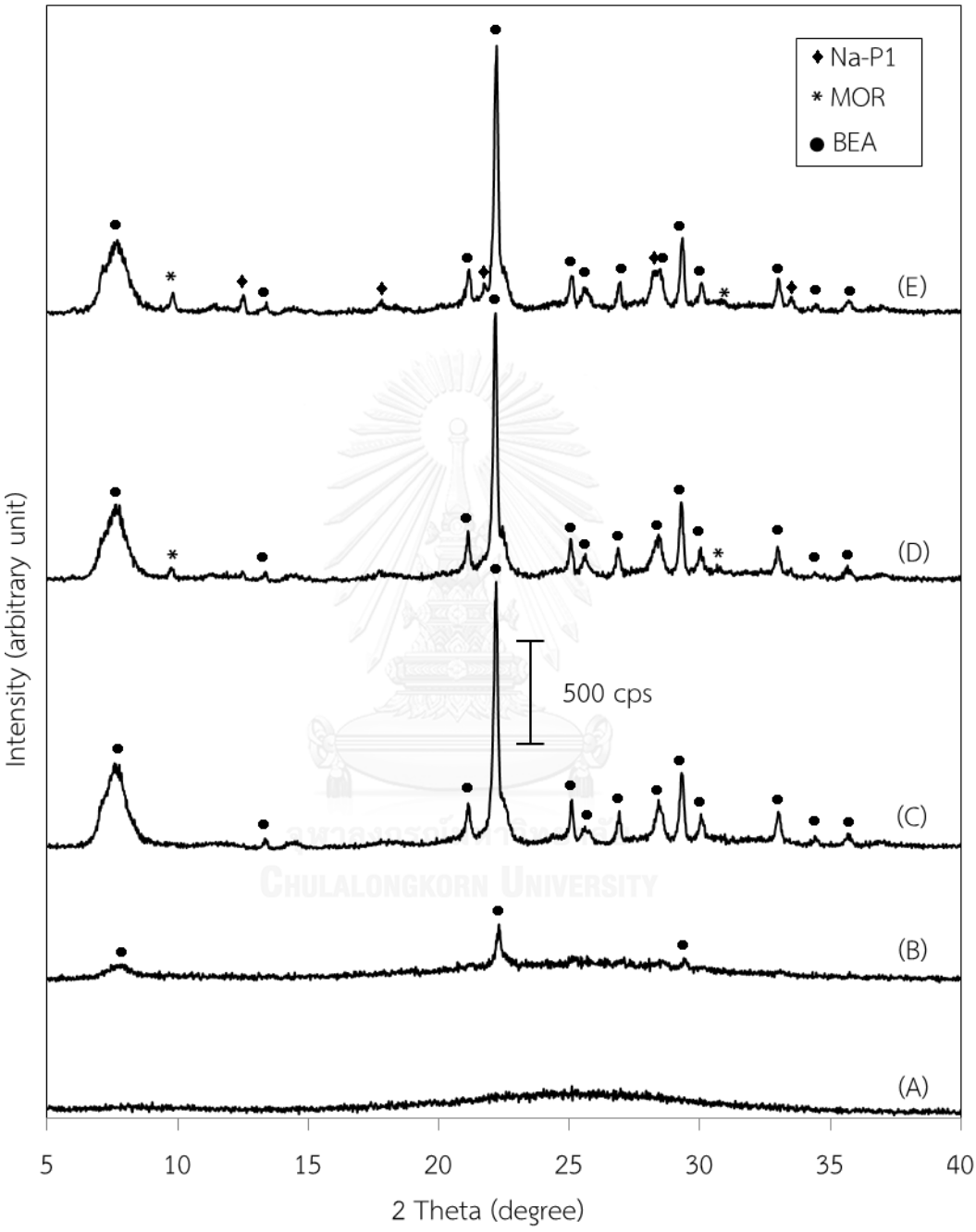

Figure 4.35 XRD patterns of as-synthesized zeolite beta products prepared in the presence of 0.33 wt% crystalline nanoseeds crystallized at 130 ℃ for various periods: (A) 1 day; (B) 2 days; (C) 3 days; (D) 4 days and (E) 5 days

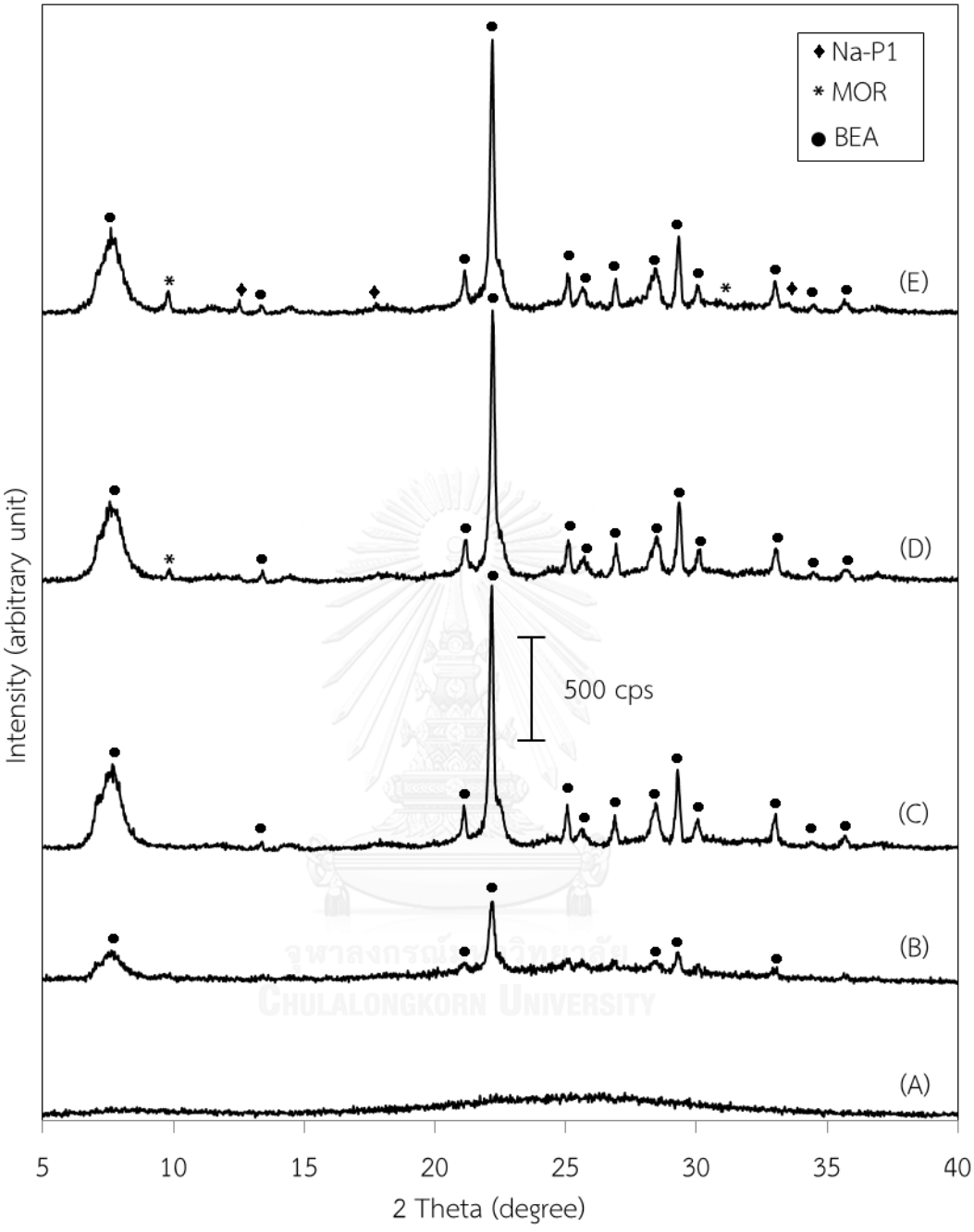

Figure 4.36 XRD patterns of as-synthesized zeolite beta products prepared in the presence of 0.50 wt% crystalline nanoseeds crystallized at 130 °C for various periods: (A) 1 day; (B) 2 days; (C) 3 days; (D) 4 days and (E) 5 days

Figure 4.37 XRD patterns of as-synthesized zeolite beta products prepared in the presence of 0.66 wt% crystalline nanoseeds crystallized at 130 °C for various periods: (A) 1 day; (B) 2 days; (C) 3 days; (D) 4 days and (E) 5 days

To shorten the crystallization period, the greater amounts of 0.83 and 1.00 wt% crystalline nanoseeds were added. According to the XRD results in Figure 4.24 and 4.25, zeolite beta samples synthesized using these two different amounts of seeds were similar. For the samples obtained after crystallization for 1 day, very low peaks of zeolite beta were found. It indicates that larger amounts of seeds can enhance the transformation of the amorphous phase into BEA phase. When the crystallization period was extended to 2 days, the peaks intensities became much higher according to more transformation from the amorphous phase into BEA crystals. During crystallization for longer than 2 days, the crystallinity did not significantly change. However, the XRD results of the corresponding product synthesized by addition of 0.83 wt% crystalline nanoseeds for 3 days, Figure 4.24(D) indicate the co-existence of zeolite beta as a major phase and zeolite Na-P1 as impurity. The longer crystallization time, the stronger intensities of zeolite Na-P1 was achieved. While the sample synthesized in the presence of 1.00 wt% seeds for 3 days provided the zeolite beta product with two impurities: zeolite Na-P1 and MOR. Thus, the optimal condition for the synthesis of zeolite beta with 0.83 and 1.00 wt% of seeds addition must be 130 °C for 2 days.

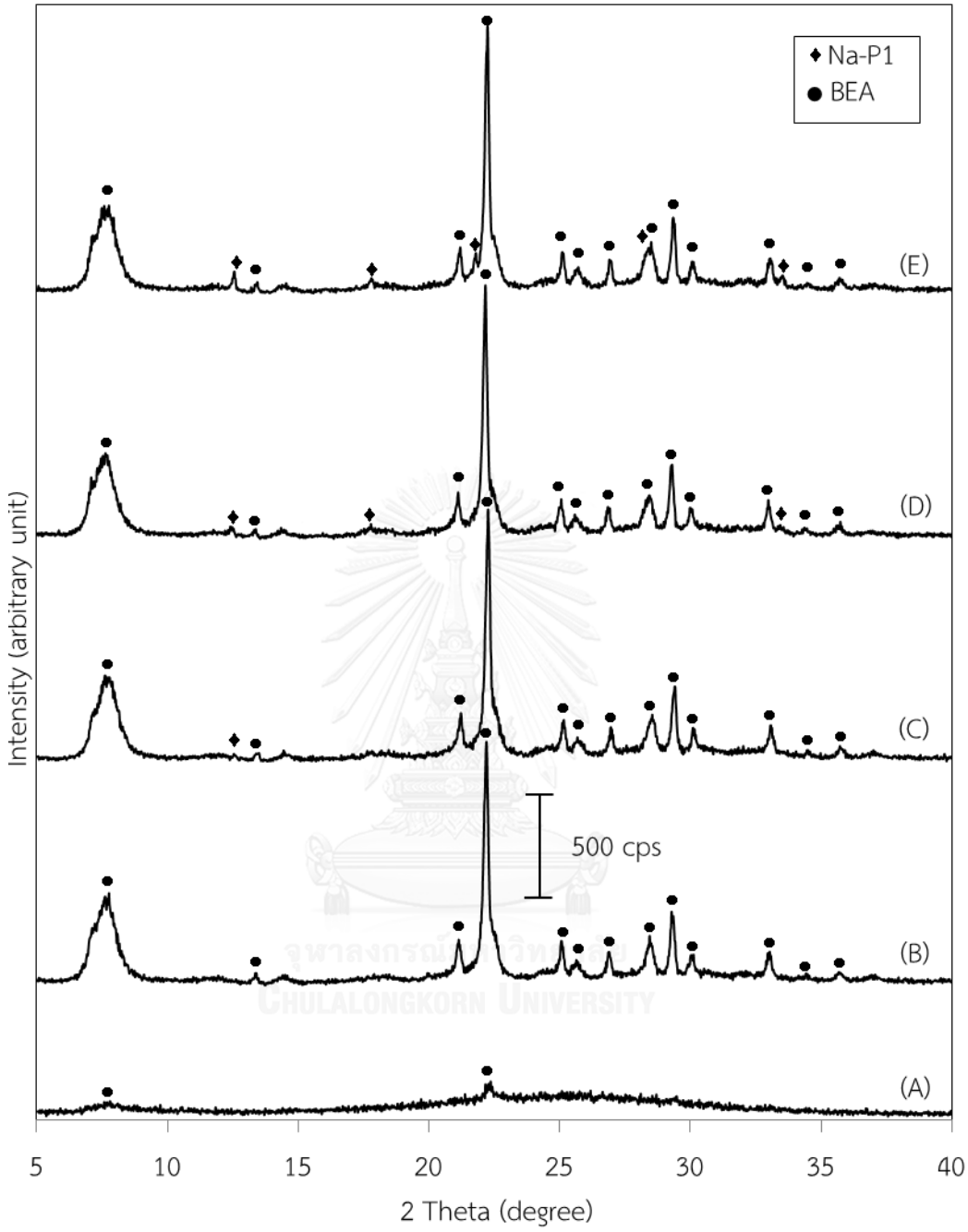

Figure 4.38 XRD patterns of as-synthesized zeolite beta products prepared in the presence of 0.83 wt% crystalline nanoseeds crystallized at 130 °C for various periods: (A) 1 day; (B) 2 days; (C) 3 days; (D) 4 days and (E) 5 days

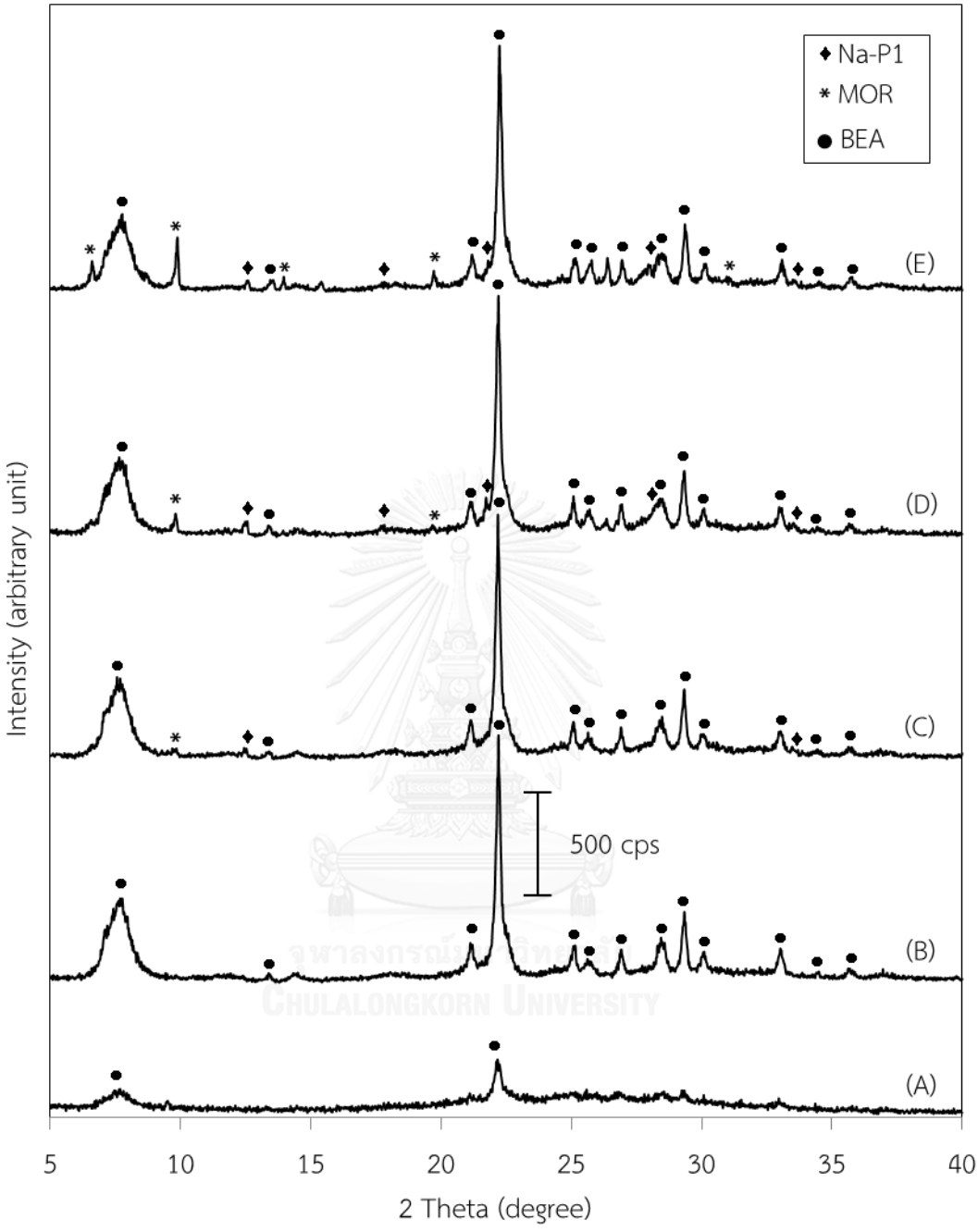

Figure 4.39 XRD patterns of as-synthesized zeolite beta products prepared in the presence of 1.00 wt% crystalline nanoseeds crystallized at 130 °C for various periods: (A) 1 day; (B) 2 days; (C) 3 days; (D) 4 days and (E) 5 days

The relation between crystallinities of zeolite beta products and crystallization periods of the samples prepared with various seed amounts are expressed in Figure 4.26. The data suggest that the amounts of crystalline nanoseeds added in the reactant gel have a strong influence on time consumed for formation and crystallinities of zeolite beta products. The larger amount of added seeds tends to shorten crystallization time required to achieve the pure zeolite beta with maximum crystallinity. The amounts of 0.83 and 1.00 wt% seeds exhibit similar profiles reaching the maximum crystallinity after 2 days. Another group of 0.33-0.66 wt% seed amounts reaches the maximum crystallinity after 3 days while the 0.17 wt% seed amount does after 5 days. However, these plots do not show the coexistence of impurity phases which was discussed previously that the use of too much seed amounts leads to formation of impurity phases earlier than those in the presence of lower seed amounts. The seed amounts and crystallization time must be optimized by considering the XRD patterns along with the crystallinity profiles.

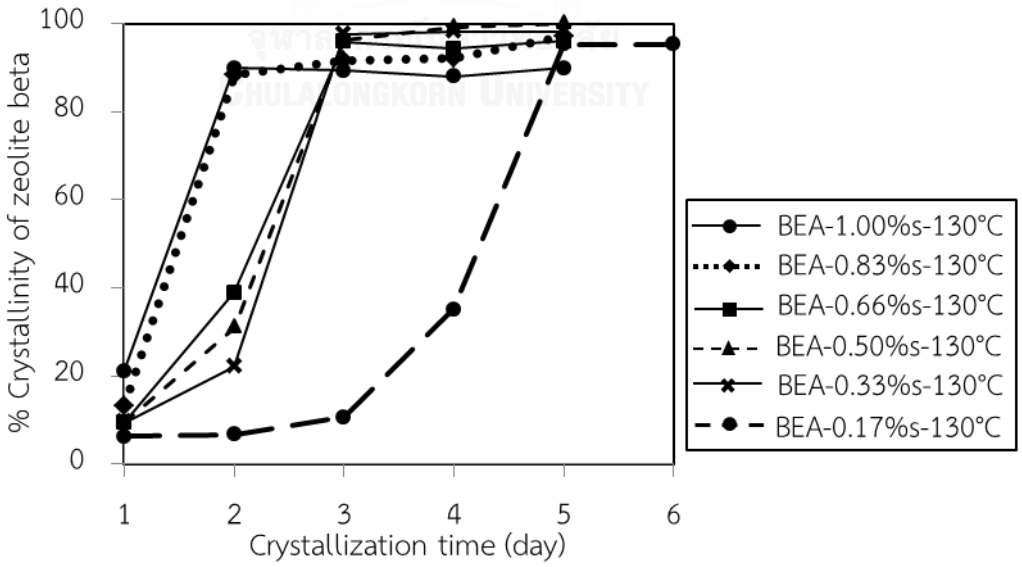

Figure 4.40 Crystallinity of zeolite beta samples prepared with various seed amounts at 130 °C for various periods

To investigate its thermal stability all of the zeolite beta products crystallized at 130 ℃ by adding various seed amounts and optimal crystallization times including BEA-0.17%s-130℃-5d, BEA-0.33%s-130℃-3d, BEA-0.50%s-130℃-3d, BEA-0.66%s-130℃-3d, BEA-0.83%s-130℃-2d and BEA-1.00%s-130℃-2d were calcined at 550 ℃ for 5 hours. The template-assisted zeolite beta was performed in parallel for comparing the thermal stability and its XRD patterns of as-synthesized and calcined samples are shown in Figure 4.27. All seed-assisted samples still show the XRD patterns comparable to that of the BEA structure with only a decrease of 8-14 wt% in crystallinity as shown in Figure 4.28 but the template-assisted sample exhibited a 50% decrease in crystallinity (Figure 4.27) as usual. The results indicated that the zeolite beta products obtained by the seed-assisted synthesis are much more thermal stable than that prepared by the template-assisted method. From the above results, BEA-0.17%s-130℃-5d, BEA-0.33%s-130℃-3d and BEA-0.83%s-130℃-2d were selected to test for their activities in catalytic acetalization, thus the zeolite beta catalysts were characterized for other properties.

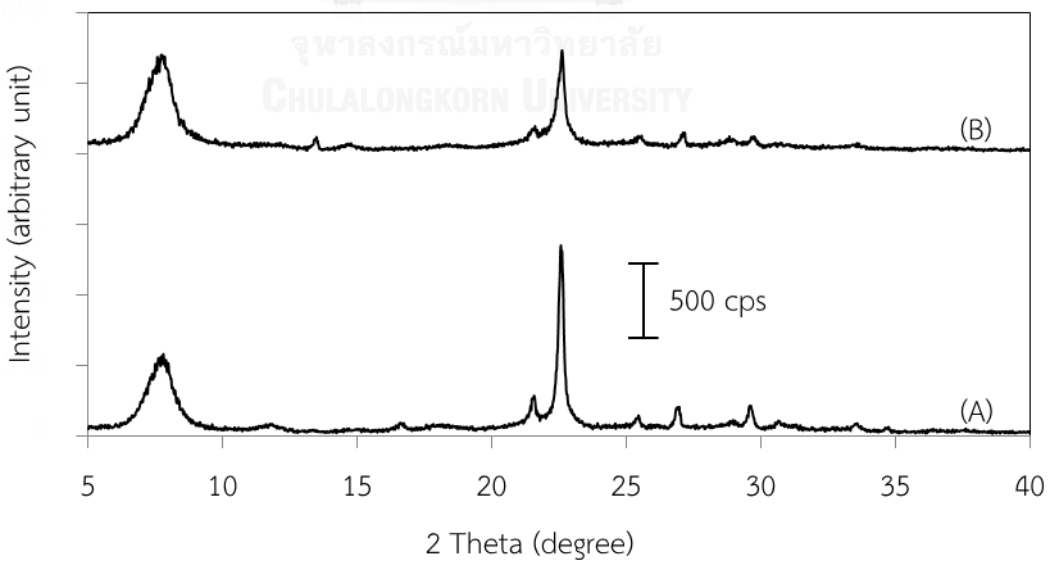

Figure 4.41 XRD patterns of (A) as-synthesized and (B) calcined zeolite beta samples prepared by the template-assisted method

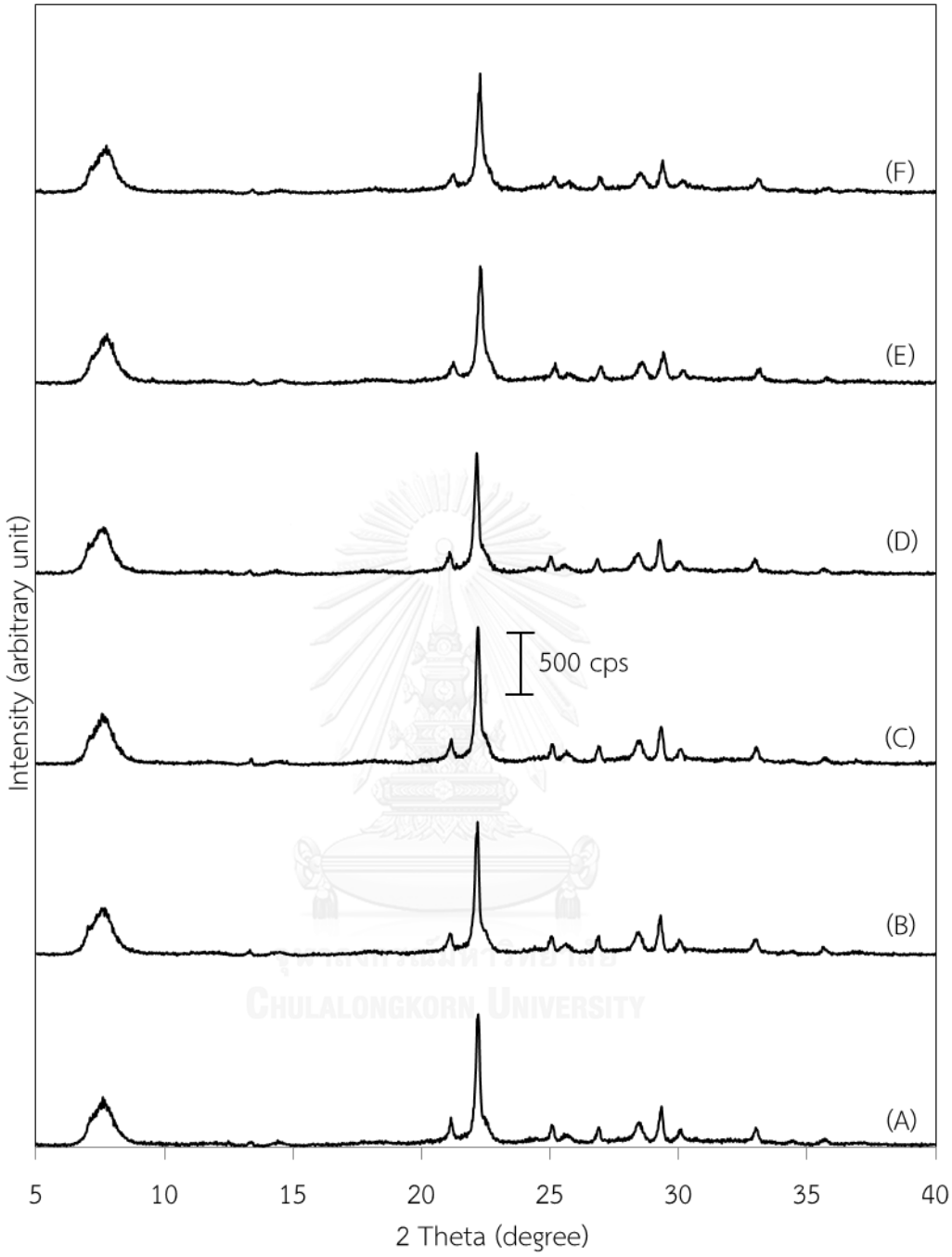

Figure 4.42 XRD patterns of calcined zeolite beta samples prepared with various seed amounts at 130 °C: (A) BEA-0.17%s-130°C-5d; (B) BEA-0.33%s-130°C-3d; (C) BEA-0.50%s-130°C-3d; (D) BEA-0.66%s-130°C-3d; (E) BEA-0.83%s-130°C-2d and (F) BEA-1.00%s-130°C-2d

4.3.3.2 Field Emission Scanning Electron Microscopy Images

The morphology of calcined zeolite beta products prepared with various seed amounts at 130 °C: BEA-0.17%s-130°C-5d; BEA-0.33%s-130°C-3d and BEA-0.83%s-130°C-2d were investigated by using FESEM. All FESEM images in Figure 4.29 exhibit truncated square bipyramidal morphology of zeolite beta crystals with different sizes in the decreasing order of BEA-0.17%s-130°C-5d>BEA-0.33%s-130°C-3d>BEA-0.83%s-130°C-2d. The BEA-0.17%s-130°C-5d product presents the largest crystal average size of 620 nm x 840 nm as shown in Figure 4.29 (A and B). The BEA-0.33%s-130°C-3d product shows smaller crystal average size which is 370 nm x 550 nm as shown in Figure 4.29 (B). The crystal average size of BEA-0.83%s-130°C-2d was about 140 nm x 150 nm as shown in Figure 4.29 (C). It can illustrate that the amount of crystalline nanoseeds strongly affects the crystal sizes depending on the crystallization rate. When lower amounts of crystalline nanoseeds were added into starting gel, crystallization rate of zeolite beta formation was slower resulting in the larger crystal size of zeolite beta. This is in agreement with, Kamimura, Y. *et al.* [24]. The small amount of crystalline nanoseeds provided small number of nuclei leading to the prolongation of nucleation step. While the longer period of synthesis, the bigger size of crystal was obtained attributed to the prolongation of crystal growth step [82].

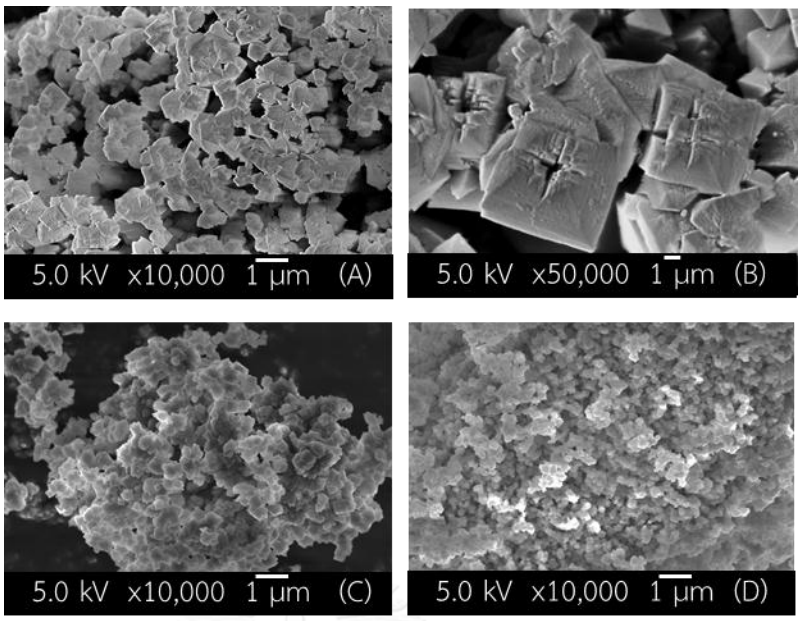

Figure 4.43 FESEM images of zeolite beta samples prepared with various seed amounts at 130 °C: (A and B) BEA-0.17%s-130°C-5d (C) BEA-0.33%s-130°C-3d and (D) BEA-0.83%s-130°C-2d

4.3.3.3 Nitrogen Adsosorption-Desorption Isotherms

The textural properties of calcined samples of BEA-0.17%s-130°C-5d, BEA-0.33%s-130°C-3d and BEA-0.83%s-130°C-2d were studied. Figure 4.30 illustrates the nitrogen adsorption-desorption isotherms of those three samples which are Type I, typical for microporous materials. At very low relative pressure the micropores was fully filled very fast due to the strong capillary effect. No adsorption behavior of mesopores at the intermediate relative pressure was observed. Adsorption at very high relative pressure indicates the adsorption on the external surface area. The isotherm of BEA-0.17%s-130°C-5d exhibits a little lower adsorbed amount of nitrogen than other two samples while the isotherms of the BEA-0.33%-130°C-3d and BEA-0.83%-130°C-2d are very close to each other. The adsorption-desorption isotherm of BEA-0.17%s-130°C-5d

exhibits no hysteresis loop indicating the uniform pore size but the others two samples exhibit hysteresis loops showing non-uniform pore sizes.

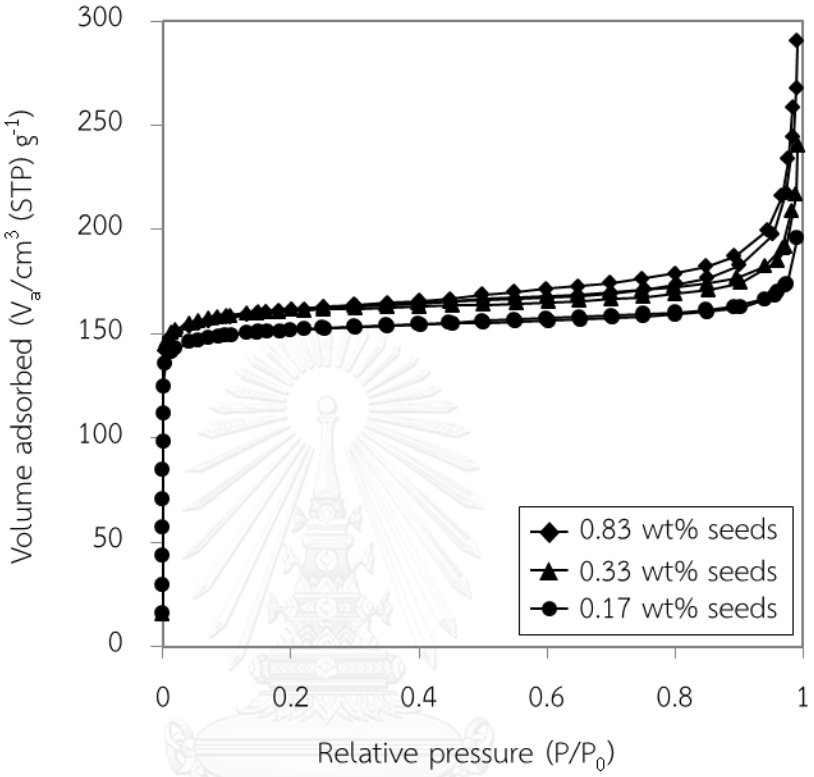

Figure 4.44 Nitrogen adsorption-desorption isotherms of calcined zeolite beta products prepared with various seed amounts at 130 °C: BEA-0.17%s-130°C-5d; BEA-0.33%s-130°C-3d and BEA-0.83%s-130°C-2d

Table 4.3 compiles the textural properties of zeolite beta samples: BEA-0.17%s-130°C-5d: BEA-0.33%s-130°C-3d and BEA-0.83%s-130°C-2d. The BET surface areas of BEA-0.17%s-130°C-5d and BEA-0.33%s-130°C-3d are about the same (621 and 618 m^2/g, respectively) but BEA-0.17%s-130°C-5d shows a little lower BET specific surface area of 595 m^2/g. The BEA-0.83%s-130°C-2d shows the greatest external surface area of 33.4 m^2/g, while BEA-0.17%-130°C-5d and BEA-0.33%-130°C-3d illustrate lower external surface areas of 22.5 and 24.6 m^2/g. All three samples

have similar micropore volumes and pore size distributions confirming the same type of zeolite structure. The distribution data of pore sizes determining by the MP-plot method was shown in Figure 4.31. Only one peak at 0.7 nm was obtained confirming the structure of zeolite beta in all three samples.

Table 4.3 Textural properties of calcined zeolite beta products synthesized at 130 ℃ with various periods of crystallization

Sample code	BET plot	t-plot		MP-plot
	specific surface area (m^2/g)	external surface area (m^2/g)	micropore volume (cm^3/g)	micropore size distribution (nm)
BEA-0.17%s-130℃-5d	595	22.5	0.23	0.7
BEA-0.33%s-130℃-3d	621	24.6	0.24	0.7
BEA-0.83%s-130℃-2d	618	33.4	0.24	0.7

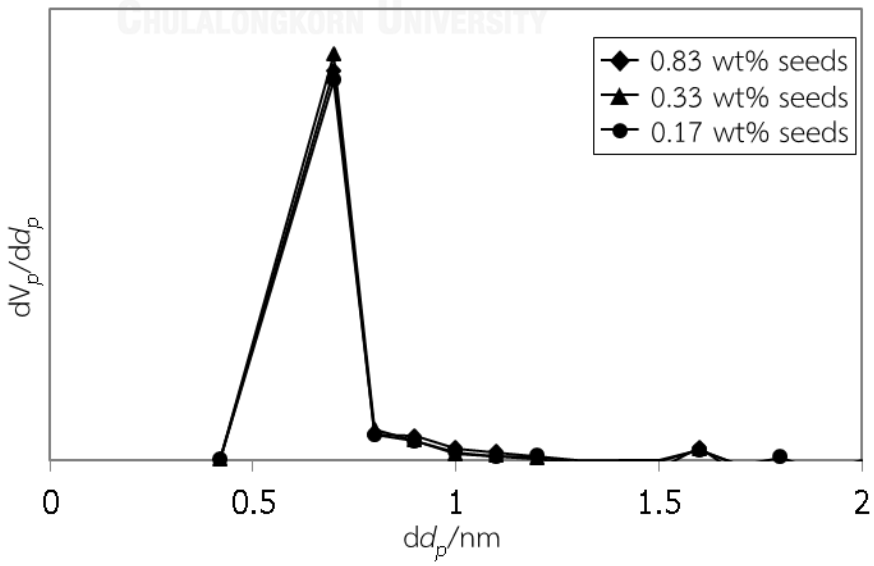

Figure 4.45 MP plots for pore size distribution of calcined zeolite beta products prepared at 130 °C: BEA-0.17%s-130°C-5d; BEA-0.33%s-130°C-3d and BEA-0.83%s-130°C-2d

4.3.3.4 ^{27}Al-MAS-NMR Spectra

^{27}Al-MAS-NMR spectra of as-synthesized and calcined zeolite beta samples crystallized at 130 °C with various seed amounts and various crystallization periods are demonstrated in Figure 4.31 and Figure 4.32. The spectra of both as-synthesized and calcined zeolite beta products present only one stong signal centered around 56 ppm which corresponds to the tetrahedral site of aluminium atoms in zeolite framework. No signal at 0 ppm was observed for both as-synthesized and calcined samples refers to the absence of octrahedrally coordination non-framework aluminium. These results confirm that there are no dealumination from the framework tetrahedral site to non-famework site upon the calcination. Thus, it can be concluded that the zeolite beta products synthesized by addition of crystalline nanoseeds have high thermal stability which is in agreement with the XRD results. In contrast to the ^{27}Al-MAS-NMR spectra of zeolite beta samples prepared by the template-assisted method where the NMR peak at 0 ppm was observed after calcination as shown in Figure 4.34. Thus, dealumination can be take place in the latter case.

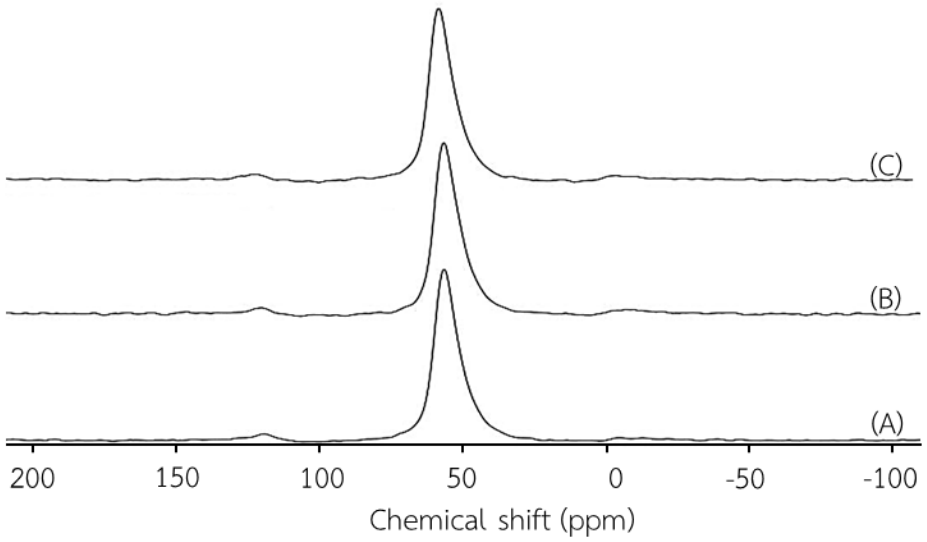

Figure 4.46 ^{27}Al-MAS-NMR spectra of as-synthesized zeolite beta products crystallized at 130 °C: (A) BEA-0.17%s-130°C-5d; (B) BEA-0.33%s-130°C-3d and (C) BEA-0.83%s-130°C-2d

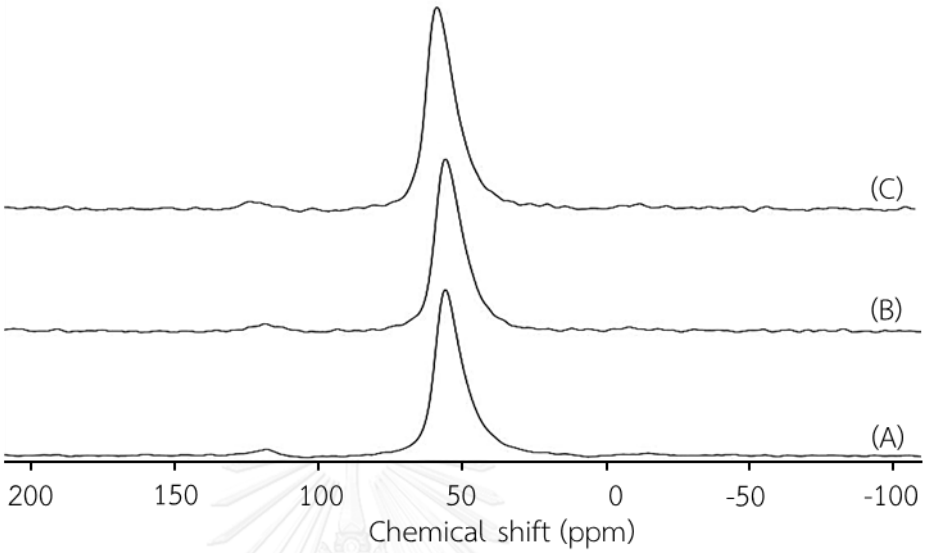

Figure 4.47 ^{27}Al-MAS-NMR spectra of calcined zeolite beta products crystallized at 130 °C: (A) BEA-0.17%s-130°C-5d; (B) BEA-0.33%s-130°C-3d and (C) BEA-0.83%s-130°C-2d

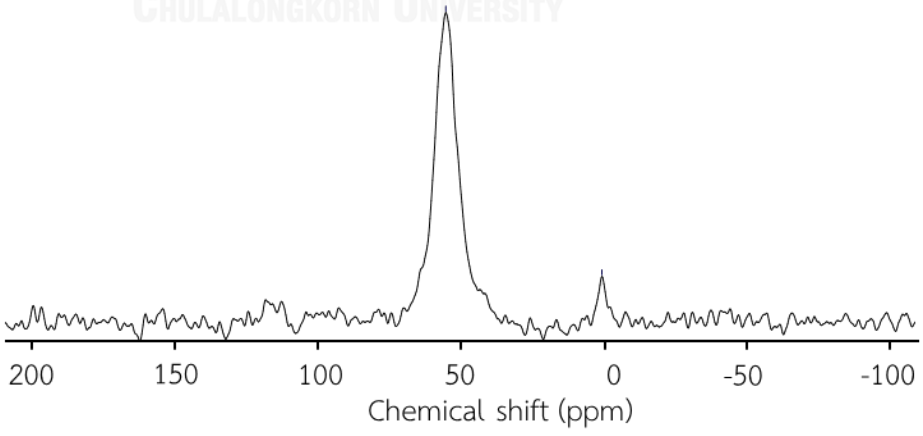

Figure 4.48 ^{27}Al-MAS-NMR spectra of calcined zeolite beta product prepared by the template-assisted method.

4.3.3.5 Elemental Analysis

Total aluminium atoms in the catalysts were determined by ICP-MS and Si was calculated by subtraction of Al from the total number of tetrahedral atoms, known as 64 atoms per unit cell of zeolite beta. The Si/Al mole ratios in gel were calculated from reagent amounts. The Si/Al mole ratios in gel and in the pure zeolite beta catalysts obtained from different seed amounts were shown in Table 4.4. It was found that the Si/Al moles ratios in gel were remarkably higher than the Si/Al moles ratios in catalysts. Even though there is no octahedral aluminium peak observed at the chemical shift near 1 ppm in ^{27}Al-MAS-NMR spectra, section 4.3.3.4 for both as-synthesized and calcined zeolite beta products. Total aluminium atoms were determined by ICP-MS. There is no significant difference between Si/Al ratios in those catalysts which are in a range of 8.8-10.0.

Table 4.4 Si/Al mole ratios of calcined zeolite beta samples prepared under different crystallization conditions

Sample	SiO_2/Al_2O_3 mole ratio in gel[a]	SiO_2/Al_2O_3 mole ratio in catalyst[b]
BEA-0.17%s-5d	37	9.9
BEA-0.33%s-3d	37	8.8
BEA-0.83%s-2d	37	10.0

[a] calculated from reagent quantities.

[b] Aluminium was determined by ICP-MS

4.4 Activities of Zeolite Beta Catalysts in Acetalization of Glycerol to Solketal

4.4.1 Effect of Catalyst Amounts

In order to study the effect of catalyst amounts on the acetalization of glycerol to solketal, different amounts of calcined H^+-BEA-0.17%s-130°C-5d catalyst were used. The reactions were carried out at the boiling temperature under reflux and atmospheric pressure with the glycerol to acetone mole ratio of 1:2. Figure 4.35 demonstrates conversions of glycerol, selectivities to solketal and solketal yields using various amounts of catalyst. Without the catalyst, no glycerol conversion was observed (not shown). The glycerol conversion increases when the catalyst loading was raised from 1 wt% to 20 wt%. It is obvious that the catalyst amount is a factor playing a key role in the conversion of glycerol. This may be explained by the increase of number of active sites available in the zeolite beta catalyst, resulting in higher glycerol conversion similarly observed in a previous study [41]. The longer spent time, the higher conversions were found for all catalyst loadings. The highest conversion of glycerol was achieved in the presence of 20 wt% of catalyst after 150 minutes of reaction. Considering Figure 4.35 (B), selectivity of H^+-BEA-0.17%s-130°C-5d catalyst to solketal was increased with the increment of the catalyst amount. Prolongation of reaction time, a small increment of selectivity was observed for all catalyst amounts. In the presence of 2 wt% of catalyst, the selectivity to solketal is around 55% while those in the presence of higher catalyst amounts are in the range of 82-98%. There are slight difference in selectivity compared among the catalyst loadings of 5, 10 and 20 wt%. The values of solketal yield can be described in the same way as conversion. The yield of solketal reaches the maximum level at around 20% after 150 minutes of reaction with 20 wt% of catalyst adding. Thus, the catalyst amount of 20 wt% referred to glycerol providing the highest glycerol conversion with the highest selectivity to solketal is selected as the optimal catalyst amount for studies on other parameters.

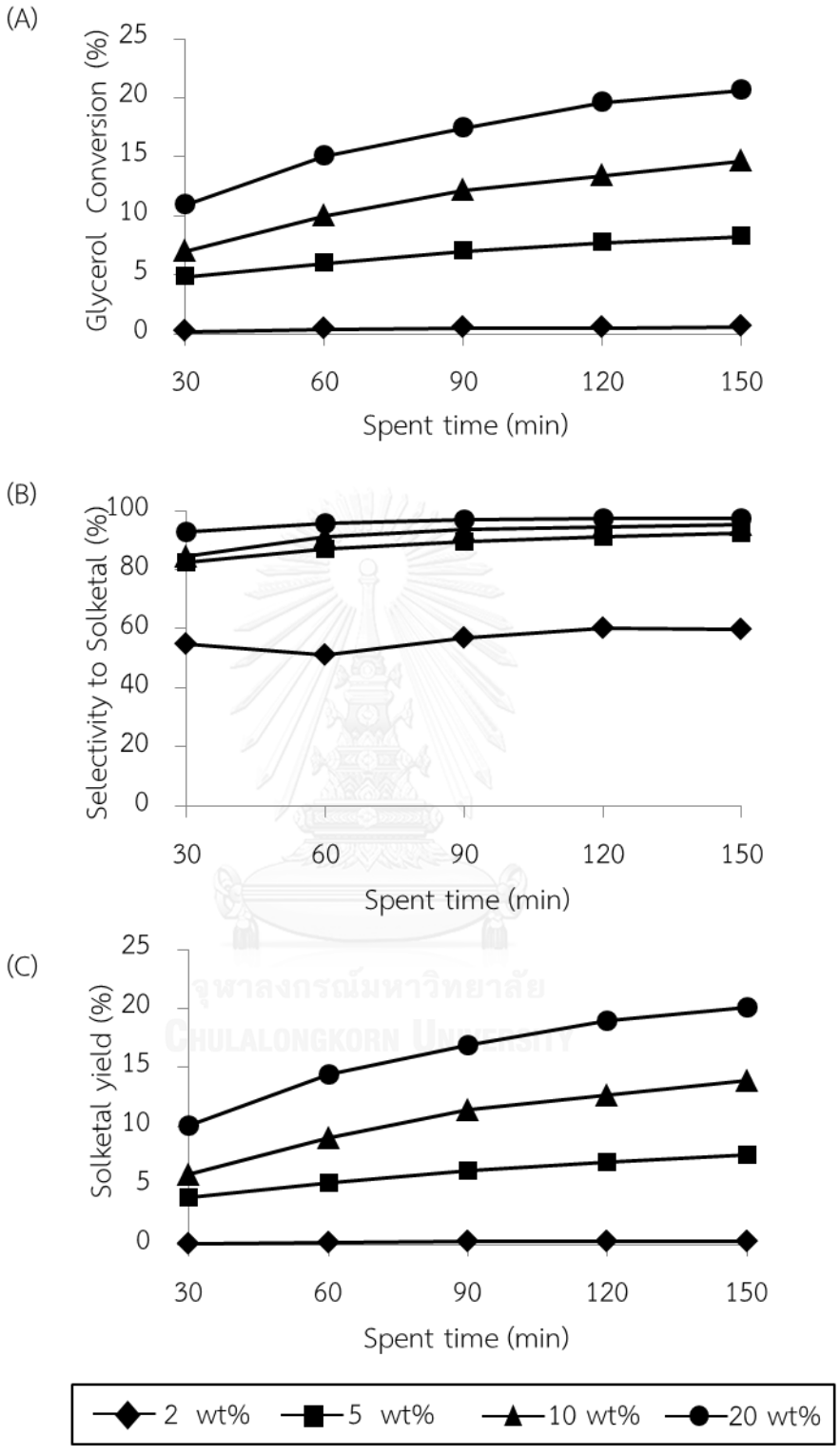

Figure 4.49 Effect of catalyst amounts on acetalization of glycerol to solketal at boiling temperature under reflux with the glycerol to acetone mole ratio of 1:2

4.4.2 Effect of Glycerol to Acetone Mole Ratio

The catalytic reaction between glycerol and acetone were carried out at boiling temperature under reflux for 150 minutes using 20 wt% of H^+-BEA-0.17%s-130°C-5d catalyst with respect to glycerol. The mole ratio of glycerol to acetone was varied in a range of 1:2, 1:4, 1:6 and 1:10 and the catalyst activities were shown in Figure 4.36. There is no significant difference in glycerol conversion with the increase of glycerol to acetone mole ratio from 1:2 to 1:6. However, slightly higher conversion was found when the mole ratio of glycerol to acetone is 1:10. This may be resulted from the increase in accessibility of acetone with glycerol according to higher amount of acetone. While selectivity values show a little lower when more acetone was used. All the mole ratios provided the high selectivities of solketal in the range of 82-97%. Glycerol to acetone mole ratio of 1:10 was found to be the optimal value for further studied since it provided the glycerol conversion up to 30% with selectivity to solketal as high as 91%.

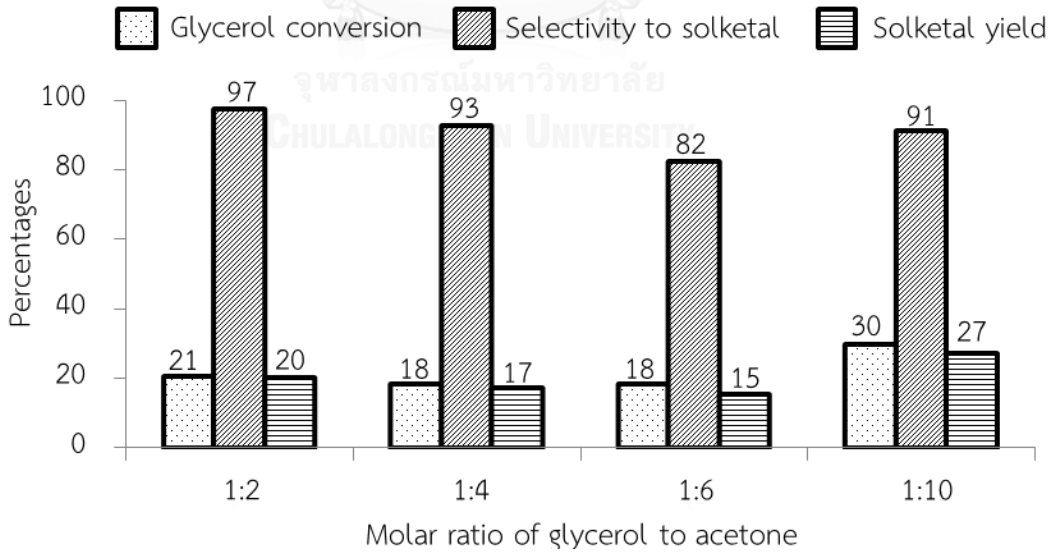

Figure 4.50 Effect of glycerol to acetone mole ratio on acetalization of glycerol to solketal after 150 minutes of reaction at boiling temperature under reflux using 20 wt% of zeolite beta catalyst

4.4.3 Effect of Crystalline Nanoseed Amounts in Catalyst

The acetalization of glycerol was carried out at boiling temperature for the reaction time 150 minutes with mole ratios of glycerol to acetone of 1:10 using 20 wt% of zeolite beta catalysts, namely H^+-BEA-0.17%s-130°C-5d, H^+-BEA-0.33%s-130°C-3d and H^+-BEA-0.83%s-130°C-2d. All of them gave slightly different glycerol conversion of 30, 32 and 35%, respectively with an average solketal selectivity of 91%. This is because all of the zeolite beta catalysts having very close values of Si/Al mole ratios of 8.8-10.0 as reported in Table 4.4 which can imply to similar acidities. Moreover, they have almost equal surface area and micropore volume as reported in the previous section. As we know that the reactants have to reach the acid sites in the zeolite pores. Thus, slightly higher activity of H^+-BEA-0.83%s-130°C-2d than other samples could be attributed to an easy diffusivity of reactant molecules in the short path length due to its smaller crystal size as shown Figure 4.29. Considering solketal yields which are in the same trend as glycerol conversion, the zeolite beta with 10 wt% of crystalline nanoseeds exhibited the highest solketal yield of 33% and 93% selectivity to solketal. Based on the above results, the H^+-BEA-0.83%s-130°C-2d was selected as the best catalyst for acetalization of glycerol to solketal.

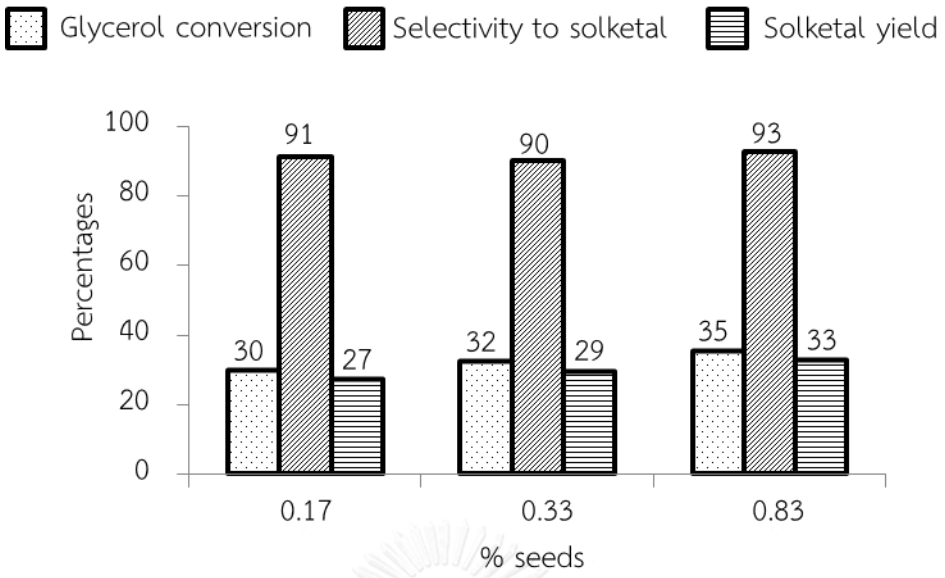

Figure 4.51 Effect of seed amounts used in preparation of the zeolite beta catalysts on acetalization of glycerol to solketal

4.4.4 Catalyst Reuse

4.4.4.1 X-ray Powder Diffraction Patterns

The H^+-BEA-0.83%s-130°C-2d catalyst was reused to study the catalytic stability. The reaction was carried out at boiling temperature for 150 minutes with the mole ratio of glycerol to acetone of 1:10. An amount of 20 wt% of the selected zeolite beta catalyst was added to the reaction medium. After the first run, the color of BEA-0.83%s-130°C-2d catalyst remained white but it became ivory after the second catalytic run. However, after calcination at 550 °C for 5 hours, the used catalyst turned to white. The XRD patterns of the calcined unused and regenerated catalyst are presented in Figure 4.38. After the catalytic reaction, the XRD patterns of fresh and used catalyst samples were still corresponded to the BEA structure. Only 5 and 11% decrease in intensities of the peak at 2θ of 22.2° was observed for the 1^{st} regenerated and 2^{nd} regenerated BEA-0.83%s-130°C-2d catalysts, respectively.

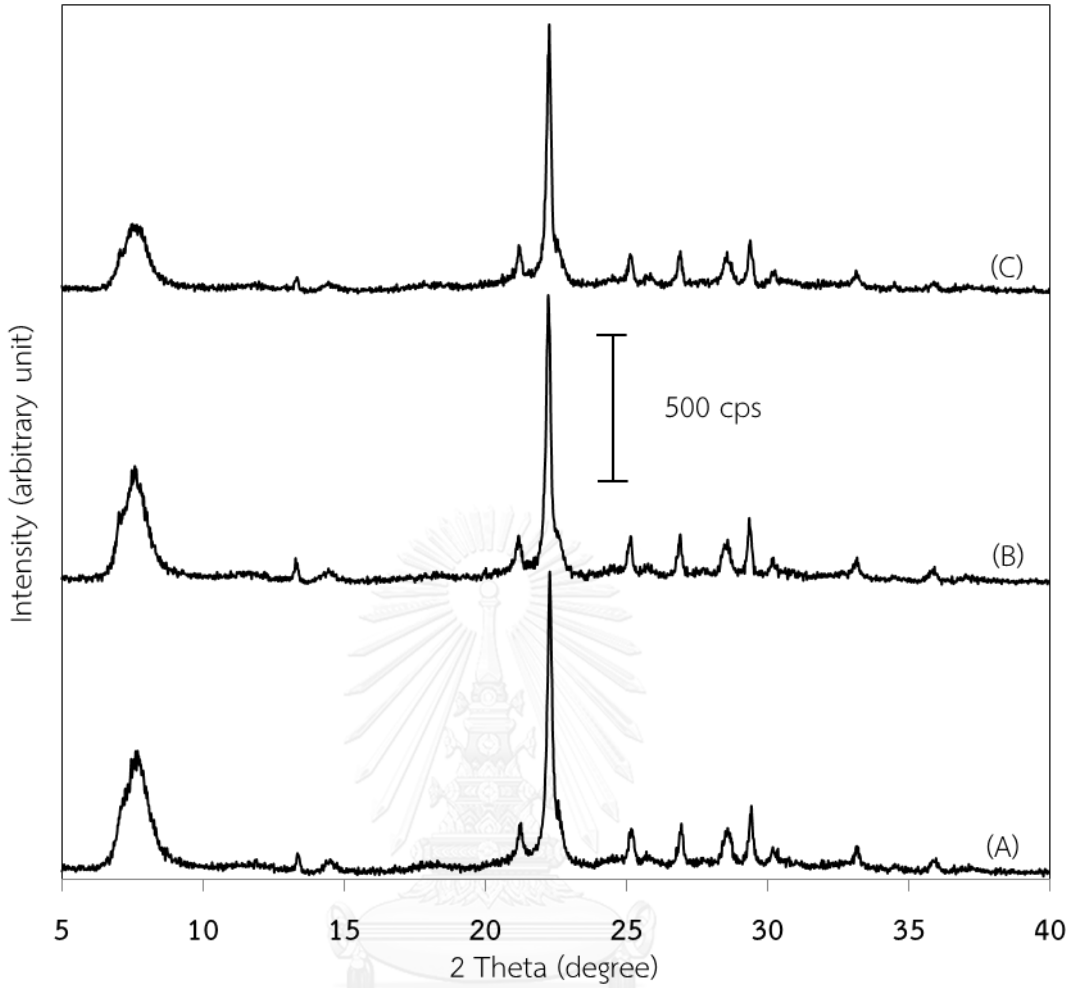

Figure 4.52 XRD patterns of (A) the fresh (B) the 1st regenerated and (C) the 2nd regenerated BEA-0.83%s-130°C-2d catalyst

4.4.4.2 Field Emission Scanning Electron Microscopy Images

FESEM images of the regenerated BEA-0.83%s-130°C-2d sample were shown in Figure 4.39 which reveals almost the same morphology and particle size of the regenerated zeolite beta particles compared to those of the fresh catalyst which has been shown in Figure 4.29 (C).

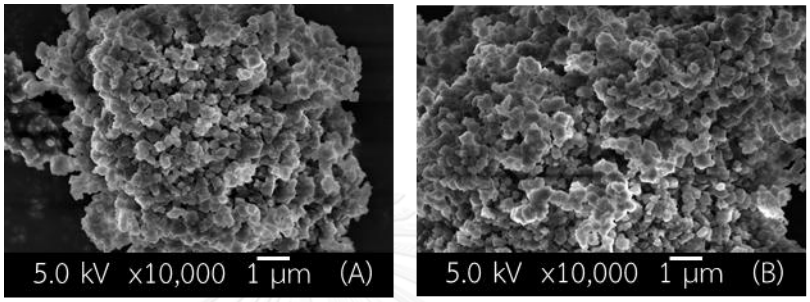

Figure 4.53 FESEM images of (A) the 1st regenerated and (B) the 2nd regenerated H^+-BEA-0.83%s-130°C-2d samples

4.4.4.3 Activity of Regenerated Zeolite Beta in Acetalization of Glycerol to Solketal

The spent zeolite beta catalyst after the first run was regenerated by calcination before reuse in order to study the catalytic activities and its life time. Figure 4.40 presents the glycerol conversion, selectivity to solketal and solketal yield of the fresh and regenerated catalysts under the same conditions. The regenerated catalyst demonstrated almost equal activity as the fresh catalyst. A slight decrease in selectivity to solketal and solketal yield was observed. This result is in agreement with the XRD results and FESEM images as reported in sections 4.4.4.1 and 4.4.4.2. The regenerated catalyst exhibited only 2% lower of glycerol conversion than that of the fresh catalyst indicating the good catalytic stability of zeolite beta sample prepared by seed-assisted method using the on-site crystalline nanoseeds.

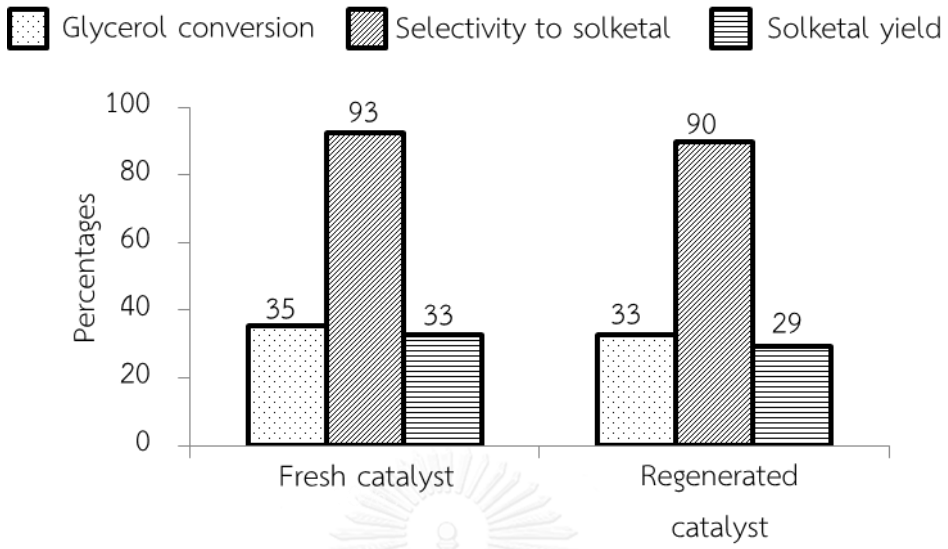

Figure 4.54 Catalytic performance of regenerated zeolite beta in acetalization of glycerol to solketal

CHAPTER V
CONCLUSION

Highly thermal stable zeolite beta was successfully synthesized by the nanoseed-assisted method using fumed silica as the silica source mixed with sodium aluminate and sodium hydroxide. The starting gel with a composition of SiO_2:0.027Al_2O_3:0.36Na_2O:35H_2O was hydrothermally crystallized under autogenous pressure. Crystallization temperature played an important role in zeolite structure and crystallinity. Adding the seed amount of 0.17 wt% to the starting gel provided pure zeolite beta with the highest crystallinity after crystallization at 130 °C for 5 days. Prolongation of crystallization period led to formation of the impurity of zeolites Na-P1 and mordenite and so did the increase in temperature. Larger seed amount than 0.17 wt% reduced crystallization time required for achievement of pure zeolite beta with maximum crystallinity. The amounts of 0.83 and 1.00 wt% seeds provided the maximum crystallinity after 2 days while 0.33 to 0.66 wt% seed amounts does after 3 days. Upon increasing nanoseed amounts from 0.17 to 0.83 wt%, the calcined samples of zeolite beta have the drastic change in crystal sizes from 620 nm x 840 nm to 140 nm x 150 nm. The zeolite samples have BET specific surface area about 600 m^2/g and micropore volume of 0.24 cm^3/g. The pore size distribution was found in a range of micropores with an average pore size of 0.7 nm. After calcination at evaluated temperature, all seed-assisted zeolite samples still show the XRD patterns comparable to those of as-synthesized ones with only a small decrease of crystallinity, indicating the high thermal stability of zeolite beta products prepared by the seed-assisted synthesis. ^{27}Al-MAS-NMR spectra suggested no dealumination upon calcination. The zeolite catalysts contained SiO_2/Al_2O_3 ratios in a range of 8.8-10.0 which is significantly lower than those in the starting gel.

The zeolite beta samples prepared by the nanoseed-assisted method were applied as catalysts in acetalization of glycerol with acetone using dimethylformamide as solvent. The highest glycerol conversion of 35% with 93% selectivity to solketal were achieved after a reaction time of 150 minutes using zeolite beta sample prepared by adding the nanoseed amount of 0.83 wt% to initial gel weight. The used catalyst was regenerated by calcinations and maintained similar activity comparing to the fresh catalyst.

The suggestions for future work

1. Zeolite beta samples with different Si/Al mole ratios should be prepared by the nanoseed-assisted method and studied for their catalytic activities.
2. Effect of solvent on catalytic activity in acetalization of glycerol to solketal should be studied.

REFERENCES

[1] Bárcia, P.S., Silva, J.A.C., and Rodrigues, A.E. Adsorption equilibrium and kinetics of branched hexane isomers in pellets of beta zeolite. Microporous and Mesoporous Materials 79(1–3) (2005): 145-163.

[2] Newsam, J.M., Treacy, M.M.J., Koetsier, W.T., and Gruyter, C.B.D. Structural Characterization of Zeolite Beta. Vol. 420. London: The Royal Society, 1988.

[3] Mohammadi-Manesh, H., Tashakor, S., and Alavi, S. Diffusion of benzene through the beta zeolite phase. Microporous and Mesoporous Materials 181 (2013): 29-37.

[4] Kim, J.-C., Cho, K., and Ryoo, R. High catalytic performance of surfactant-directed nanocrystalline zeolites for liquid-phase Friedel–Crafts alkylation of benzene due to external surfaces. Applied Catalysis A: General 470 (2014): 420-426.

[5] Sridevi, U., Bokade, V.V., Satyanarayana, C.V.V., Rao, B.S., Pradhan, N.C., and Rao, B.K.B. Kinetics of propylation of benzene over H-beta and SAPO-5 catalysts: a comparison. Journal of Molecular Catalysis A: Chemical 181(1–2) (2002): 257-262.

[6] Wu, Y., Tian, F., Liu, J., Song, D., Jia, C., and Chen, Y. Enhanced catalytic isomerization of ***α***-pinene over mesoporous zeolite beta of low Si/Al ratio by NaOH treatment. Microporous and Mesoporous Materials 162 (2012): 168-174.

[7] Ha, L., Mao, J., Zhou, J., Zhang, Z.C., and Zhang, S. Skeletal isomerization of unsaturated fatty acids on beta zeolites: Effects of calcination temperature and additives. Applied Catalysis A: General 356(1) (2009): 52-56.

[8] Ramos, M.J., de Lucas, A., Jiménez, V., Sánchez, P., and Valverde, J.L. Hydroisomerization of different refinery naphtha streams by using a beta zeolite catalyst. Fuel Processing Technology 89(8) (2008): 721-727.

[9] Taufiqurrahmi, N., Mohamed, A.R., and Bhatia, S. Deactivation and coke combustion studies of nanocrystalline zeolite beta in catalytic cracking of used palm oil. Chemical Engineering Journal 163(3) (2010): 413-421.

[10] Tarach, K., et al. Catalytic cracking performance of alkaline-treated zeolite beta in the terms of acid sites properties and their accessibility. Journal of Catalysis 312 (2014): 46-57.

[11] Renzini, M.S., Lerici, L.C., Sedran, U., and Pierella, L.B. Stability of ZSM-11 and beta zeolites during the catalytic cracking of low-density polyethylene. Journal of Analytical and Applied Pyrolysis 92(2) (2011): 450-455.

[12] Peters, T.A., Benes, N.E., Holmen, A., and Keurentjes, J.T.F. Comparison of commercial solid acid catalysts for the esterification of acetic acid with butanol. Applied Catalysis A: General 297(2) (2006): 182-188.

[13] Satyarthi, J.K., Radhakrishnan, S., and Srinivas, D. Factors influencing the kinetics of esterification of fatty acids over solid acid catalysts. Energy and Fuels 25(9) (2011): 4106-4112.

[14] da Silva, C.X.A. and Mota, C.J.A. The influence of impurities on the acid-catalyzed reaction of glycerol with acetone. Biomass and Bioenergy 35(8) (2011): 3547-3551.

[15] Maksimov, A.L., Nekhaev, A.I., Ramazanov, D.N., Arinicheva, Y.A., Dzyubenko, A.A., and Khadzhiev, S.N. Preparation of high-octane oxygenate fuel components from plant-derived polyols. Petroleum Chemistry 51(1) (2011): 61-69.

[16] da Silva, C.X.A., Goncalves, V.L.C., and Mota, C.J.A. Water-tolerant zeolite catalyst for the acetalisation of glycerol. Green Chemistry 11(1) (2009): 38-41.

[17] Wadlinger, R.L.K., G.T.; and Rosinski, E.J. Catalytic composition of a crystalline zeolite. 1967.

[18] Bekkum, H.V. and Kouwenhoven, H.W. Progress in the use of zeolites in organic synthesis. in Cejka, J., Bekkum, H.V., Corma, A., and Schuth, F. ,Introduction to Zeolite Molecular Sieves, pp. 947-998. London: Elsevier, 2007.

[19] Mintova, S., Valtchev, V., Onfroy, T., Marichal, C., Knözinger, H., and Bein, T. Variation of the Si/Al ratio in nanosized zeolite beta crystals. Microporous and Mesoporous Materials 90(1–3) (2006): 237-245.

[20] Otomo, R., Yokoi, T., Kondo, J.N., and Tatsumi, T. Dealuminated beta zeolite as effective bifunctional catalyst for direct transformation of glucose to 5-hydroxymethylfurfural. Applied Catalysis A: General 470 (2014): 318-326.

[21] Zhang, H., et al. Rational synthesis of beta zeolite with improved quality by decreasing crystallization temperature in organotemplate-free route. Microporous and Mesoporous Materials 180 (2013): 123-129.

[22] Majano, G., Delmotte, L., Valtchev, V., and Mintova, S. Al-rich zeolite beta by seeding in the absence of organic template. Chemistry of Materials 21(18) (2009): 4184-4191.

[23] Xie, B., Song, J., Ren, L., Ji, Y., Li, J., and Xiao, F.-S. Organotemplate-free and fast route for synthesizing beta zeolite. Chemistry of Materials 20(14) (2008): 4533-4535.

[24] Kamimura, Y., Chaikittisilp, W., Itabashi, K., Shimojima, A., and Okubo, T. Critical factors in the seed-assisted synthesis of zeolite beta and "green beta" from OSDA-free Na^{+}-aluminosilicate gels. Asian Journal of Chemistry 5(10) (2010): 2182-91.

[25] Kamimura, Y., et al. Crystallization behavior of zeolite beta in OSDA-free, seed-assisted synthesis. The Journal of Physical Chemistry C 115(3) (2011): 744-750.

[26] Xie, B., et al. Seed-directed synthesis of zeolites with enhanced performance in the absence of organic templates. Chemical Communications 47(13) (2011): 3945-3947.

[27] Zheng, B., et al. Mechanism of seeding in hydrothermal synthesis of zeolite beta with organic structure-directing agent-free gel. Chinese Journal of Catalysis 35(11) (2014): 1800-1810.

[28] Atabani, A.E., Silitonga, A.S., Badruddin, I.A., Mahlia, T.M.I., Masjuki, H.H., and Mekhilef, S. A comprehensive review on biodiesel as an alternative energy resource and its characteristics. Renewable and Sustainable Energy Reviews 16(4) (2012): 2070-2093.

[29] Behr, A., Eilting, J., Irawadi, K., Leschinski, J., and Lindner, F. Improved utilisation of renewable resources: New important derivatives of glycerol. Green Chemistry 10(1) (2008): 13-30.

[30] Leoneti, A.B., Aragão-Leoneti, V., and de Oliveira, S.V.W.B. Glycerol as a by-product of biodiesel production in Brazil: Alternatives for the use of unrefined glycerol. Renewable Energy 45 (2012): 138-145.

[31] Lauriol-Garbay, P., Millet, J.M.M., Loridant, S., Bellière-Baca, V., and Rey, P. New efficient and long-life catalyst for gas-phase glycerol dehydration to acrolein. Journal of Catalysis 280(1) (2011): 68-76.

[32] Kinage, A.K., Upare, P.P., Kasinathan, P., Hwang, Y.K., and Chang, J.-S. Selective conversion of glycerol to acetol over sodium-doped metal oxide catalysts. Catalysis Communications 11(7) (2010): 620-623.

[33] Lee, S.-H. and Moon, D.J. Studies on the conversion of glycerol to 1,2-propanediol over Ru-based catalyst under mild conditions. Catalysis Today 174(1) (2011): 10-16.

[34] Witsuthammakul, A. and Sooknoi, T. Direct conversion of glycerol to acrylic acid via integrated dehydration–oxidation bed system. Applied Catalysis A: General 413–414 (2012): 109-116.

[35] Silva, P.H.R., Gonçalves, V.L.C., and Mota, C.J.A. Glycerol acetals as anti-freezing additives for biodiesel. Bioresource Technology 101(15) (2010): 6225-6229.

[36] Ozorio, L.P., Pianzolli, R., Mota, M.B.S., and Mota, C.J.A. Reactivity of glycerol/acetone ketal (solketal) and glycerol/formaldehyde acetals toward acid-catalyzed hydrolysis. Journal of the Brazilian Chemical Society 23 (2012): 931-937.

[37] Royon, D., Locatelli, S., and Gonzo, E.E. Ketalization of glycerol to solketal in supercritical acetone. The Journal of Supercritical Fluids 58(1) (2011): 88-92.

[38] Monbaliu, J.-C.M., et al. Effective production of the biodiesel additive STBE by a continuous flow process. Bioresource Technology 102(19) (2011): 9304-9307.

[39] Suriyaprapadilok, N. and Kitiyanan, B. Synthesis of solketal from glycerol and its reaction with benzyl alcohol. Energy Procedia 9 (2011): 63-69.

[40] Menezes, F.D.L., Guimaraes, M.D.O., and da Silva, M.J. Highly selective $SnCl_2$-catalyzed solketal synthesis at room temperature. Industrial & Engineering Chemistry Research 52(47) (2013): 16709-16713.

[41] Ferreira, P., Fonseca, I.M., Ramos, A.M., Vital, J., and Castanheiro, J.E. Valorisation of glycerol by condensation with acetone over silica-included heteropolyacids. Applied Catalysis B: Environmental 98(1–2) (2010): 94-99.

[42] Nandan, D., Sreenivasulu, P., Sivakumar Konathala, L.N., Kumar, M., and Viswanadham, N. Acid functionalized carbon–silica composite and its application for solketal production. Microporous and Mesoporous Materials 179 (2013): 182-190.

[43] Zhao, W., Yi, C., Yang, B., Hu, J., and Huang, X. Etherification of glycerol and isobutylene catalyzed over rare earth modified Hβ-zeolite. Fuel Processing Technology 112 (2013): 70-75.

[44] Tesana, S. and Koovimol, A. Conversion of glycerol with acetone using zeolite beta as catalyst. Bachelor, Chemistry Chulalongkorn university, 2012.

[45] Clarkson, J.S., Walker, A.J., and Wood, M.A. Continuous reactor technology for ketal formation: An improved synthesis of solketal. Organic Process Research & Development 5(6) (2001): 630-635.

[46] Blakeman, P.G., et al. The role of pore size on the thermal stability of zeolite supported Cu SCR catalysts. Catalysis Today 231 (2014): 56-63.

[47] Nanda, M.R., Yuan, Z., Qin, W., Ghaziaskar, H.S., Poirier, M.-A., and Xu, C.C. Thermodynamic and kinetic studies of a catalytic process to convert glycerol into solketal as an oxygenated fuel additive. Fuel 117, Part A (2014): 470-477.

[48] Khayoon, M.S. and Hameed, B.H. Solventless acetalization of glycerol with acetone to fuel oxygenates over Ni–Zr supported on mesoporous activated carbon catalyst. Applied Catalysis A: General 464–465 (2013): 191-199.

[49] Breck, D.W. Zeolite Molecular Sieve: Structure, Chemistry, and use. New York: John Wiley & Sons, 1997.

[50] Secondary Building Units (SBU's) in zeolites [Online]. Available from: http://www.ch.ic.ac.uk/vchemlib/course/zeolite/structure.html [June 1]

[51] Xu, R., Pang, W., Yu, J., Huo, Q., and Che, J. Chemistry of Zeolites and Related Porous Materials: Synthesis and Structure. Singapore: John Wiley & Sons (Asia), 2007.

[52] Flanigen, M., Broach, R.W., and Wilson, S.T. Zeolites in Industrial Separation and Catalysis. Weinheim: WILEY-VCH Verlag GmbH & Co. KGaA, 2010.

[53] Santen, R.A.v. Theory of Brønsted acidity in zeolites. in Jansen, J.C., Stocker, M., Karge, H.G., and Weitkamp, J. ,Advance Zeolite Science and Applications, pp. 273-294. Netherlands: Elsevier Science B.V., 1994.

[54] Bhatia, S. Zeolite Catalysis: Principles and Applications. USA: CRC PRESS, 1990.

[55] Stöcker, M. Gas phase catalysis by zeolites. Microporous and Mesoporous Materials 82(3) (2005): 257-292.

[56] Payra, P. and Dutta, P.K. Zeolites: A primer. in Auerbach, S.M., Carrado, K.A., and Dutta, P.K. ,Handbook of Zeolite Science and Technology, p. 11. USA: Marcel Dekker, Inc., 2003.

[57] Cundy, C.S. and Cox, P.A. The hydrothermal synthesis of zeolites: Precursors, intermediates and reaction mechanism. Microporous and Mesoporous Materials 82(1–2) (2005): 1-78.

[58] Higgins, J.B., et al. The framework topology of zeolite beta. Zeolites 8(6) (1988): 446-452.

[59] Jansen, J.C., Creyghton, E.J., Njo, S.L., van Koningsveld, H., and van Bekkum, H. On the remarkable behaviour of zeolite beta in acid catalysis. Catalysis Today 38(2) (1997): 205-212.

[60] Sun, J., et al. Synthesis, surface and crystal structure investigation of the large zeolite beta crystal. Microporous and Mesoporous Materials 102(1–3) (2007): 242-248.

[61] Corma, A., Navarro, M.T., Rey, F., Rius, J., and Valencia, S. Pure polymorph C of zeolite beta synthesized by using framework isomorphous substitution as a structure-directing mechanism. Angewandte Chemie International Edition 40(12) (2001): 2277-2280.

[62] Lesley, E.S. and Elaine, A.M. Solid State Chemistry: An Introduction. Third ed. New York: CRC Press Taylor & Francis Group, 2005.

[63] Kokotailo, G.T. and Fyfe, C.A. Zeolite structure analysis with powder x-ray diffraction and solid-state NMR techniques The Rigaku Journal 12 (1995): 3-10.

[64] Powder pattern simulations of disordered intergrowths. in Treacy, M.M.J. and Higgins, J.B. (eds.),Collection of Simulated XRD Powder Patterns for Zeolites (fifth), pp. 477-485. Amsterdam: Elsevier Science B.V., 2007.

[65] Huggett, J.M. and Shaw, H.F. Field emission scanning electron microscopy; a high-resolution technique for the study of clay minerals in sediments. Clay Minerals 32(2) (1997): 197-203.

[66] Mukhopadhyay, S.M. Sample preparation for microscopic and spectroscopic characterization of solid surfaces and films. in Sample Preparation Techniques in Analytical Chemistry, pp. 377-411: John Wiley & Sons, Inc., 2003.

[67] Cauda, V., Onida, B., Platschek, B., Muhlstein, L., and Bein, T. Large antibiotic molecule diffusion in confined mesoporous silica with controlled morphology. Journal of Materials Chemistry 18(48) (2008): 5888-5899.

[68] Sing, K.S.W., et al. Reporting physisorption data for gas/solid systems. in Handbook of Heterogeneous Catalysis: Wiley-VCH Verlag GmbH & Co. KGaA, 2008.

[69] Balbuena, P.B. and Gubbins, K.E. Theoretical interpretation of adsorption behavior of simple fluids in slit pores. Langmuir 9(7) (1993): 1801-1814.

[70] Lowell, S., Shields, J., Thomas, M., and Thommes, M. Surface area analysis from the Langmuir and BET theories. in Characterization of Porous Solids and Powders: Surface Area, Pore Size and Density, pp. 58-81: Springer Netherlands, 2004.

[71] Batsala, M., Chandu, B., Sakala, B., Nama, S., and Domatoti, S. Inductively coupled plasma mass spectrometry (ICP-MS). International journal of research in pharmacy and chemistry 2(3) (2012): 671-680.

[72] Vollhardt, K., C., P., and Schore, N.E. Organic Chemistry: Structure and Function. New York: W.H. Freeman and Company, 2007.

[73] Klein, D.R. Organic Chemistry. Second ed.: Wiley, 2013.

[74] Zhao, D., et al. Triblock copolymer syntheses of mesoporous silica with periodic 50 to 300 angstrom pores. Science 279(5350) (1998): 548-552.

[75] Wanchai, K. and Chaisuwan, A. Catalytic cracking of polypropylene waste over zeolite beta. Chemistry and Materials Research 3(4) (2013): 31-41.

[76] Manjunathan, P., Maradur, S.P., Halgeri, A.B., and Shanbhag, G.V. Room temperature synthesis of solketal from acetalization of glycerol with acetone: Effect of crystallite size and the role of acidity of beta zeolite. Journal of Molecular Catalysis A: Chemical 396 (2015): 47-54.

[77] Sagarzazu, A. and González, G. Influence of TEA_2O/SiO_2 ratio on the polymorph formation and crystallization of zeolite beta. Materials Chemistry and Physics 138(2–3) (2013): 640-649.

[78] Liu, X.-d., Wang, Y.-p., Cui, X.-m., He, Y., and Mao, J. Influence of synthesis parameters on NaA zeolite crystals. Powder Technology 243 (2013): 184-193.

[79] Novembre, D., Gimeno, D., Pasculli, A., and Sabatino, B.D. Synthesis and characterization of solidalite using natural kaoline: An analytical and mathematical approach to simulate the loss in weight of chlorine during synthesis process. Fresenius Environmental Bulletin 19 (2010): 1109-1117.

[80] Halgeri, A.B. and Das, J. Novel catalytic aspects of beta zeolite for alkyl aromatics transformation. Applied Catalysis A: General 181(2) (1999): 347-354.

[81] Szostak, R. and Stepto, R.F.T. Molecular Sieves: Principles of Synthesis and Identification. Second ed. London: Blackie Academic & Professional, 1998.

[82] Cubillas, P. and Anderson, M.W. Synthesis mechanism: Crystal growth and nucleation. in Zeolites and Catalysis, pp. 1-55: Wiley-VCH Verlag GmbH & Co. KGaA, 2010.

APPENDIX

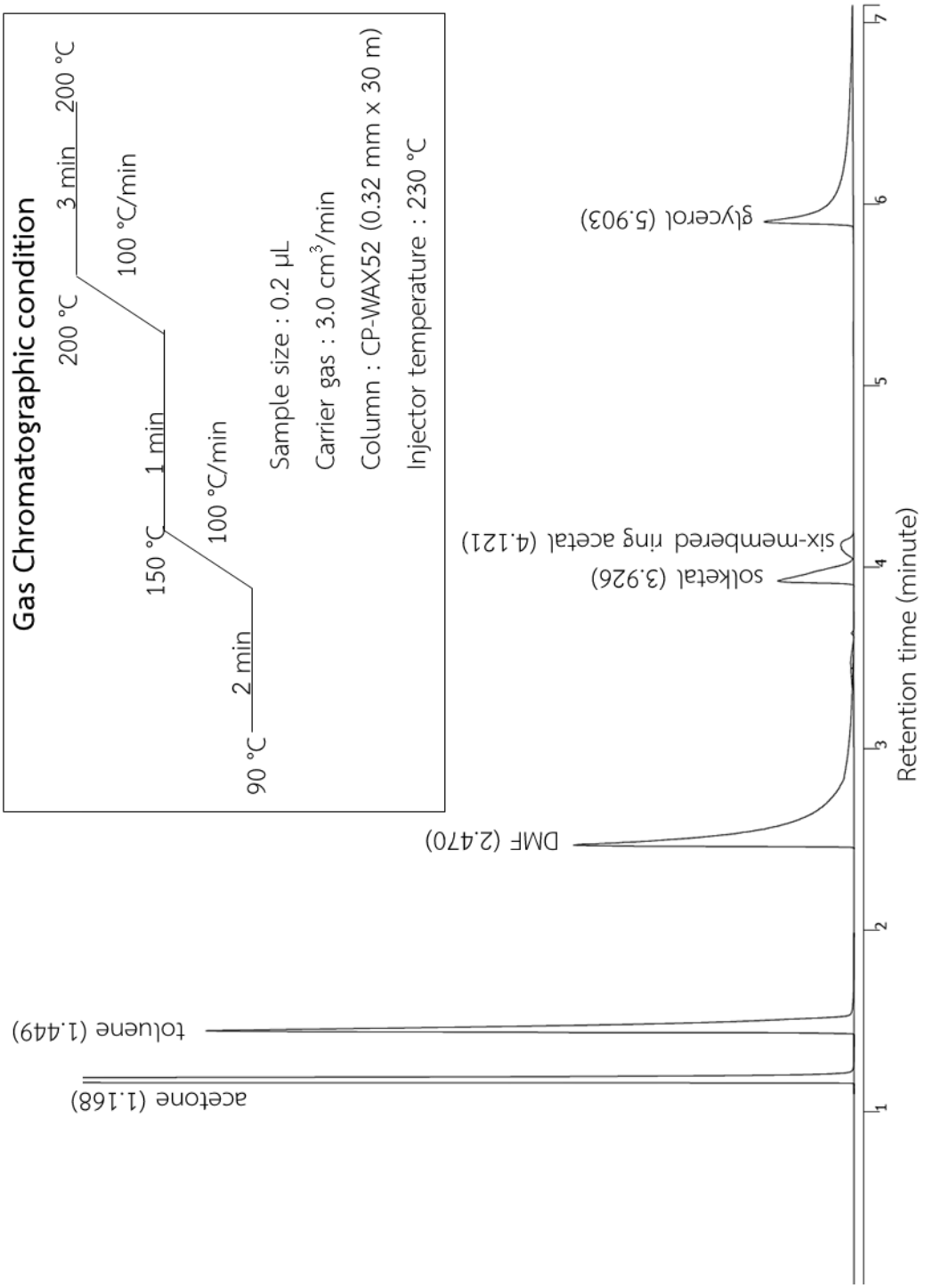

Figure A-1 A gas chromatogram illustrating the sample analysis of products (solketal and six-membered ring acetal) from the reaction of acetone and glycerol using DMF as solvent and toluene as the internal standard

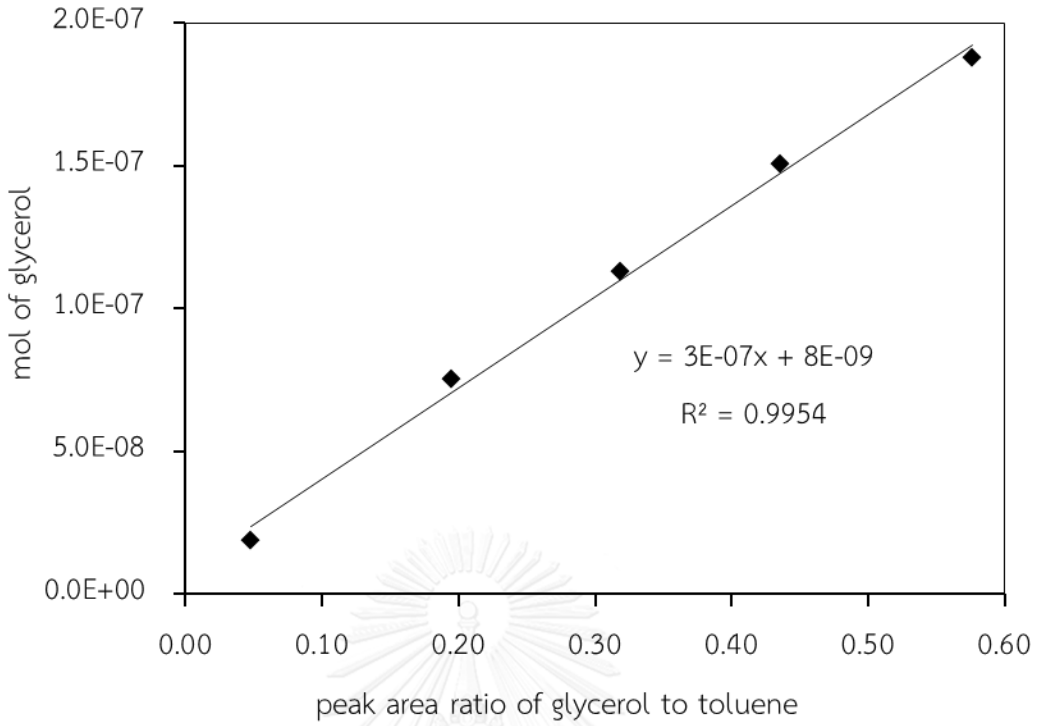

Figure A-2 Calibration curve of glycerol concentration analyzed by GC using toluene as the internal standard

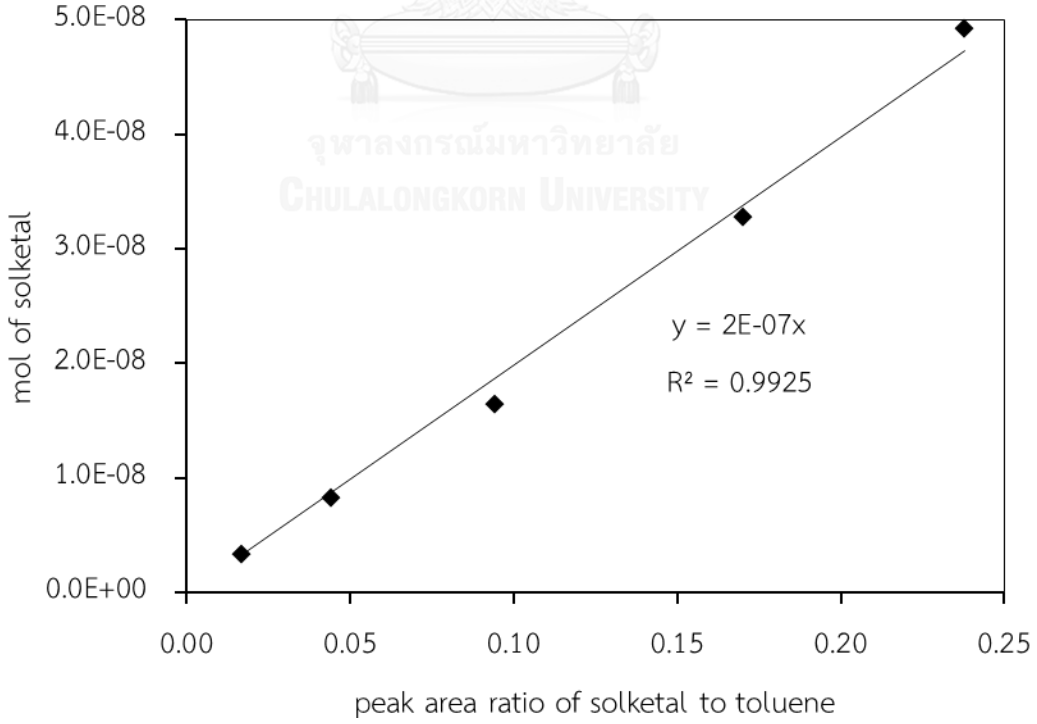

Figure A-3 Calibration curve of solketal analyzed by GC using toluene as the internal standard

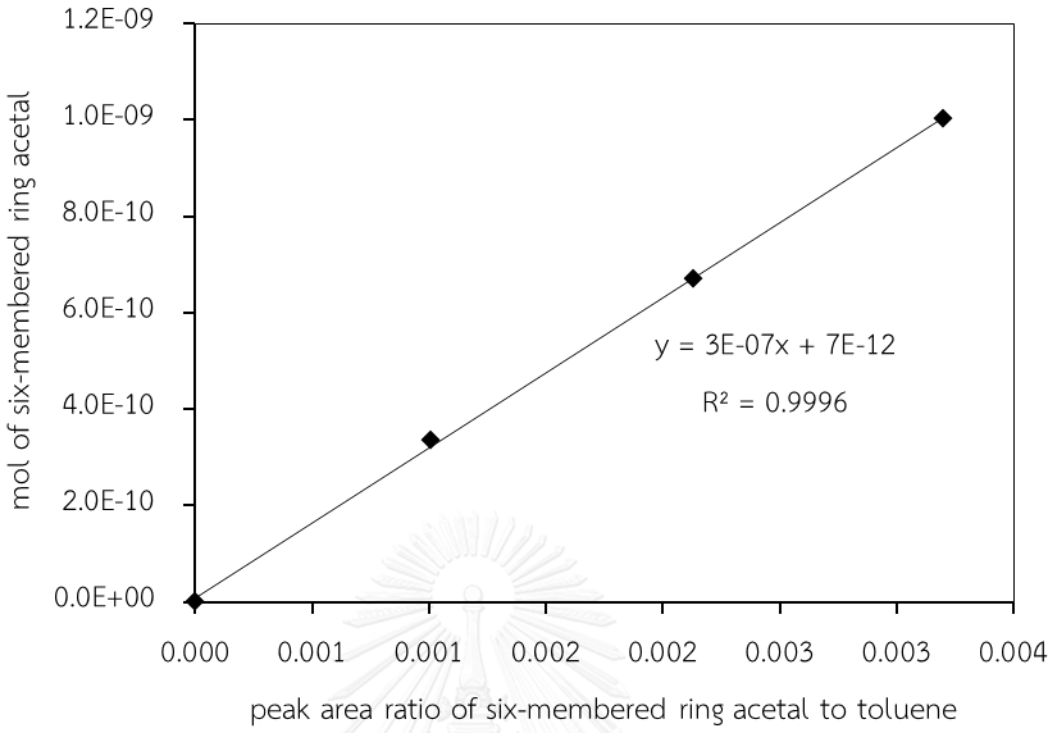

Figure A-4 Calibration curve of six-membered ring acetal analyzed by GC using toluene as the internal standard

VITA

Miss Siriluck Tesana was born on November 7, 1991 in Bangkok, Thailand. She graduated with Bachelor's Degree in Chemistry from Faculty of Science, Chulalongkorn University in 2013. She continued her study in Chemistry, Faculty of Science, Chulalongkorn University in 2013 and completed in 2015. She received the Science Achievement Scholarship of Thailand from Office of the Higher Education Commission for both undergraduate and graduate studies. She presented her research in Pure and Applied Chemistry International Conference (PACCON 2015) in the title of "Preparation of crystalline nanoseeds of BEA structure to induce formation of zeolite beta"

Her present address is 109/41, Chauncheun Modus, Pakkred-Bypass Road, Bangpood, Pakkred, Nonthaburi, Thailand 11120.